# NOSC

AD **A085399**

Technical Report 530

IONOSPHERIC PROFILES FOR PREDICTING NIGHTTIME VLF/LF PROPAGATION

Determination of an effective (exponential) model for use in design and deployment of resources for communication and navigation

JA Ferguson

25 February 1980

Final Report for Period January 1974 — September 1979

Prepared for
Defense Communications Agency
Code C650
and
US Coast Guard
Omega Navigation System Operations Detail

Approved for public release; distribution unlimited.

**NAVAL OCEAN SYSTEMS CENTER
SAN DIEGO, CALIFORNIA 92152**

80 6 12 015

BLANK PAGES
IN THIS
DOCUMENT
WERE NOT
FILMED

NAVAL OCEAN SYSTEMS CENTER, SAN DIEGO, CA 92152

AN ACTIVITY OF THE NAVAL MATERIAL COMMAND

SL GUILLE, CAPT, USN
Commander

HL BLOOD
Technical Director

ADMINISTRATIVE INFORMATION

Work was performed under Program Element FGOV, Project USCG, Task Area O (NOSC 532-MP01), by a member of the Ionospheric Propagation Branch (Code 5323) for the Defense Communications Agency, Code C650 and the US Coast Guard, Omega Navigation System Operations Detail. This report covers work from January 1974 to September 1979 and was approved for publication 25 February 1980.

Released by
JH Richter, Head
EM Propagation Division

Under authority of
JD Hightower, Head
Environmental Sciences Department

REPORT DOCUMENTATION PAGE		READ INSTRUCTIONS BEFORE COMPLETING FORM
1. REPORT NUMBER NOSC Technical Report 530 (TR 530)	**2. GOVT ACCESSION NO.** AD-A085 399	**3. RECIPIENT'S CATALOG NUMBER**
4. TITLE (and Subtitle) IONOSPHERIC PROFILES FOR PREDICTING NIGHTTIME VLF/LF PROPAGATION, Determination of an effective (exponential) model for use in design and deployment of resources for communication and navigation		**5. TYPE OF REPORT & PERIOD COVERED** Final rept. January 1974 – September 1979 **6. PERFORMING ORG. REPORT NUMBER**
7. AUTHOR(s) J. A. Ferguson		**8. CONTRACT OR GRANT NUMBER(s)**
9. PERFORMING ORGANIZATION NAME AND ADDRESS Naval Ocean Systems Center San Diego, CA 92152		**10. PROGRAM ELEMENT, PROJECT, TASK AREA & WORK UNIT NUMBERS** FGOV, USCG, O (NOSC 532-MP01)
11. CONTROLLING OFFICE NAME AND ADDRESS Defense Communications Agency, Code C650 and US Coast Guard, Omega Navigation System Operations Detail		**12. REPORT DATE** 25 February 1980 **13. NUMBER OF PAGES** 78
14. MONITORING AGENCY NAME & ADDRESS(if different from Controlling Office)		**15. SECURITY CLASS. (of this report)** Unclassified
		15a. DECLASSIFICATION/DOWNGRADING SCHEDULE

16. DISTRIBUTION STATEMENT (of this Report)

Approved for public release; distribution unlimited

NOSC/TR-530

17. DISTRIBUTION STATEMENT (of the abstract entered in Block 20, if different from Report)

18. SUPPLEMENTARY NOTES

19. KEY WORDS (Continue on reverse side if necessary and identify by block number)

Ionospheric profiles	MEECN link resources
Ionospheric models	Omega navigation system
Ionospheric propagation	
Vlf/lf propagation	

20. ABSTRACT (Continue on reverse side if necessary and identify by block number)

The regression analysis of ionospheric profiles from the literature fails to show the high ionospheric variability that is observed in the propagation measurements. Neither does it show the rapid transition in altitude between high and middle latitudes. The measured propagation data are more directly related to the MEECN and Omega system requirements for predicting vlf and lf field strengths. Profiles are suggested on the basis of the analysis of these data.

DD $_{1 JAN 73}^{FORM}$ **1473** EDITION OF 1 NOV 65 IS OBSOLETE
S/N 0102-LF-014-6601
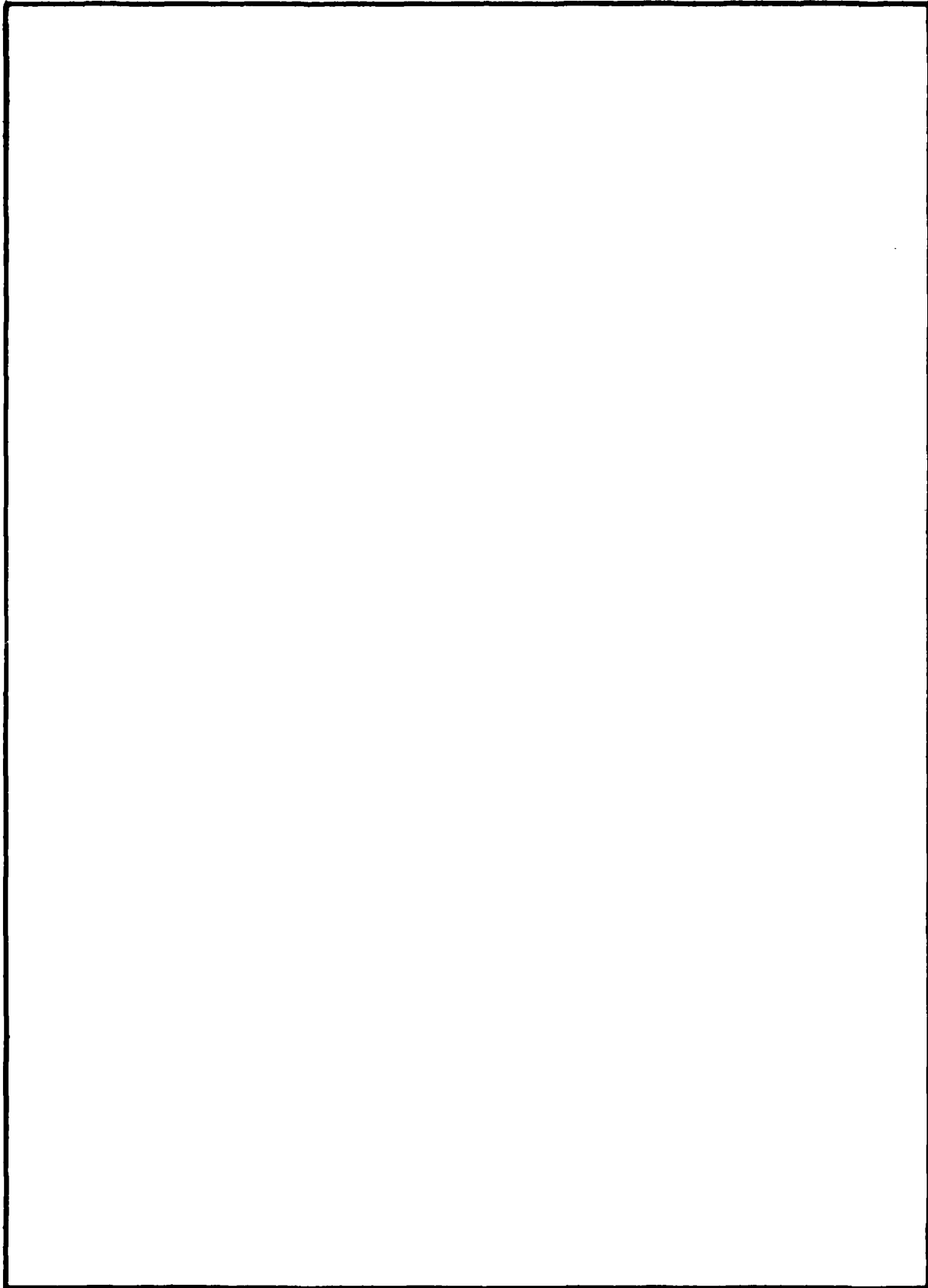
EXECUTIVE SUMMARY

OBJECTIVE

Establish a more accurate description of the lower ionosphere than heretofore available, to refine vlf and lf propagation prediction parameters.

BACKGROUND

To design and deploy resources to be used in the vlf/lf Minimum Essential Emergency Communication Network (MEECN) communication links requires a reliable knowledge of radio signal propagation. Furthermore, assessment of the coverage of the Omega vlf navigation system requires reliable ionospheric profile specification. The Tri-Service Propagation Program was established by the Defense Communication Agency (DCA) to refine the propagation prediction parameters appropriate to vlf and lf. Many of the experimental data reported here were obtained as part of the Tri-Service Propagation Program. The final propagation analysis and profile assessments were carried out as part of the Omega validation project.

Considerable theoretical work in vlf and lf propagation has been done since the early 1960s. As a result, a number of computer codes were generated and quite successfully applied to experimental data. However, vlf and lf propagation strongly depends on the lower ionosphere (D region). Consequently the model of the ionosphere used in propagation predictions must be accurate. An error of 5 km in the effective height of reflection of a nighttime ionospheric model can result in 20-dB errors in signal amplitude calculations. The Tri-Service Propagation Program sought to establish a more accurate description of the lower ionosphere.

APPROACH

Improvement of the ionospheric model was approached from two separate directions. The first approach was to survey the literature for published profiles of electron density vs height. The lower parts of these profiles were then analyzed to determine the best fit to a profile in which electron density varies exponentially with height. A regression analysis was performed to determine the temporal and geographical variations of the exponential profile.

The second approach was to acquire experimentally measured long-path propagation data, then to "fit" these data by calculating the field-strength amplitude along the appropriate propagation path through the use of a variety of ionospheric profiles. The profile was selected that gave the best agreement between calculations and measurements.

Propagation Model

The computer codes used to calculate signal levels in this report employ state-of-the-art full-wave solutions to the anisotropic earth-ionosphere waveguide. The lower boundary has an arbitrarily adjustable conductivity. The upper boundary has an arbitrary distribution of electrons and ions with height. Through the use of a mode conversion model, the effects of rapid changes in the waveguide parameters along the direction of propagation are accounted for and the effects of elevated and arbitrarily oriented transmitters and receivers can be calculated.

The principal unknown in the earth-ionosphere waveguide model, especially for nighttime propagation, is the ionosphere conductivity, which is in part a function of the electron

1

and ion density distribution with height. Fixed-location sounding systems are somewhat in-accurate because the ionization densities are quite low in the region of importance to vlf and lf propagation.

Propagation studies using long-path vlf and lf data provide an indirect but more use-ful description of the ionosphere for propagation prediction. Much success has been achieved with such studies by using an exponential electrons-only ionospheric profile specified by a scale height, β, and a reference height, h′. DCA surveyed the available data and determined that the best nighttime profile was given by the parameters β = 0.5 km^{-1} and h′ = 87 km, for all seasons and latitudes. It was also clear from this DCA study that nighttime propaga-tion data were not very extensive and that further refinements of the profile were needed.

Some of the measurements made by NOSC as part of the Tri-Service Propagation Program used as a transmission source a ten-frequency vlf/lf sounder. The data obtained provide simultaneous evaluation of the ionospheric profile at all ten frequencies. One of the first results of this evaluation was the discovery that β must be made to vary with frequency, from 0.3 km^{-1} at 10 kHz to 0.8 km^{-1} at 60 kHz. Varying β in this way improves the agree-ment between measured and calculated amplitudes by better than 5 dB and sometimes as much as 25 dB.

Measured Data

In a further effort to improve prediction capabilities for nighttime propagation, data from a set of 28 aircraft flights were examined. These flights spanned the western half of the northern hemisphere. Many of these flights recorded transmissions from stations at both ends. This type of data provides the best empirical evaluation of the propagation prediction computer codes and model ionospheres.

Profiles from Propagation Modeling

Ionospheric profiles obtained for the 28 data paths show that the nighttime values of h′ for high latitudes are much lower than the value expected from previous studies. The range of values is found to be from 82 down to 76 km. It is remarkable that 76 km is only 2 km above typical daytime values. The range of values is also much larger than previously encountered.

The available data suggested that the boundary of the very low values of h′ is in the vicinity of 70° magnetic dip and further that geomagnetic coordinates are useful in defining latitudinal variations of the ionosphere. For propagation paths at latitudes south of this 70° dip line, the previously determined h′ of 87 km is found. Calculations of the field amplitudes at high latitudes are improved up to 20 dB by using the lowered values of h′ rather than 87 km.

Profiles from the Literature

Observations of the D region have been made at scattered stations since 1948. The analysis of these observations rests on the assumption that for the purpose of predicting vlf/lf propagation, the variation of electron density with height can be represented by an exponential relationship.

570 electron density profiles were used in the final analysis. The parameters of the exponential profiles derived from these data were subjected to a multiparameter linear re-gression analysis. The coefficients of terms representing zenith angle of the sun, geographic

latitude, season, sunspot number, and normal vs disturbed conditions were determined. The resultant expressions from this approach give the reference height, h′, and scale height, α, as follows:

$$h' = 74.37 - 8.097X_1 + 5.779X_2 - 1.213X_3 - 0.0440X_4 - 6.038X_5$$

where

$$\alpha = 0.3849 - 0.1658X_1 - 0.08584X_3 + 0.1296X_3$$

X_1 = cos of solar zenith angle

X_2 = cos of geographic latitude

X_3 = cos $[2\pi (m - \frac{1}{2})/12]$ (m = month number)

X_4 = Zurich smoothed relative sunspot number

X_5 = magnetic absorption index: 0 for quiet conditions, 1 for disturbed conditions.

Predictions of the ionospheric profiles determined by means of this model — derived from the literature — were compared with the profiles determined by propagation modeling. The aircraft data indicate that the ionosphere varies more than predicted by this model. The comparison disclosed differences in h′ of 2 to 4 km, which can cause up to 20 dB error on calculating vlf field strength.

RESULTS

The regression analysis of ionospheric profiles from the literature does not show the high ionospheric variability that is observed in the propagation measurements. Neither does it show the rapid transition in reference height between high and middle latitudes. The measured propagation data are more directly related to the MEECN requirement for predicting vlf and lf field strengths. On the basis of the analysis of these data, the following profiles are suggested, where F = frequency, in kHz.

Seasonal-Diurnal Propagation Condition	h′ (km)	β (km⁻¹)	Magnetic Dip (°)
Summer day	70	0.5	
Summer night	87	0.0077F + 0.31	
Winter day	74	0.3	
Winter night	80	0.035F − 0.025 (10 < F < 35)	90–75 (high latitudes)
	Linear change between high and middle latitudes		75–70 (transition latitudes)
	87	0.0077F + 0.31	< 70 (middle latitudes)

The frequency dependence of β is based on NOSC data. The latitude variation represents typical conditions; very quiet conditions would be treated by moving the transition region several degrees northward, whereas very disturbed conditions would be treated by moving it only a few degrees southward and by lowering the high-latitude h′ to 76 km.

3

RECOMMENDATIONS

1. Collect and analyze more data from systems such as ten-frequency sounders, to better establish the nighttime profile latitude variation.

2. Correlate these data with satellite measurements.

CONTENTS

INTRODUCTION

To design and deploy resources to be used in the vlf/lf Minimum Essential Emergency Communication Network (MEECN) communication links requires a reliable knowledge of radio signal propagation. The Tri-Service Propagation Program was established by the Defense Communications Agency (DCA) to refine propagation prediction parameters appropriate to vlf and lf. Many of the experimental data reported here were obtained as part of the Tri-Service Propagation Program. The final propagation analysis and profile assessment were carried out as part of the Omega validation project.

Considerable theoretical work in vlf and lf propagation has been done since the early 1960s. As a result, a number of computer codes have been generated. The most significant of these codes were documented in a series of Defense Nuclear Agency (DNA) and Defense Atomic Support Agency (DASA) reports, references 1-5 being the most recent. NOSC has extensively reviewed the use of these computer programs in modeling experimental data (ref 6).

Vlf and lf propagation is strongly dependent on the lower ionosphere. Consequently it is essential that the model of the ionosphere used in propagation predictions be accurate. An error of 5 km in the effective height of reflection of a nighttime ionospheric model can result in 20 dB errors in signal amplitude calculations. Examples of these kinds of errors are shown in this report.

Within the Tri-Service Propagation Program, improvement of the ionospheric model was approached from two separate directions. The first approach was to survey the literature for published profiles of electron density versus height. The lower parts of these profiles were then analyzed to determine the best fit to a profile which has an exponential variation of electron density versus height. A regression analysis was performed to determine the geographical and temporal variations of the exponential profile. This analysis was carried out for DCA by the Institute for Telecommunication Sciences (ITS) (ref 7, 8).

The second approach taken to improve the ionospheric model was to acquire experimental long-path data, then to determine an exponential profile by comparing these measurements with calculations made by means of the assumed profile. This approach expands the data base that shows the behavior of the vlf/lf fields along propagation paths. These

1. DASA Interim Report 702, A FORTRAN Program for Waveguide Propagation which Allows for Both Vertical and Horizontal Dipole Excitation, by RA Pappert, WF Moler, and LR Shockey, 15 June 1970.

2. DASA Interim Report 713, WKB Mode Summing Program for Vlf/Lf Antennas of Arbitrary Length, Shape and Elevation, by RA Pappert and LR Shockey, 2 June 1971.

3. DNA Interim Report 722, Mode Conversion Program for an Inhomogeneous Anisotropic Ionosphere, by RA Pappert and LR Shockey, 1 May 1972.

4. DNA Interim Report 771, Simplified Vlf/Lf Mode Conversion Program with Allowance for Elevated, Arbitrarily Oriented Electric Dipole Antennas, by RA Pappert and LR Shockey, 10 October 1976.

5. DNA Interim Report 77T, "MODESRCH" — An Improved Computer Program for Obtaining Elf/Vlf/Lf Mode Constants in an Earth-Ionosphere Waveguide, by DG Morfitt and CH Shellman, 1 October 1976.

6. NOSC TR 141, Effective Electron Density Distributions Describing Vlf/Lf Propagation Data, by DG Morfitt, 21 September 1977.

7. DCA TR 111-77, A Revised Model of the Electron Density in the Lower Ionosphere, by RM Davis and LA Berry, 1977.

8. DCA Report C600-TP-76-2, A Statistical Model of the Lower Ionosphere, 1976.

long-path data also permit a more direct evaluation of the performance of the propagation prediction codes at a large number of points. This analysis was performed by NOSC.

The purpose of this report is to document and compare the results of these two approaches for nighttime propagation conditions.

PROPAGATION MODEL

The vlf/lf propagation models and computer programs used to calculate the signal levels plotted in this report employ a full-waveguide solution to the anisotropic earth-ionosphere waveguide problem. The lower boundary has an arbitrarily adjustable conductivity and premittivity. Conductivity values are typically obtained from the ten-level map published in reference 9. Other values often used are 4.64 S/m for sea water and 0.0124 S/m as an average for good-conducting land.* The effects of earth curvature are included.

The anisotropy of the ionospheric upper boundary is due to the presence of the earth's magnetic field. This field varies along any propagation path. The effects of this variation are negligible for daytime propagation conditions, but they can severely affect calculated vlf signal levels for nighttime propagation. These effects are also observed in measurements (ref 10). Values for the magnetic field are typically obtained from computer codes that use high-order polynomials (ref 11). Alternative sources are maps of the magnetic field variations, such as those published by the Hydrographic Office.

The upper boundary of the earth-ionosphere waveguide in the propagation model is specified by an arbitrary distribution of electrons and ions with height. The frequency with which each constituent collides with the surrounding neutral particles is also an arbitrary function of height. The ionization densities and collision frequencies define a conductivity profile. The ionospheric region of greatest importance to vlf/lf propagation is that from about 50 km up to about 120 km (the D and E regions). This region is not easily studied by ground-based probing experiments, which tend to be plagued either by large error factors in estimates of the ionization densities at various heights or by poor height resolution (ref 12). Rocket soundings provide more accurate measurements but are very limited in their temporal and geographical distributions.

Propagation studies such as the one described in this report apply a propagation model to experimental data and attempt to determine the conductivity profile indirectly, by comparing calculated fields with measured fields and varying the ionospheric model until acceptable agreement is found.

One of the simplest ionospheric profiles is an exponential variation of conductivity with height. It can be specified by only two parameters — typically scale height and reference height (to be defined later). The process of varying the ionospheric model, calculating fields, and

---

* The siemen (S) is the metric equivalent of the mho.

9. NRL TM 5460-315, Vlf Effective Ground Conductivity Map, by JP Hauser, 5 October 1970.

10. Experimental Observation of Magnetic Field Effects on Vlf Propagation at Night, by JE Bickel, JA Ferguson, and GV Stanley; Radio Science, vol 5, January 1970, p 19-25.

11. An Interim Magnetic Field, by DC Jensen and JC Cain; JGR, vol 67, 1962, p 3568-3569.

12. Ionospheric Profiles up to 160 km: A Review of Techniques and Profiles, by EV Thrane; Methods of Measurements and Results of Lower Ionosphere Structure, Akademie-Verlag, Berlin, 1974.

comparing the calculations with measurements is greatly facilitated by the use of these profiles. Furthermore, exponential conductivity profiles have already been used to provide excellent agreement with experimentally measured vlf/lf fields (ref 6, 10, 13, 14).

The elements of the waveguide propagation model described so far are used to calculate a set of complex modal solutions (modes) for the specified earth-ionosphere waveguide. These modes are then summed at arbitrarily selected distances from the transmitter to obtain the calculated vlf/lf field at those distances. This simple model is called horizontally homogeneous and can be applied to most daytime propagation paths with unvarying ground conductivity. Generally the parameters of the waveguide must be varied to describe the real propagation paths properly. Such paths cross land-sea and day-night boundaries and regions through which the geomagnetic field variations are significant. The modeling of such paths is accomplished by dividing them into horizontally homogeneous segments. As an example, a land-sea boundary might mark the end of one segment and the beginning of the next. At each boundary conversion, coefficients are calculated to relate modes in one segment to those in the next (ref 3). The mode conversion model allows for an arbitrary number and order of modes on each side of each waveguide discontinuity.

The mode conversion model can be applied even in the event that the propagation path has only slowly varying waveguide parameters. The results of such an application reproduce those obtained by means of the so-called WKB mode-summing technique (ref 2). This model also allows for the calculation of both horizontal and vertical components of the electric field at an arbitrary height in the waveguide. Consequently, an arbitrary antenna can be treated.

As already described, the principal unknown in the propagation model is the ionospheric conductivity, which is a function of the height variation of electron and ion density distributions and collision frequencies. For an electrons-only ionospheric model, the conductivity parameter is defined as follows:

$$\omega_r(h) = \frac{e^2}{\epsilon_0 m} \frac{N(h)}{\nu(h)} , \tag{1}$$

where

$$
\begin{aligned}
e &= \text{electron charge} \\
m &= \text{electron mass} \\
\epsilon_0 &= \text{permittivity of free space} \\
N(h) &= \text{electron density at height h} \\
\nu(h) &= \text{collision frequency of the electrons with the surrounding neutrals at} \\
&\quad \text{height h.}
\end{aligned}
$$

The conductivity profile used in this report is that of reference 15, in which

$$\omega_r(h) = 2.5 \times 10^5 \exp [\beta(h-h')] , \tag{2}$$

13. DCA Report 960-TP-74-5, Comparison of Predicted Vlf/Lf Signal Levels with Propagation Data, by DG Morfitt, 21 January 1974.

14. DCA Report C650-TP-74-4, Determination of Effective Ionospheric Electron Density Profiles for Vlf/Lf Propagation, by DG Morfitt, 1 January 1976.

15. NBS TN 300, Characteristics of the Earth-Ionosphere Waveguide for Vlf Radio Waves, by JR Wait and KP Spies, 30 December 1964.

where β is a scale height in km^{-1} and h' is a reference height in km. (Height h is also in km.) The collision frequency

$$\nu(h) = 1.816 \times 10^{11} \exp [- 0.15 h] , \qquad (3)$$

where ν is the number of collisions per second (ref 15). The electron density at height h is thus found as follows:

$$N(h) = 1.4276 \times 10^7 \exp [\beta(h-h') - 0.15 h] , \qquad (4)$$

where N is the number of electrons per cubic centimeter.

The determination of the parameters of the above model for application to communication systems performance is achieved by comparing measured data with theoretical calculations and adjusting the parameters in the latter until a subjective acceptable agreement is obtained. The most straightforward method of comparison is obtained when the measured data are collected at a large number of points along a great circle propagation path that includes the transmitter. The easiest way to collect such data is aboard an inflight aircraft, and that is the way all the propagation data examined in this report were collected.

At the beginning of the DCA Tri-Service Propagation Program, DCA surveyed the available vlf/lf propagation data and the exponential profiles that gave the best agreement with them (ref 13). The profiles determined are given in table 1. Subsequent experimental measurements and analyses have produced little change in the recommended daytime profiles (ref 6, 14) but have produced a much more complicated relationship for nighttime propagation, which is the main subject of this report.

	Day		Night
Latitudes	Summer	Winter	All Seasons and Latitudes
High	$\beta = 0.3, h' = 72$	$\beta = 0.3, h' = 72$	$\beta = 0.5, h' = 87$
Middle	$\beta = 0.5, h' = 70$	$\beta = 0.3, h' = 72$	

Table 1. 1974 recommended profiles (β in km^{-1}, h' in km).

Table 1 recommends the profile $\beta = 0.5$ km^{-1}, $h' = 87$ km for nighttime propagation for all frequencies described in reference 14. When data from the NOSC multifrequency vlf/lf oblique incidence sounder were used, it became necessary to modify β as a function of frequency in order to fit simultaneous data at ten frequencies. This frequency dependence probably occurs because the ionospheric profile is not truly exponential and because its slope increases with height. Since the principal height of reflection increases with frequency, the model parameter β must increase to more readily match the true profile. Unfortunately, the variation of β with frequency changes from one set of measurements to the next. The data analyzed in reference 14 are for middle latitudes and were collected on three separate nights in February 1969, January 1974, and February 1974. Fitting the values of β from the best fit profiles against the frequency (F), in kHz, produces the following three equations:

$$\beta = 0.35 + 0.0070F, \text{ for 7 February 1969} \qquad (5a)$$
$$\beta = 0.242 + 0.020F, \text{ for 30 January 1974} \qquad (5b)$$
$$\beta = 0.25 + 0.0089F, \text{ for 1 February 1974} \qquad (5c)$$

The values of β at various frequencies in (5a) and (5c) are fairly close, about 0.55 at 30 kHz and 0.70 at 50 kHz. On the other hand, (5b) gives 0.85 at 30 kHz and 1.26 at 50 kHz. The cause for this variability has not been determined. The location of amplitude minima as a function of distance from the transmitter is principally a function of h' for the range of β values used. For the data reported in reference 14, the value of h' was between 87 and 88 km. This variation is very small, considering the range of β obtained, and is consistent with table 1. The variation of β is highly significant in predicting signal amplitudes at lf, where 5- to 25-dB improvements were obtained (ref 6).

PROPAGATION DATA

Data from fixed vlf operational transmitters are next examined, along with one set of NOSC ten-frequency sounder data. The data were recorded in flights along propagation paths all but a few of which had a transmitter in operation at each end. A summary of the data flights is given in table 2.

Data were collected in 1957, 1969, and 1974–1977. The data for the latter three years were obtained by the DCA Tri-Service Propagation Program. The 1957 data are included because they were not originally modeled by using full-wave calculations. The 1969 data have not been reported previously. Table 3 lists the transmitting stations used to obtain the data, along with the magnetic dip at the ground at each station.

The aircraft flight paths are shown in figure 1. Also shown (shaded line) is the locus of points for which the magnetic dip angle at the ground is 70°. (This line will enter the discussion later.) The dashed lines are each an arc of a great circle that passes through the indicated transmitter locations. They represent the optimum flight paths for collecting data and in general represent the paths used in the propagation analysis.

The propagation data plots, figures 2–41, are located at the end of the report, for the convenience of the reader. Each plot shows normalized received signal amplitude at points along a particular flight path. The signal amplitude (vertical scale) is shown in dB above one microvolt per metre, normalized to one kilowatt of power radiated by an equivalent vertical monopole. The horizontal scale is in megametres from the transmitter.

The ordinate unit of amplitude (dB/μV/m/kW) is an abbreviation for dB above one microvolt per metre for one kilowatt of radiated power. The number in parentheses after the date of each set of data indicates the flight number from table 2 and figure 1.

Figures 2 through 14 provide easy comparison of vertical field strength data from each individual combination of transmitter and propagation path. Data from the 16 November and 16 December 1957 Annapolis–Seattle flights, shown in the top part of figures 2 (NSS transmitting) and 3 (NLK transmitting) are similar, with each frequency set showing only about 100 km offset in the location of its minima and maxima for the two dates. The two corresponding sets of 1969 data were taken over the same flight path and recorded within 3 days of each other, but they show considerably less agreement, especially with NLK transmitting. The data from NLK transmissions (fig 3) show the largest differences, with 500-km separation between the minima near 2 Mm. These data clearly indicate that care must be taken when attempting to generalize the results of only a few measurements. The data from NLK transmissions measured in 1969 and 1977 (fig 3) show similar variation in amplitude structure as a function of distance. The data in this particular figure will be addressed in more detail later.

Table 2. Data flight summary.

Flt No	Date and Origin	Destination	Departure Date GMT	Arrival GMT	SSN (6)	Transmitting Stations
1	1957 Annapolis MD	Seattle WA	16 Nov 0118	1017	201	NSS, NLK
2	Seattle	Annapolis	16 Dec 0220	0848	200	NSS, NLK
3	1969 Seattle	Patuxent River MD	24 Jan 0126	1111		NSS, NLK
4	Patuxent River	Seattle	26 Jan 0146	1315	110	NSS, NLK
5	Seattle	Honolulu HI	27 Jan 0522	1701		NLK, NPM
6	1974 Sentinel AZ	Glasgow MT	5 Feb 0508	0918	34	NOSC sdr
7	Glasgow	Thule, Greenland	6 Feb 0925	1410		NOSC sdr
8 (1)	1975 Griffiss AFB NY	Griffiss AFB	18 May 2213	0514	17	NAA
9	Griffiss AFB	Mildenhall AFB, UK	21 May 2230	0507		NAA
10	Griffiss AFB	Mildenhall AFB	3 Oct 2000	0300	14	NAA
11	Mildenhall AFB	Griffiss AFB	5 Oct 2315	0600		NAA, GBR
12 (2)	1976 Wright Patterson AFB OH	Bodo, Norway	1 Dec 2250	0920		NAA
13 (5)	Bodo	Fairbanks AK	3 Dec 2323	0610		—
14 (5)	Fairbanks	Honolulu	4 Dec 0822	1526	15	—
15	Honolulu	Seattle	6 Dec 0400	1006		NAA, NPM
16	Seattle	Wright Patterson AFB	7 Dec 0208	0900		NAA
17 (3)	1977 Wright Patterson AFB	Mildenhall AFB	6 Jan 1915	0609		NAA, JHZ
18 (3)	Mildenhall AFB	Bodo	9 Jan 0034	0547		JHZ, GBR
19	Bodo	Fairbanks	10 Jan 0129	0757	17	GBR
20	Fairbanks	Honolulu	11 Jan 0758	1455		NPM
21	Honolulu	Seattle	12 Jan 0438	1006		NAA, NLK
22	Seattle	Wright Patterson AFB	14 Jan 0220	0926		NAA, NLK
23	Wright Patterson AFB	Bodo	2 Feb 2156	0815		NAA, JHZ
24 (4)	Bodo	Bodo	4 Feb 1800	2348		GBR
25	Bodo	Fairbanks	6 Feb 0012	0700	18	GBR, JHZ
26 (5)	Fairbanks	Honolulu	8 Feb 0742	1420		—
27	Honolulu	Seattle	10 Feb 0413	0934		NAA, NLK
28	Seattle	Wright Patterson AFB	11 Feb 0235	0746		NAA, NLK

NOTES

1. Flight went half way to Mildenhall AFB, UK, then returned.
2. Time includes 2-hour refueling stop in Keflavik, Iceland.
3. Flight was via Keflavik, Iceland.
4. Flight was via Mildenhall AFB, UK.
5. No useful data were obtained.
6. Zurich smoothed sunspot number.
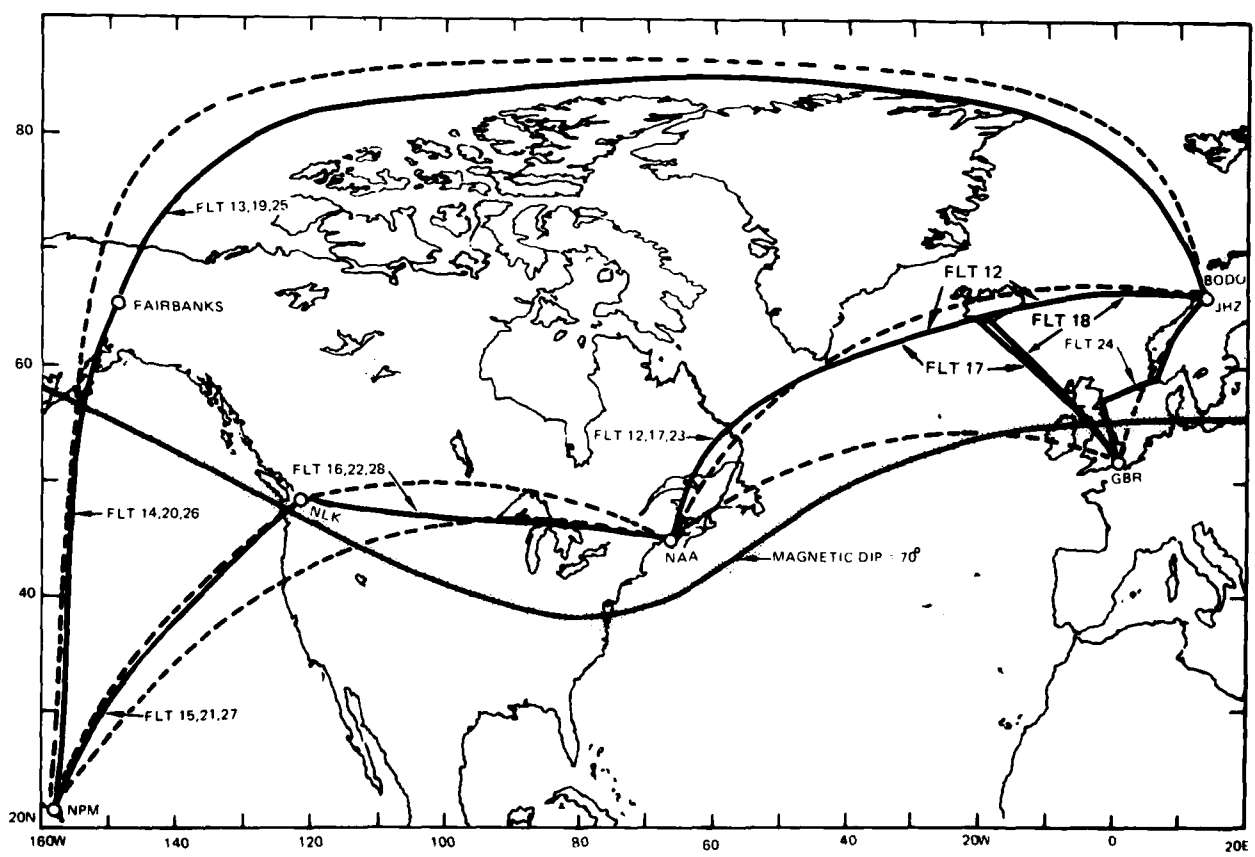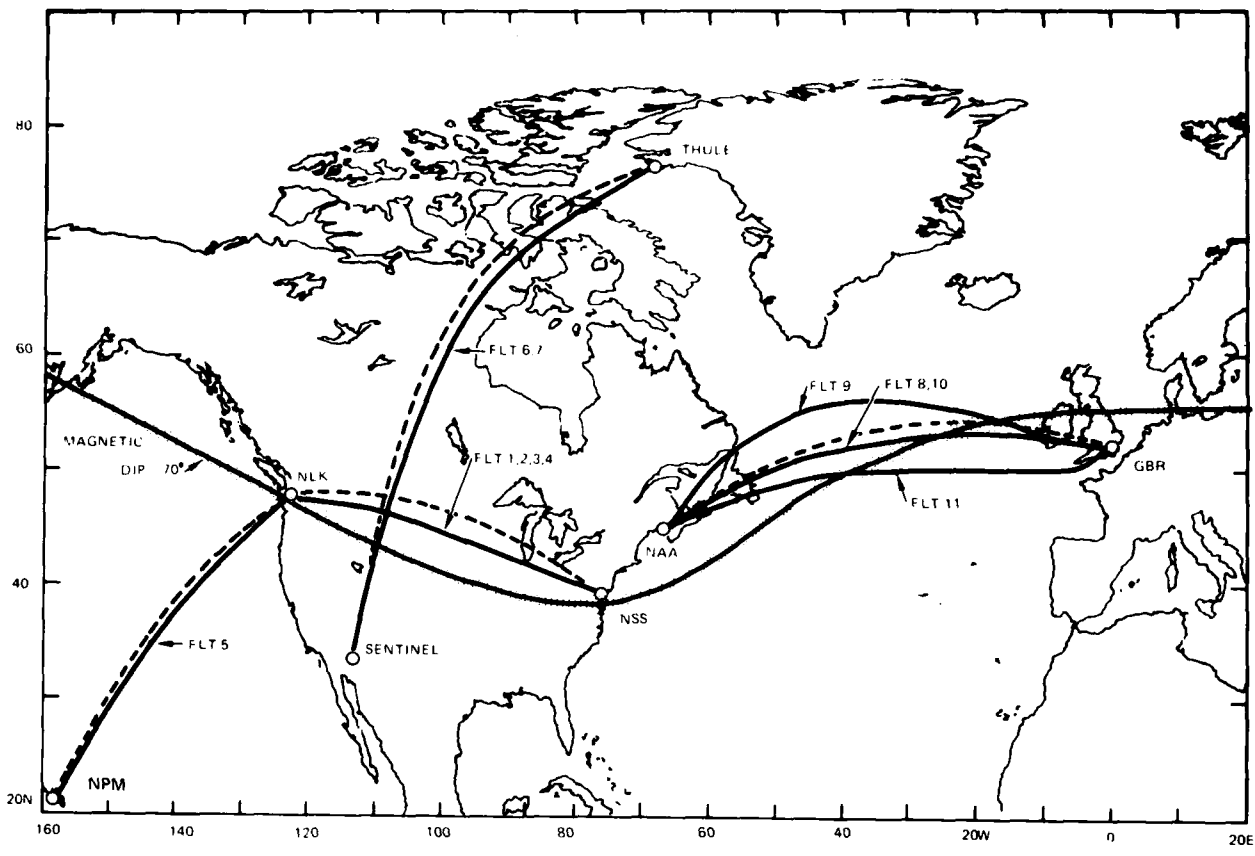
Figure 1. Flight paths (solid) and corresponding propagation radials (dashed).

13

Call Sign	Freq (kHz)	Location	Longitude	Latitude	Dip ($^{\circ}$)
NSS	15.5, 21.4	Annapolis MD	76.450° W	38.983° N	70.6
NAA	17.8	Cutler ME	67.283° W	44.633° N	73.4
NLK	18.6	Jim Creek WA	121.917° W	48.200° N	71.0
NPM	23.4	Lualualei HI	158.150° W	21.417° N	39.1
GBR	16.0	Rugby, UK	1.183° W	52.367° N	67.7
JHZ	16.4	Helgeland, Norway	13.004° E	66.417° N	76.1
NOSC	10-freq sounder	Sentinel AZ	113.150° W	32.817° N	59.5

Table 3. Transmitting stations.

Data from NAA transmissions, recorded in 1976 and 1977 during flights from Hawaii to Seattle and from Seattle to Cutler, are plotted in figure 4. The overall amplitudes in this figure are questionable because the receivers were unstable. Nevertheless, the locations of the minima are correct and allow a determination of the h' parameter. In this respect, the data show a clear trend of the minima toward the transmitter in each successive data set, indicating a lowering of the average ionospheric profile.

Data from NLK transmissions, recorded in 1969 and 1977 during flights between Hawaii and Seattle, are plotted in figure 5. 1976 NLK data are lacking because the station was shut down for maintenance during the data flights. The two sets of data for 1977 are similar. The amplitude minimum near 3 Mm for 1969 is shifted toward the transmitter by about 400 km relative to the corresponding minimum for the 1977 data. Data recorded from NPM transmissions on similar flights in 1969 and 1976 are shown in figure 6. Here the 1969 amplitude minimum near 3 Mm is shifted toward the transmitter by about 300 km. Only one set of data was obtained from NPM transmissions recorded during flights from Fairbanks to Hawaii, plotted in figure 7.

Figure 8 plots two sets of data from NAA transmissions measured in 1975. The large amplitude differences in the October data are attributed to an error in the calibration procedure, but the locations of the maxima and minima are correct and can be used to determine h'. Additional data from NAA obtained in 1976 and 1977 are plotted in figure 9.

During the 5 October 1975 flight, data from GBR transmissions were obtained. These data, plotted in figure 10, are on a path reciprocal to one of the sets of NAA data and are used to determine β for the October 1975 data. Additional data for east-to-west propagation across the Atlantic, plotted in figure 11, are from JHZ transmissions recorded in January and February 1977.

One set of data from GBR transmissions, plotted in figure 12, is perhaps the most difficult to analyze of all the data taken. The data in this plot were recorded on a sequence of two flights: GBR to Bodo, Norway, and Bodo to Fairbanks (flights 24 and 25). The flight path from Bodo to Fairbanks is not a radial with respect to GBR. In propagation modeling, non-radial propagation paths are cumbersome and expensive to analyze because to model them accurately requires computations for a large number of radial paths whose end points are on the nonradial path. Computing such radial paths is particularly difficult here because of the large number of such radials that must be considered for various portions of the Greenland ice cap.

Data from JHZ transmissions in February 1977 are plotted in figure 13. The problems associated with the data in figure 12 do not exist for these data since the radial path from Bodo, Norway, to Fairbanks is almost all over ocean.

Data collected on successive flights 6 and 7 on a path from the NOSC sounder at Sentinel AZ via Glasgow MT to Thule, Greenland, in January 1974 are plotted in figure 14a-c. At some frequencies, the signal amplitudes recorded at the end of flight 6 and at the beginning of flight 7 are not the same. This indicates that the ionosphere differed somewhat between the two flights.

Horizontal field strength data obtained on some of the data flights are shown in figures 15-22. The variation of horizontal field strength with distance and time does not repeat from one sample to the next as well as does the corresponding variation of vertical field strength. This difference is due in part to the more rapid variation with distance of the horizontal fields. Consequently, ionospheric changes which produce relatively minor shifts in the vertical field amplitude structure may produce complex changes in the horizontal field amplitude structure. The difference can be seen by comparing figures 4 and 16, which show simultaneous vertical and horizontal field strength data.

PROFILES FROM PROPAGATION MODELING

The best fit theoretical results for figures 2-14 (vertical field strength measurements) are shown by the next series of figures, 23-37. The best fit β and h' values are given, as well as the result for the profile $\beta = 0.5$, h' = 87 (dashed curve) for comparison, from table 1. The notation used in the figures to denote the profile is β/h'. Table 4 is a summary of the best fit profiles. For flights 5, 17, and 23, two profiles were needed: one to fit the set of data from one transmitter and the other to fit the corresponding reciprocal path data. The table indicates in parentheses for these particular flights the appropriate transmitter identifier for whose transmission data plot the fit was derived. For the other data flights it was assumed that the ionosphere varied slowly throughout each of them and that the best fit profile is a reasonable compromise.

These best fits are obtained by first determining which features of the amplitude versus distance pattern are most important — usually the locations of major amplitude minima and the amplitudes of the maxima. As an example, the best fit for the NSS data from flight 1 (fig 23) is $\beta = 0.6$, h' = 77 (0.6/77). This profile provides excellent agreement between the measured and calculated locations of the amplitude minima, at 0.6 and 2 Mm, and the overall amplitude. The choices of best fit are not always clearly indicated, however. As an example, the NSS data from flight 4 (fig 24) could not be acceptably fit with any homogeneous ionospheric model. The best profile was chosen by using the reciprocal path data from NLK (fig 26), for which spectacular agreement exists between the calculations and measurements.

Profiles were not obtained for flights 13 and 14 because no usable propagation data were obtained on those flights. There is no profile given for flight 26, since the principal propagation radial is NPM to Fairbanks and the transmitter was shut down during the flight. Furthermore, no analysis was performed for flight 19. The principal data for this flight (from GBR — fig 12) involve nonradial propagation over the Greenland ice cap. The difficulties involved in analyzing data taken over such paths have already been described.

15

Propagation Path*	Flight	Date	Best-Fit Profiles
NLK–NSS	1	16 Nov 1957	0.6/77
	2	16 Dec 1957	0.6/76
	3	24 Jan 1969	0.6/82
	4	26 Jan 1969	0.6/76
NLK–NAA	16	7 Dec 1976	0.4/88
(segment 2 data)	22	14 Jan 1977	0.4/82
	28	11 Feb 1977	0.4/80
NAA–JHZ	12	1 Dec 1976	0.3/87
	17	6 Jan 1977	0.3/84 (NAA), 0.4/80 (JHZ)
	18	9 Jan 1977	0.4/78
	23	2 Feb 1977	0.3/84 (NAA), 0.4/76 (JHZ)
NAA–GBR	8	18 May 1975	0.4/85
	9	21 May 1975	0.4/85
	10	3 Oct 1975	0.4/87
	11	5 Oct 1975	0.4/87
JHZ → Pole	25	6 Feb 1977	0.5/80
NPM → Pole	20	11 Jan 1977	0.6/87
NPM–NLK	5	27 Jan 1969	0.6/82 (NLK), 0.6/85 (NPM)
	15	6 Dec 1976	0.4/89
(segment 1 data)	21	12 Jan 1977	0.6/87
	27	10 Feb 1977	0.6/87
NAA → NPM	15	6 Dec 1976	0.4/88
(segment 1 data)	21	12 Jan 1977	0.4/87
	27	10 Feb 1977	0.4/87
Sentinel → Pole	6 + 7	5–6 Feb 1974	β varies with frequency
			$h' = 87$ km south of $69°$ dip
			$h' = 77$ km north of $72°$ dip

* The symbol – indicates two-way propagation path.

 The symbol → indicates one-way propagation path in the direction indicated.

Table 4. Summary of β/h' for best fits to the data.

Of the available data, the most extensive set for any transmitter is shown in figure 3 for NLK eastward propagation. Some very interesting results follow from the analysis of this set of data. An essential feature is the location of the minimum between 2 and 3 Mm. There is a 400 km variation of the location of the minimum.

The data taken on 26 January 1969 (flt 4) and 16 December 1957 (flt 2) indicate a disturbance of the ionosphere. An h' value of 76 km fits the data well, especially those from the NLK transmissions (fig 25). This low value of h' and the 82-km value for the data of

24 January 1969 are remarkable since the nominal range of h' for nighttime data at lower latitudes is 86–90 km. The 76-km value is nearly as low as the nominal daytime range of 70–74 km. These results are consistent with those of reference 16 for a very short path (350 km) from Omega Norway to Kiruna, Sweden.

Middle-latitude propagation modeling results indicate a model ionosphere with h' from 86 to 90 km. For the NLK-NSS and NLK-NAA data (table 4), h' varies from 76 to 82 km except on flight 16. Values of h' lower than the middle-latitude nighttime profile indicate a source of ionization not present at low latitudes. A likely reason for this additional ionization is particle precipitation (ref 16, 17). In a study to coordinate satellite measurements of electron fluxes and ground-based measurements of D-region ionization, references 18 and 19 showed that precipitating electrons can be the dominant source of ionization at D-region heights. The satellite results clearly indicate that the southernmost boundary of the precipitation varies from day to day. In one instance, on a northward swing of the satellite, the minimum detectable flux level was exceeded at a magnetic latitude of about 57° (magnetic dip at the ground = 72°). The electron flux increased to a plateau at about 61° (dip = 74.5°). In another instance this transition took place from about 44° (dip = 62.5°) to 48° (dip = 65.8°). In both instances the transition region is about 4° of magnetic latitude. Dip-angle figures are used here instead of the more commonly used L values because the former are more directly related to vlf/lf propagation parameters. It is important to consider the energy levels of these precipitating particles.

The above observations are used in establishing a tentative geophysical model for propagation calculations. Latitudes north of the transition region will be called high latitudes. The propagation paths included in flights 1–4 are at places within the transition region and at other places totally within the high latitudes.

In table 4 note that flights 15, 21, and 27 have two significantly different best-fit profiles given. Most of these discrepancies can be accounted for acceptably. The differences in β for flights 21 and 27 are due to receiver problems for the NAA data (fig 28). Therefore the value $\beta = 0.6$ km^{-1}, obtained from the NLK data (fig 29), is probably more accurate.

Each set of data shown in figure 28 was obtained in two segments of flight, as shown in figure 1. Segment 1 data (4–9 Mm) were collected during flight from Hawaii to Seattle and are listed in table 4 as NAA → NPM. Segment 2 data (0–4 Mm) were collected on another night during flights from Seattle to Cutler and are listed in table 4 under NLK-NAA. The available reciprocal path data for these segments are plotted in figures 29 and 30 (segment 1) and figure 27 (segment 2). It can be seen in figure 1 that the propagation path between NLK and NAA may be affected by precipitating particles whereas the path between NPM and NLK and between NAA and NPM may not be thus affected. Hence, the h' value of 87 km for data

16. Vlf Radio Signals Propagating Over the Greenland Ice-Sheet, by S Westerlund and FH Reder; JATP, vol 35, 1973, p 1475–1491.

17. Energetic Electron Precipitation as a Source of Ionization in the Nighttime D-Region Over the Mid-Latitude Rocket Range, South Uist, by MP Gough and HL Collin; JATP, vol 35, 1973, p 835–850.

18. A Coordinated Study of Energetic Electron Precipitation and D-Region Electron Concentrations Over Ottawa During Disturbed Conditions, by TR Larsen, JB Reagan, WL Imhof, LE Montbriand, and JS Belrose; JGR, vol 81, 1976, p 2200–2211.

19. L-Dependent Energetic Electron Precipitation and Mid-Latitude D-Region Pair Production Profiles, by TR Larsen, WL Imhof, and JB Reagan; JGR, vol 81, 1976, p 3444-3446.

recorded on segment 1 is not inconsistent with h' values of 80 and 82 km for segment 2, on flights 28 and 22, respectively. The segment 2 data of flight 16 (fig 28a) indicate that the particle precipitation boundary must have been north of the propagation path, giving a middle-latitude value for h' of 88 km.

Other data for which more than one profile was obtained were recorded on flights 17, 18, and 23 between NAA and JHZ (fig 33 and 35). The choice of β for the JHZ data (fig 35) was made on the basis of the qualitative agreement between the theory and measurements rather than on the overall amplitude. Higher values of β tend to fill in the distinctive minimum near 500 km, so were not used. Comparison of figures 33 and 35 shows that no single profile fits each set of data and indicates that the ionosphere varied significantly during the data flights.

For flight 5, h' values of 82 km for the NLK data (fig 29) and 85 km for the NPM data (fig 30) were obtained. This may be the result of the effect of a slow southward movement of the particle precipitation boundary during the airplane flight from NLK to NPM. Such a movement would affect the NLK data but not the NPM data.

If the location and extent of particle precipitation could be determined on each of the nights for which two profiles were required, the calculations could be made with a latitudinally varying ionospheric model. Lacking such detailed data, the NOSC ten-frequency sounder data collected on flights 6 and 7 (fig 14) have been analyzed with an empricially derived latitude variation of h' that is consistent with the satellite data (ref 18, 19). This is the only path so analyzed because it is essentially along a magnetic meridian and is therefore an ideal one from which to derive the h' latitude variation. The results of this modeling are shown in table 4 and figure 37. In this model, h' south of 69° dip is 87 km; north of 72° dip it is 77 km. Between these two dip angles h' is varied linearly in four equally spaced steps of h' over equal distances, as illustrated at the bottom of the figure. The variations of the magnetic dip and ground conductivity were included in the waveguide mode calculations.

The improvement in the fit of the calculations to the sounder measurements is evident in the distances beyond about 2 Mm. Taking into account the lowered ionosphere tends to move the calculated minima and maxima toward the transmitter, bringing them into better alignment with the measurements. This effect is particularly easy to see in the 14.003-kHz data.

The usual range of h' is from 76 to 84 km for winter data (November–February) along propagation paths with magnetic dip angles greater than about 70° (flights 1–4, 12, 16–18, 22–25, 28). The improvement gained from using reduced values of h' is shown in figures 38–41. These figures display for each flight as a function of distance the ratios of the measured amplitude to each of the two calculated amplitudes resulting from the use of the 0.5/87 profile and the best-fit profile. The ratios are displayed in dB so that perfect agreement between measured and calculated amplitudes would be a horizontal line at zero. The new profiles produce fits that are closer to the measurements and have less amplitude variation about them. More quantitative results are shown in table 5, which shows the mean and standard deviation of the ratios, in dB, for each 1-Mm distance range. The new profiles produce dB ratios close to zero more consistently than the previous profile (0.5/87) produces, particularly for flights 1–3, 5, 12, 17, 23, and 28. The high-latitude ionosphere must be treated as having a lower effective height of reflection (h') than the middle-latitude ionosphere, but the geophysical parameters that control the location of the boundary between the two ionospheric regions are not understood. A comparison of tables 2 and 4 shows that h' values of 76 and 77 km are derived from data taken during high sunspot numbers while values of 80 and 82 km are more typical of lower sunspot numbers. However, the NLK–NAA

18

data show an h′ variation of 8 km for a sunspot range of 15 to 18. Furthermore, the magnetic index ranged from 3 to 5 for these same data. The variation of these two parameters indicates that these indices are not sufficient to describe the ionospheric variation.

| Distance Range, Mm | NSS → NLK | | | | | NLK → NSS | | | |
	Flt	$\overline{R}_1$	σ_1	$\overline{R}_2$	σ_2	Flt	$\overline{R}_1$	σ_1	$\overline{R}_2$	σ_2
1 - 2	1	0.7	4.3	0.9	1.0	1	0.8	5.8	-1.2	1.1
2 - 3		6.0	8.3	0.3	1.7		-1.2	6.4	1.2	5.0
3 - 4		-3.3	1.7	-0.5	1.3		7.7	4.1	-2.6	1.0
1 - 2	2	-0.7	4.2	1.5	2.0	2	1.6	6.3	-1.6	2.3
2 - 3		8.0	8.2	2.3	1.8		-1.5	7.2	0.9	3.8
3 - 4		0.0	0.8	2.9	1.0		5.9	4.8	2.3	2.4
1 - 2	3	-0.5	4.0	-0.5	3.4	3	3.3	5.8	1.5	3.6
2 - 3		1.4	4.2	2.3	2.9		-3.8	5.0	0.4	3.8
3 - 4		-3.9	10.3	0.5	2.7		5.5	3.0	0.2	1.4
1 - 2	4	-0.6	3.4	2.2	2.7	4	4.7	6.1	1.0	0.5
2 - 3		-0.2	3.8	7.1	5.7		-0.8	9.2	1.7	2.3
3 - 4		-4.9	3.5	-1.4	2.7		4.0	7.2	1.9	2.8

| Distance Range, Mm | NAA → NLK | | | | | NLK → NAA | | | |
	Flt	$\overline{R}_1$	σ_1	$\overline{R}_2$	σ_2	Flt	$\overline{R}_1$	σ_1	$\overline{R}_2$	σ_2
1 - 2	16	-3.3	3.9	-2.0	3.1					
2 - 3		3.8	5.6	0.7	3.3					
3 - 4		0.2	5.8	2.9	8.6					
1 - 2	22	0.0	1.9	-1.9	3.2	22	1.9	5.4	1.3	2.2
2 - 3		4.4	6.4	1.9	4.7		-5.8	7.5	0.2	3.4
3 - 4		4.9	8.3	-2.2	1.0		-1.9	5.7	-3.2	1.2
1 - 2	28	1.3	2.2	0.2	1.6	28	2.8	5.3	-0.4	1.0
2 - 3		4.3	10.6	1.5	1.4		-2.9	7.3	0.2	2.0
3 - 4		-0.4	7.8	-5.4	1.8		-3.8	7.6	-4.1	0.8

NOTES $\overline{R}_1$, σ_1 are mean and standard deviation of difference of measured and calculated amplitudes for the 0.5/87 profile.

$\overline{R}_2$, σ_2 are same as $\overline{R}_1$, σ_1, but for the best-fit profile.

Table 5. Statistics for ratios (dB) of measured to calculated amplitudes for high-latitude nighttime paths.

19

		NAA → JHZ					JHZ → NAA			
Distance Range, Mm	Flt	$\bar{R}_1$	σ_1	$\bar{R}_2$	σ_2	Flt	$\bar{R}_1$	σ_1	$\bar{R}_2$	σ_2
1 – 2	12	– 4.5	5.2	–1.0	1.7					
2 – 3		– 7.6	5.2	0.6	3.2					
1 – 2	17	– 2.4	4.9	–0.8	1.3	17 + 18	2.3	4.2	3.3	1.0
2 – 3		– 6.8	7.0	–0.4	2.4		– 0.2	5.9	2.3	0.8
3 – 4		0.1	3.2	0.7	0.6					
1 – 2	23	– 5.0	5.8	–3.2	2.0	23	0.5	4.7	2.0	1.0
2 – 3		– 7.6	7.9	–1.2	2.1		8.1	8.8	1.0	1.0
3 – 4		– 4.9	7.5	–1.5	2.6		–1.7	1.2	1.2	0.5
4 – 5		– 0.8	6.7	1.1	1.4					

		NPM → NLK					NLK → NPM			
Distance Range, Mm	Flt	$\bar{R}_1$	σ_1	$\bar{R}_2$	σ_2	Flt	$\bar{R}_1$	σ_1	$\bar{R}_2$	σ_2
1 – 2	5	1.9	2.3	0.8	1.6	5	1.7	3.5	0.8	2.0
2 – 3		– 2.7	6.7	2.6	1.7		0.5	1.6	-0.7	1.2
3 – 4		12.7	9.3	0.2	1.4		– 0.4	2.8	–1.2	3.0
1 – 2	21	1.0	1.5	–0.3	2.1	15	– 0.5	2.6	2.2	2.5
2 – 3		2.0	1.7	0.1	0.7		–1.1	3.6	2.9	3.2
3 – 4		2.9	5.5	–2.1	2.6		– 2.2	1.1	1.7	1.0
1 – 2	27	0.2	1.3	–1.1	2.0					
2 – 3		2.5	1.7	1.1	1.1					
3 – 4		6.1	6.6	1.6	1.0					

Table 5. (Continued)

PROFILES FROM THE LITERATURE

Observations of the D region have been made at scattered stations since 1948. The period of greatest activity was perhaps 1964–1970. Since that time fewer observations have been made each year. Due to the difficulty and expense of this work, it is doubtful that it will be resumed on a large scale. Thus, the present body of D-region observations may not be greatly amplified in the future. The analyses presented here are extracted from references 7, 8 and private communication with RM Davis and LA Berry (1978).

The analysis presented in this section rests on the assumption that for the purpose of predicting vlf/lf propagation, the variation of electron density with height can be represented by the exponential relationship

$$N(h) = N_o \exp [\alpha(h-h_o)] , \qquad (6)$$

where

N_o = electron density at some reference height, h_o

α = scale height.

Reference 8 discusses the errors arising from assuming an exponential profile. It concludes that the assumption is reasonable in view of the random variation of D-region profiles applicable to a given propagation calculation.

From equations 4 and 6 it follows that

$$N_0 = 1.4276 \times 10^7 \exp\left\{-[(\alpha + 0.15)h' + \alpha h_0]\right\} , \tag{7}$$

with $h = h'$. It follows from equation 7 that

$$h' = \left[\ln\left(\frac{1.4276 \times 10^7}{N_0}\right) + \alpha h_0\right](\alpha + 0.15)^{-1} . \tag{8}$$

Thus, if N_0, h_0, and α are known for a given D-region profile, the profile can be specified in terms of the two parameters α and h' by means of equation 8. Equations 4, 6 and 7 show that

$$\beta = \alpha + 0.15 , \tag{9}$$

where β and h' are the parameters discussed in previous sections.

In the present analysis, N_0, h_0, and α are determined from the published electron density profiles by assuming that most of the energy is reflected near the level at which

$$B(h_0) = \frac{\omega_r(h_0)}{\omega}$$

$$= \sqrt{2}\cos^2\phi , \tag{10}$$

where

ω = angular frequency of the radio wave
ϕ = angle of incidence on the ionosphere (ref 20).

If we take $\phi = 81°$ and frequency = 30 kHz as typical values for long-distance vlf/lf propagation, it follows that

$$N_0 = 2.05 \times 10^{-6} \nu(h_0) , \tag{11}$$

where

$\nu(h_0)$ is the collision frequency at h_0.

Figure 42 (from reference 21) shows how N_0 and h_0 are determined. It shows an electron density profile along with the assumed collision frequency profile. An exponential collision frequency is fitted to this collision frequency at 70 km. The exponential collision frequency is used in equation 11 to define $N_0(h)$, whose intersection with the measured profile gives the required values of N_0 and h_0. The slope of the log of the measured profile variation with height at the intersection is α.

According to correspondence with RM Davis and LA Berry in 1978, 570 electron density profiles were used in the final analysis. This is an increase of 66 profiles over the

20. The Detection of Daytime Nuclear Bursts Below 150 km by Prompt Vlf Phase Anomalies, by EC Field and RD Engel; Proc IEEE, vol 53, 1965, p 2009-2017.

21. Study of the Lower Ionosphere Using Partial Reflections — 1. Experimental Technique and Method of Analysis, by JS Belrose and MJ Burke; JGR, vol 69, 1964, p 2799-2818.
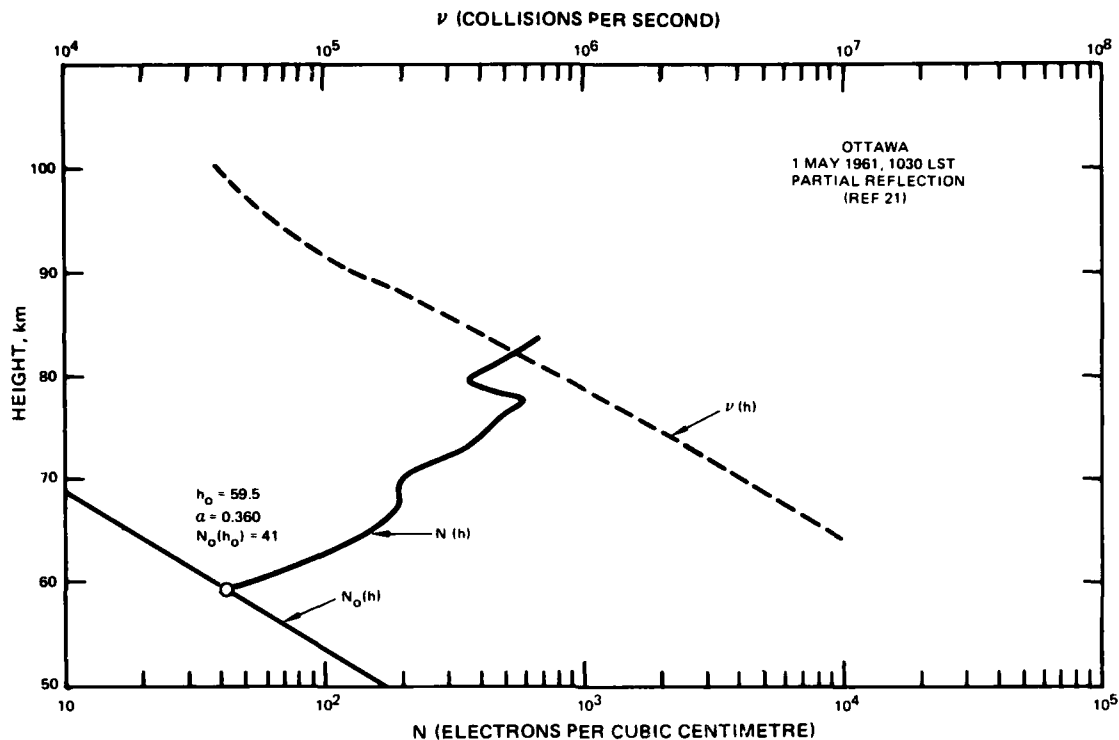
Figure 42. An example of an electron density profile, N(h), and the use of the associated collision
frequency profile, ν(h), to determine the electron density N_0 and slope at the height of reflection h_0.

number they used in 1977 (ref 7). The OMNITAB computer program at ITS was used for
doing a multiparameter least-squares fit to determine the coefficient of α and h'. The param-
eters used are defined in the following results:

$$h' = 74.37 - 8.097 \, X_1 + 5.779 \, X_2 - 1.213 \, X_3 - 0.044 \, X_4 - 6.038 \, X_5 \tag{12}$$

$$\alpha = 0.3849 - 0.1658 \, X_1 - 0.08584 \, X_3 + 0.1296 \, X_5 , \tag{13}$$

where

X_1 = cos X, solar zenith angle
X_2 = cos θ, geographical latitude
X_3 = cos ϕ, a seasonal variable in which

$$\phi = \frac{m - 0.5}{12} \, (2\pi)$$

m = month number, as 1 for January

X_4 = SSN, the Zurich smoothed relative sunspot number.
X_5 = magnetic-absorption index: 0.0 for quiet conditions, 1.0 for disturbed con-
ditions.

22

The model presented here is similar in general to the model in reference 7. The new model differs from the old primarily in the smaller variation of h' with latitude — a total variation of 5.8 km, in contrast to the 8.0-km value in reference 7. The change was probably caused by the 45% increase in the number of observations made at latitudes of 61° or higher. For the α prediction, the present model yields a larger variation with sun's zenith angle (local time and season) and a smaller change between quiet and disturbed conditions.

The new regression analysis of h' resulted in almost the same residual standard deviation as the earlier analysis: 5.39 km vs 5.22 km. The residual standard deviation for α is larger in the present model, however; 0.287 vs 0.227.

The possibility of using a trapezoidal rather than a cosine dependence for local time has been investigated. Under the trapezoid assumption, the local time variable is represented by a linear change in value from +1 to –1 over a given solar zenith angle interval. Several intervals were tried, such as 90–97°, 60–100°, and 80–110°.

The coefficients computed by OMNITAB for the trapezoid assumption were compared with those for the cosine assumption. Under the cosine assumption, the maximum day-to-night difference in h' is more than 16 km, while the corresponding difference under the trapezoid assumption is only 9 km. Since independent evidence strongly indicates that the day-to-night change in height of reflection is at least 16 km, it is concluded that the cosine dependence should be retained in this D-region model. Another disadvantage of the trapezoid model is that the seasonal dependence, X_3, is not statistically significant and would have to be discarded.

The variations of h' and α with their independent variables can be compared in some instances with the corresponding variations found by other researchers (ref 22), and with experimental results of the Tri-Service Propagation Program. Reference 22 uses electron density profiles developed from vlf and lf propagation data. The effects of the five variables are next considered in turn.

Cos X — Under the model, h' increases from a minimum at midday to a maximum at midnight. The same is true of α, in general agreement with NOSC results. The profiles of reference 22 indicate the same increase in height with increasing X in daytime hours. Reference 19 shows α larger at night.

Cos θ — The model predicts a decreasing value of h' with increasing latitude. The results of reference 22 are not given in terms of latitude, but the analysis of data taken during the Tri-Service Propagation Program presented in the previous section does show the same behavior.

Cos ϕ — The model includes a seasonal dependence, apart from the effect of X, that increases h' in summer and decreases it in winter. α has a similar dependence. The profiles of reference 22 show very little seasonal dependence in height of reflection, but NOSC data indicate a winter lowering. The slope of the reference 22 profiles shows some increase in gradient from winter to summer, in agreement with the model.

SSN — The sunspot effect in the model is a decrease in h' as sunspot number increases. The same tendency is evident in the summer profiles of reference 22.

Magnetic-absorption index — The effect of magnetic disturbance or abnormal absorption is to decrease h' or increase α substantially, according to the model. No corresponding

22. Diurnal, Seasonal, and Solar-Cycle Variations of Electron Densities in the Ionospheric D- and E-Regions, by J Bremer and W Singer; JATP, vol 39, 1977, p 25–34.

results are available in reference 22, but studies showing the same disturbance effects are cited in reference 23.

COMPARISON OF PROFILES

Table 6 shows the results of using equations 12 and 13 to predict the exponential profiles for the propagation data of the previous section. The predicted values shown are nearly all for midnight at the midpoint of the indicated propagation path. The exceptions are those followed by the transmitter identifiers, which are for midnight at the indicated transmitter locations. The sunspot parameter (SSN) for each prediction is given in table 2. No predictions for disturbed conditions are given, because they were generally too low in h' and too high in β. In two cases the disturbed profiles are closer to the propagation modeling results: for flight 4 the disturbed profile is 0.73/74, and the JHZ end of flight 23 has a disturbed profile of 0.71/74.

There is very good agreement between the predictions and the empirically derived profiles for the first four flights, which occurred in months with very high sunspot numbers. The agreement between the two sets of profiles is not as consistently good for the NLK-NAA path. The NLK-NAA and NLK-NSS paths are very similar geographically. Since the propagation data were obtained in the months November through February, the solar zenith angle varied only slightly. The only parameter in the prediction model that produces variations in the profile under these circumstances is the sunspot number. For the NLK-NAA data this parameter varied from 15 to 18, an amount insufficient to produce the profile variations observed in the propagation modeling results.

On the NAA-JHZ path the predictions agree with the propagation results only when the latter indicate depressed ionospheres. Flights 12 and 18 show the middle-latitude value of h' (87 km), which is 5-6 km higher than the value predicted. The same is true for the NAA-GBR path, where the propagation results are 5 km higher than the predicted values.

The profiles agree well for the paths from NPM and JHZ toward the north pole, but there are only two sets of data. On the remaining paths, NLK-NPM and NPM-NAA, the values obtained from the propagation modeling are 2-4 km higher than the predictions.

The values of h' are most commonly discussed, because they have the most significant effect on the accuracy of the predictions. To illustrate this point, consider the theoretical curves shown in figure 32 for the NAA-GBR path. In the bottom part of the figure are curves for 0.5/87 and 0.4/87. This difference in β causes a fairly uniform offset in the overall amplitude. In the upper part of the figure are curves for 0.5/87 and 0.4/85. Here the locations of the minima and maxima are offset. A difference of 3 to 6 dB can be accounted for by the values of β, but the difference due to h' varies from 0 to 20 dB depending on the range from the transmitter. It is clear that predicting ionospheric profiles for vlf/lf system calculations requires more data if better accuracy is to be achieved than is currently possible. Empirical modeling from propagation data seems to be more reliable.

23. The Temporal and Geographic Variations of D Region Electron Concentrations, by L Thomas; Methods of Measurements and Results of Lower Ionosphere Structure, Akademie-Verlag, Berlin, 1974.

24

Path	Flight	Date	Measured	Predicted
NLK – NSS	1	16 Nov 1957	0.6/77	0.62/76
	2	16 Dec 1957	0.6/76	0.61/76
	3	24 Jan 1969	0.6/82	0.60/80
	4	26 Jan 1969	0.6/76	0.73/74*
NLK – NAA	16	7 Dec 1976	0.4/88	0.60/84
	12	14 Jan 1977	0.4/82	0.60/83
	28	11 Feb 1977	0.4/80	0.61/83
NAA – JHZ	12	1 Dec 1976	0.3/87	0.58/81
	17	6 Jan 1977	0.3/84 (NAA),0.4/80(JHZ)	0.61/84(NAA) 0.57/80(JHZ)
	18	9 Jan 1977	0.4/78	0.58/82
	23	2 Feb 1977	0.3/84(NAA), 0.4/76(JHZ)	0.62/84(NAA) 0.71/74(JHZ)*
NAA – GBR	8	18 May 1975	0.4/85	0.64/80
	9	21 May 1975	0.4/85	0.64/80
	10	3 Oct 1975	0.4/87	0.62/82
	11	5 Oct 1975	0.4/87	0.62/82
JHZ ⟶ Pole	25	6 Feb 1977	0.5/80	0.57/80(JHZ)
NPM ⟶ Pole	20	11 Jan 1977	0.6/87	0.62/86(NPM)
NPM – NLK	5	27 Jan 1969	0.6/82(NLK), 0.6/85(NPM)	0.60/79(NLK) 0.62/82(NPM)
	15	6 Dec 1976	0.4/89	0.61/85
	21	12 Jan 1977	0.6/87	0.61/85
	27	10 Feb 1977	0.6/87	0.63/85
NAA ⟶ NPM	15	6 Dec 1976	0.4/88	0.61/85
	21	12 Jan 1977	0.4/87	0.61/85
	27	10 Feb 1977	0.4/87	0.63/85

*Predictions for disturbed conditions.

Table 6. Predicted β/h' for propagation paths.

CONCLUSIONS

Two approaches for determining effective nighttime ionospheric parameters have been described in this report. One is to build a data base of exponential profiles from the nonexponential profiles to be found in the literature. This data base is then subjected to a multiparameter linear regression analysis. The other approach is to build a data base of vlf/lf field strength amplitude measurements along a variety of propagation paths. For a variety of ionospheric models, the calculated field strength is compared to the measured fields until acceptable agreement is obtained. Since there is only a small volume of data available, the latter approach does not allow a statistical description of the results.

The propagation data examined in this report, aside from a single set of NOSC multi-frequency sounder data, were obtained from in-flight recordings of transmissions from existing vlf communication stations. Much of these data are for high-latitude or polar-cap propagation conditions at night. A surprising result is the significant profile change from previously expected values; in one case, the value of h' was only 2 km above typical daytime values. The transition region between high and middle latitudes is suggested to be in the vicinity of 70° dip. The width of the transition region from middle to high latitudes is about 4° of geomagnetic latitude. The location of the boundary, the amount of ionospheric disturbance, and the width of the boundary are all indications of the variability of the winter nighttime ionosphere. The correlation of this variability with standard geophysical disturbance indices has not been possible to date. One study that would clearly be of value is a comparison of satellite measurements of precipitating electron fluxes over some of the propagation paths for which there are data. Such a study would probably result in the ability to use forecasting programs in predicting disturbances in vlf communications. The transition region suggests that the cosine variation in latitude used in the regression analysis should be replaced by a more complicated functional form such as a trapezoid. The failure of the trapezoid model in the regression analysis described earlier cannot be explained.

The variability of the ionosphere as indicated by the propagation data is greater than that predicted by the results of the regression analysis. The agreement between the profiles obtained by both methods is best when very high sunspot numbers prevail. In such conditions the nighttime high-latitude ionosphere has h' values close to typical daytime values. When the sunspot numbers are less than 20, the profiles derived from the two methods are in less agreement.

Another result of the propagation modeling for nighttime conditions is the variability of β. Analysis of simultaneous ten-frequency data collected for the Tri-Service Propagation Program shows that the values for β must be made to vary with frequency. However, data collected on different dates show that the numerical relationship between frequency and β is not constant. The regression analysis performed on the profiles from the literature cannot show a β dependence on frequency since the reflection height and slope were determined at an assumed 30 kHz.

Most of the propagation data examined in this report are for paths tangent to the high-latitude boundary, sometimes outside and sometimes inside the transition region. The model ionosphere therefore represents an average of the actual ionosphere during the aircraft flight. The degree to which a single ionospheric model fits reciprocal path data on the same night is an indication of the variability of the location of the high-latitude boundary during the aircraft flight. From a MEECN propagation prediction standpoint, the foregoing considerations suggest the simplified ionospheric model given in table 7.

26

Seasonal-Diurnal Propagation Condition	h′ (km)	β (km⁻¹)	Magnetic Dip (°)
Summer day	70	0.5	
Summer night	87	$0.0077F + 0.31$	
Winter day	74	0.3	
Winter night	80	$0.035F - 0.025$ $(10 < F < 35)$	90–75 (high latitudes)
	Linear change between high and middle latitudes		75–70 (transition latitudes)
	87	$0.0077F + 0.31$	< 70 (middle latitudes)

Table 7. Suggested profiles based on long-path vlf/lf propagation data.
(Frequencies, F, are in kHz.)

The frequency-dependent variations for β are based on a different functional form fit to the results of reference 6 than was used in equation 5. The latitude variation represents typical conditions. One would expect that very quiet conditions would move the transition region northward by several degrees and that very disturbed conditions would move it southward a few degrees and lower the high-latitude h′ to 76 km.

RECOMMENDATIONS

It is highly recommended that satellite measurements of precipitating electron fluxes during appropriate aircraft data flights be studied with a view toward forecasting vlf/lf communication disturbances. It is also recommended that further data be obtained on propagation paths normal to the transition latitudes. Such data should be obtained for multiple simultaneous frequencies.

REFERENCES

1. DASA Interim Report 702, A FORTRAN Program for Waveguide Propagation which Allows for Both Vertical and Horizontal Dipole Excitation, by RA Pappert, WF Moler, and LR Shockey, 15 June 1970.

2. DASA Interim Report 713, WKB Mode Summing Program for Vlf/Lf Antennas of Arbitrary Length, Shape and Elevation, by RA Pappert and LR Shockey, 2 June 1971.

3. DNA Interim Report 722, Mode Conversion Program for an Inhomogeneous Anisotropic Ionosphere, by RA Pappert and LR Shockey, 1 May 1972.

4. DNA Interim Report 771, Simplified Vlf/Lf Mode Conversion Program with Allowance for Elevated, Arbitrarily Oriented Electric Dipole Antennas, by RA Pappert and LR Shockey, 10 October 1976.

5. DNA Interim Report 77T, "MODESRCH" — An Improved Computer Program for Obtaining Elf/Vlf/Lf Mode Constants in an Earth–Ionosphere Waveguide, by DG Morfitt and CH Shellman, 1 October 1976.

6. NOSC TR 141, Effective Electron Density Distributions Describing Vlf/Lf Propagation Data, by DG Morfitt, 21 September 1977.

7. DCA TR 111-77, A Revised Model of the Electron Density in the Lower Ionosphere, by RM Davis and LA Berry, 1977.

8. DCA Report C600-TP-76-2, A Statistical Model of the Lower Ionosphere, 1976.

9. NRL TM 5460-315A, Vlf Effective Ground Conductivity Map, by JP Hauser, 5 October 1970.

10. Experimental Observation of Magnetic Field Effects on Vlf Propagation at Night, by JE Bickel, JA Ferguson, and GV Stanley; Radio Sci, vol 5, January 1970, p 19–25.

11. An Interim Magnetic Field, by DC Jensen and JC Cain; JGR, vol 67, 1962, p 3568–3569.

12. Ionospheric Profiles up to 160 km: A Review of Techniques and Profiles, by EV Thrane; Methods of Measurements and Results of Lower Ionosphere Structure, Akademie-Verlag, Berlin, 1974.

13. DCA Report 960-TP-74-5, Comparison of Predicted Vlf/Lf Signal Levels with Propagation Data, by DG Morfitt, 21 January 1974.

14. DCA Report C650-TP-74-4, Determination of Effective Ionospheric Electron Density Profiles for Vlf/Lf Propagation, by DG Morfitt, 1 January 1976.

15. NBS TN 300, Characteristics of the Earth-Ionosphere Waveguide for Vlf Radio Waves, by JR Wait and KP Spies, 30 December 1964.

16. Vlf Radio Signals Propagating Over the Greenland Ice-Sheet, by S Westerlund and FH Reder; JATP, vol 35, 1973, p 1475-1491.

17. Energetic Electron Precipitation as a Source of Ionization in the Nighttime D-Region over the Mid-Latitude Rocket Range, South Uist, by MP Gough and HL Collin; JATP, vol 35, 1973, p 835-850.

18. A Coordinated Study of Energetic Electron Precipitation and D-Region Electron Concentrations Over Ottawa During Disturbed Conditions, by TR Larsen, JB Reagan, WL Imhof, LE Montbriand, and JS Belrose; JGR, vol 81, 1976, p 2200-2211.

19. L-Dependent Energetic Electron Precipitation and Mid-Latitude D-Region Pair Production Profiles, by TR Larsen, WL Imhof, and JB Reagan; JGR, vol 81, 1976, p 3444-3446.

20. The Detection of Daytime Nuclear Bursts Below 150 km by Prompt Vlf Phase Anomalies, by EC Field and RD Engel; Proc IEEE, vol 53, 1965, p 2009-2017.

21. Study of the Lower Ionosphere Using Partial Reflections — 1. Experimental Technique and Method of Analysis, by JS Belrose and MJ Burke; JGR, vol 69, 1964, p 2799-2818.

22. Diurnal, Seasonal, and Solar-Cycle Variations of Electron Densities in the Ionospheric D- and E-Regions, by J Bremer and W Singer; JATP, vol 39, 1977, p 25-34.

23. The Temporal and Geographic Variations of D Region Electron Concentrations, by L Thomas; Methods of Measurements and Results of Lower Ionosphere Structure, Akademie-Verlag, Berlin, 1974.
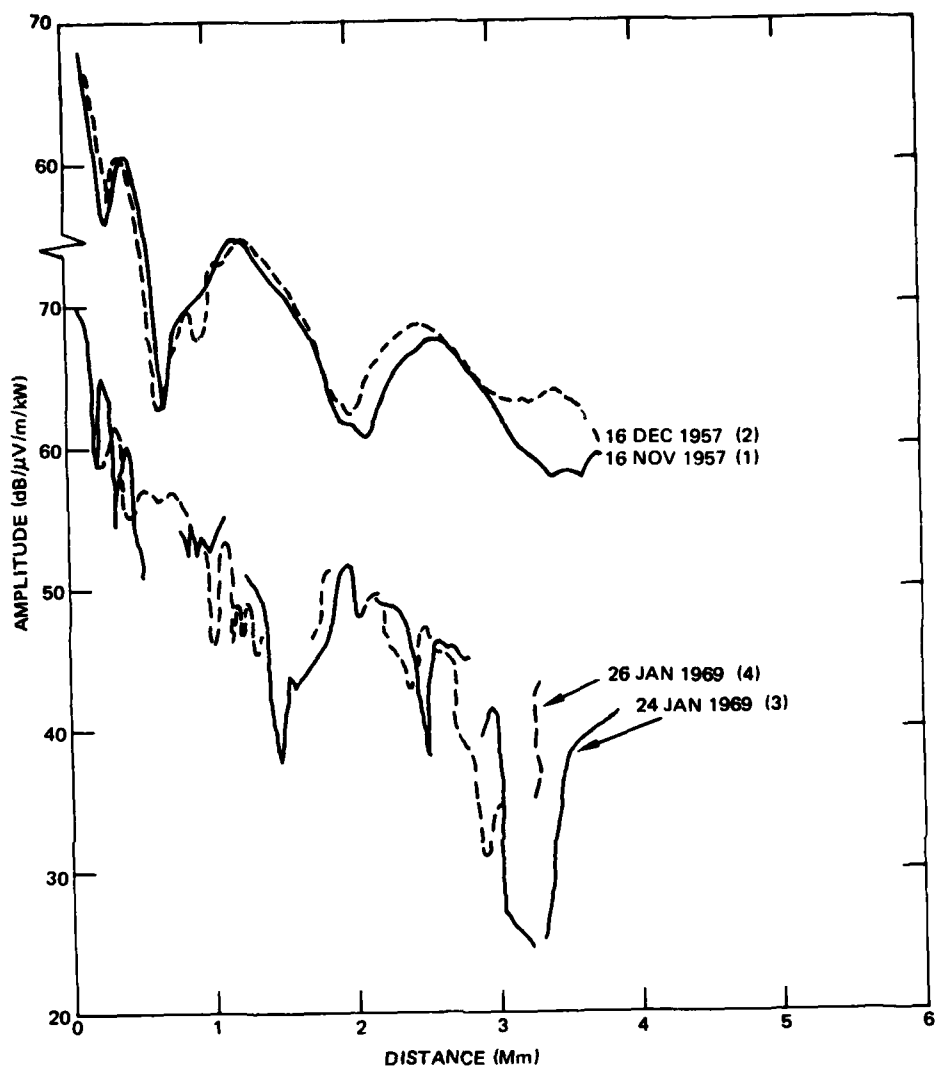
Figure 2. NSS (15.5 kHz) measured while flying between NLK and NSS in 1957. NSS (21.4 kHz) measured while flying between NLK and NSS in 1969. Vertical field strength.

30
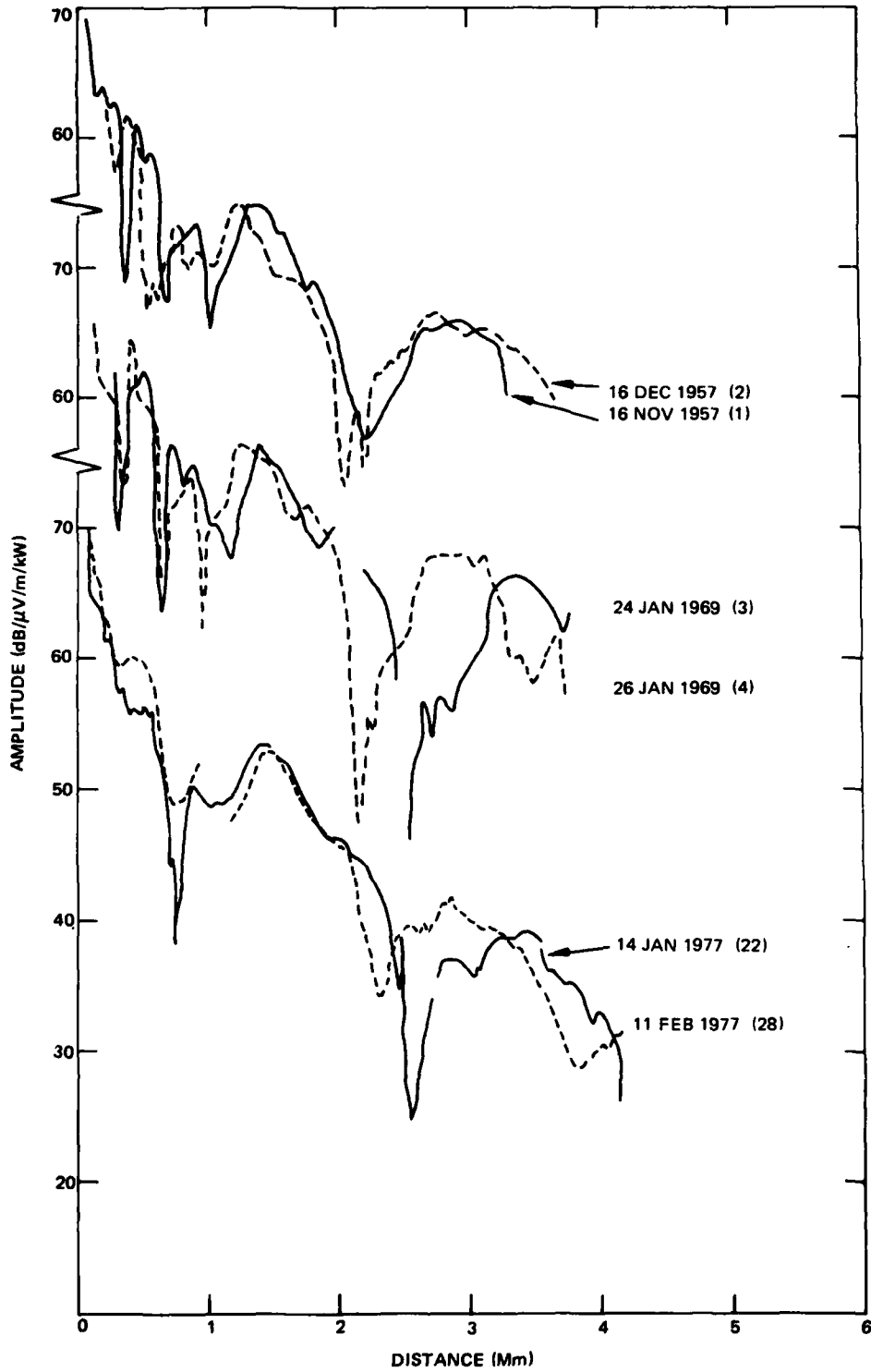
Figure 3. NLK (18.6 kHz) measured while flying between NLK and NSS in 1957 and 1969, and between NLK and NAA in 1977. Vertical field strength.

31
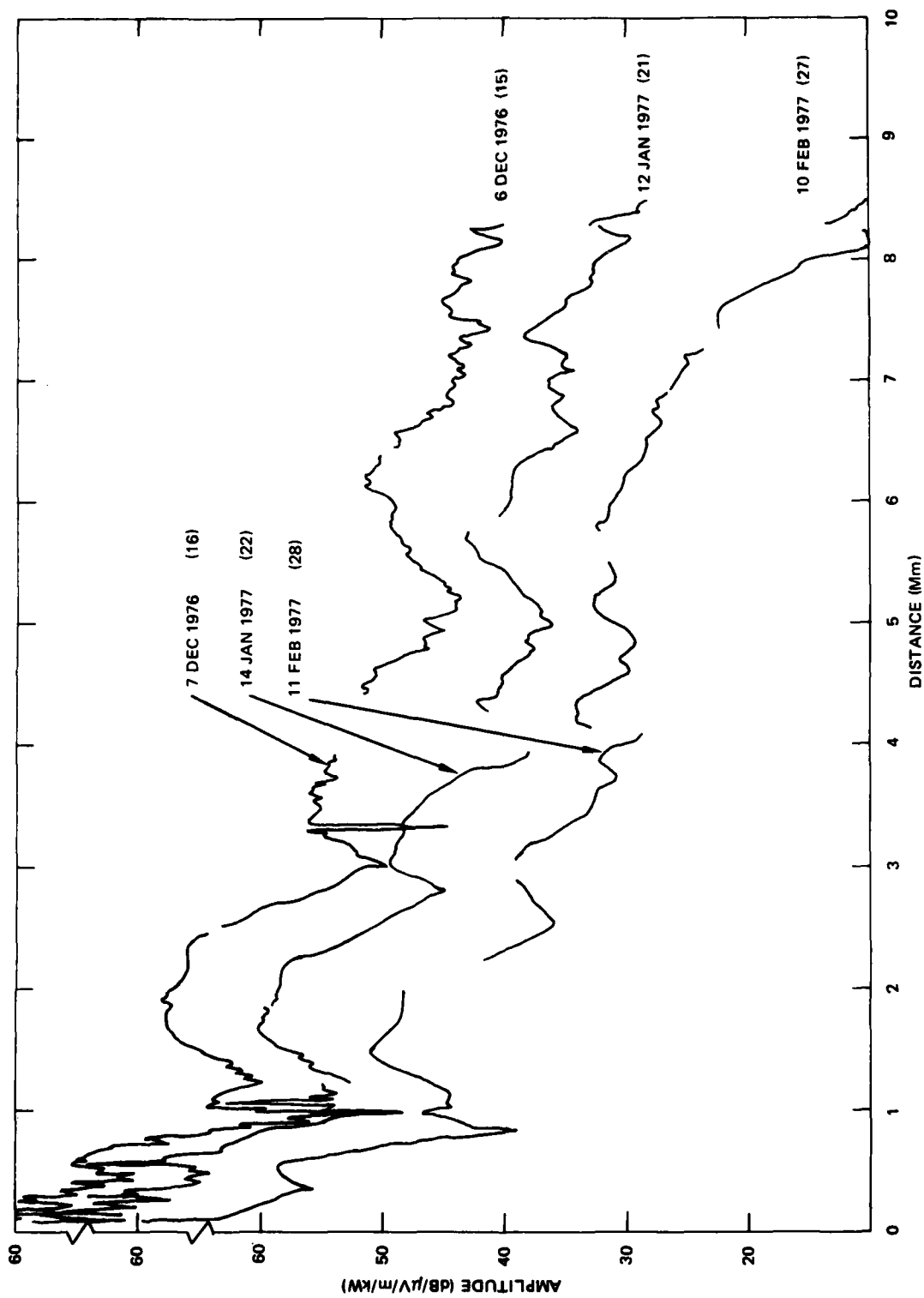
Figure 4. NAA (17.8 kHz) measured while flying from NPM to NLK to NAA in 1976 and 1977. Vertical field strength.
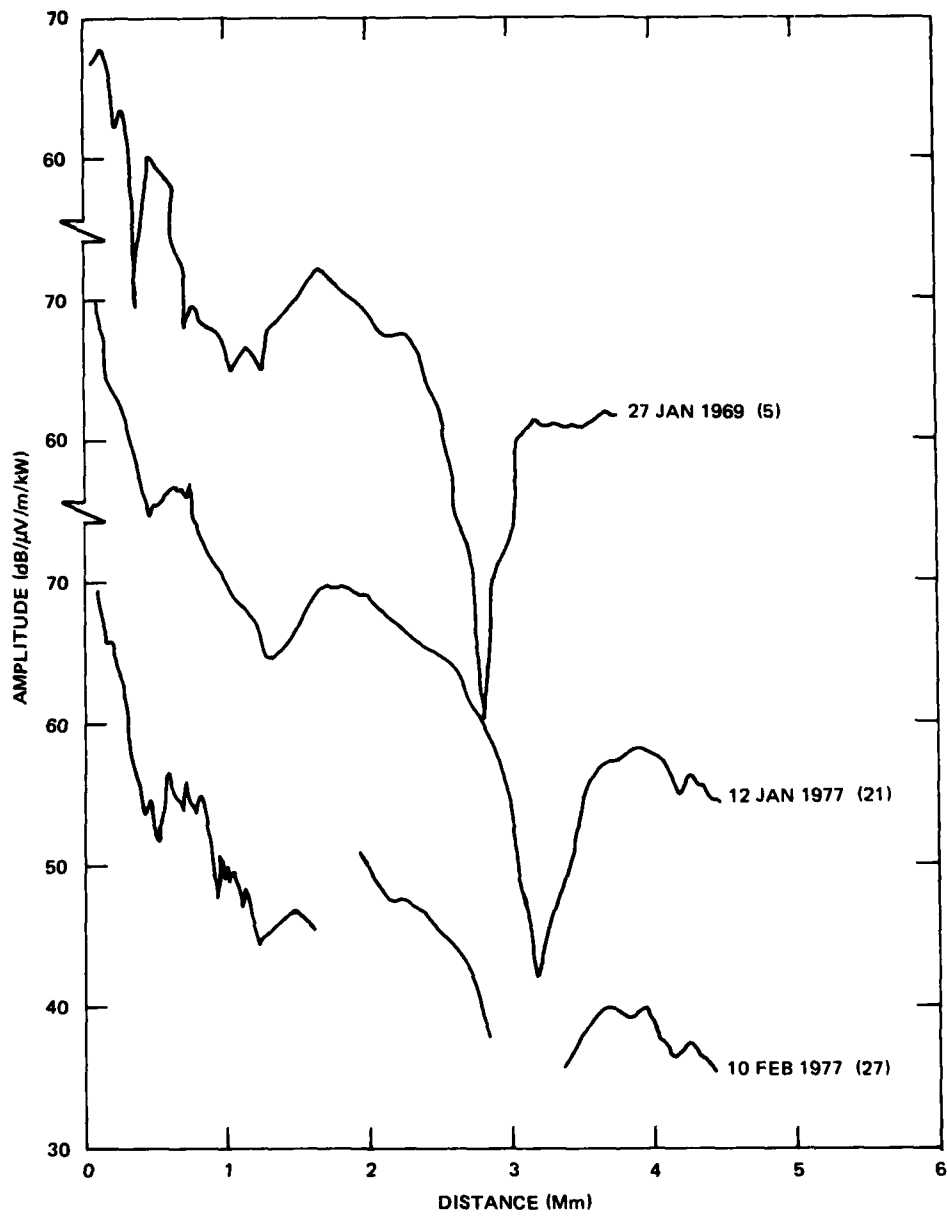
Figure 5. NLK (18.6 kHz) measured while flying between NLK and NPM in 1969 and 1977. Vertical field strength.

33
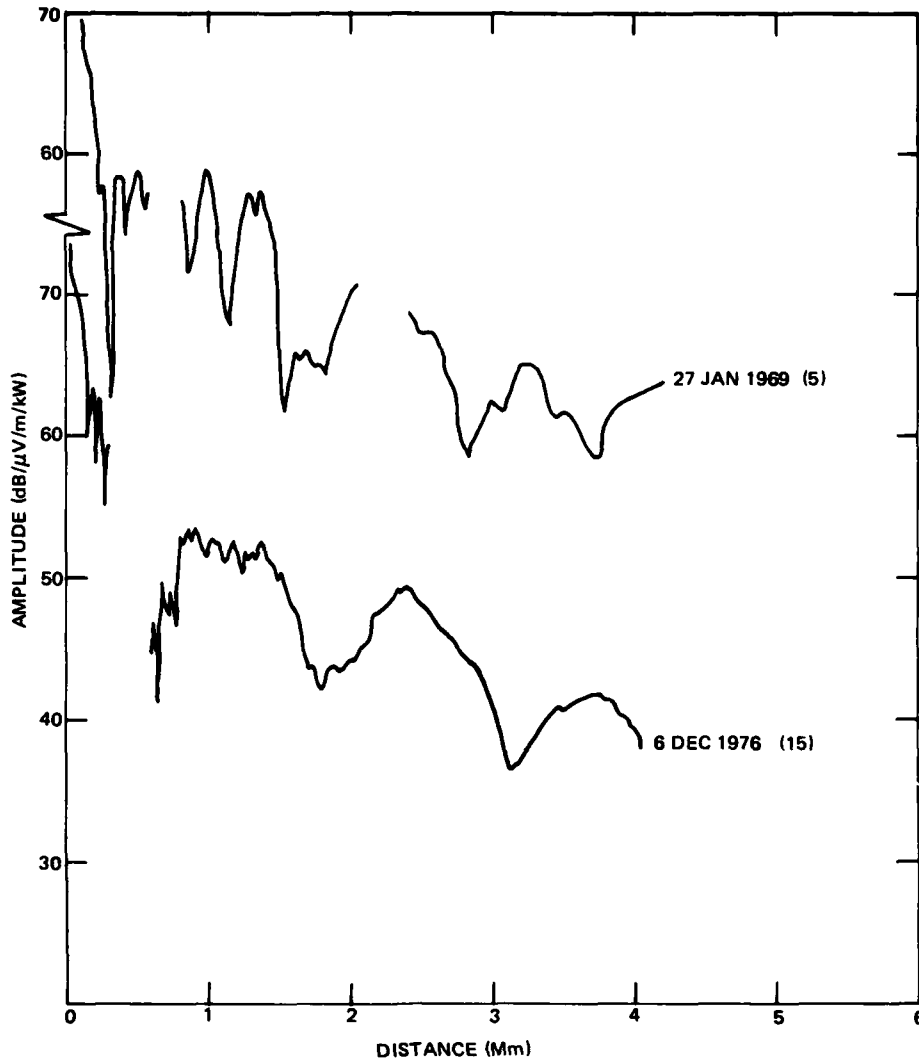
Figure 6. NPM (23.4 kHz) measured while flying between NLK and NPM in 1969 and 1976. Vertical field strength.
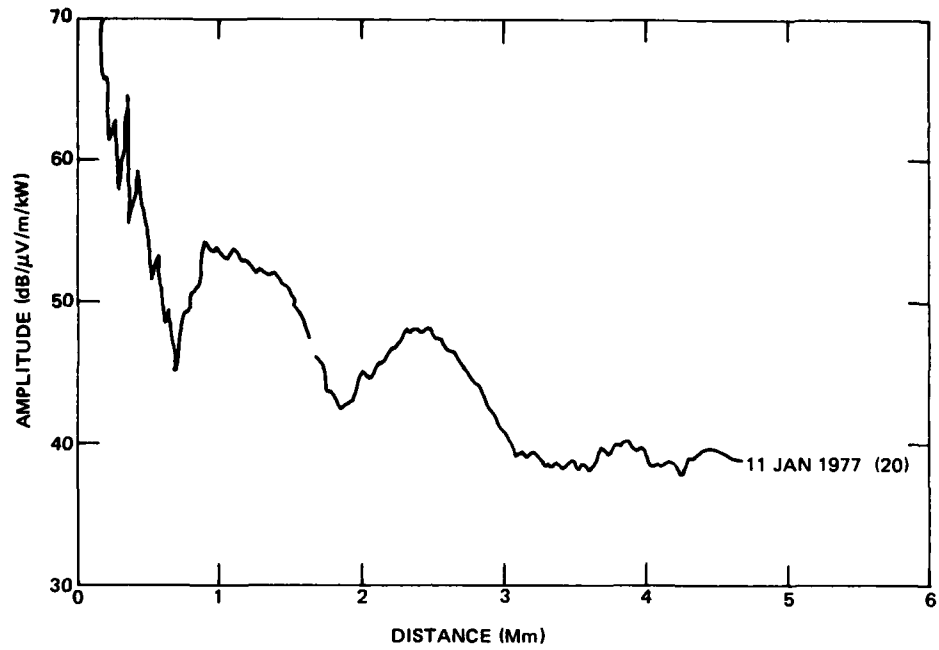
Figure 7. NPM (23.4 kHz) measured while flying between JHZ and NPM in 1977. Vertical field strength.
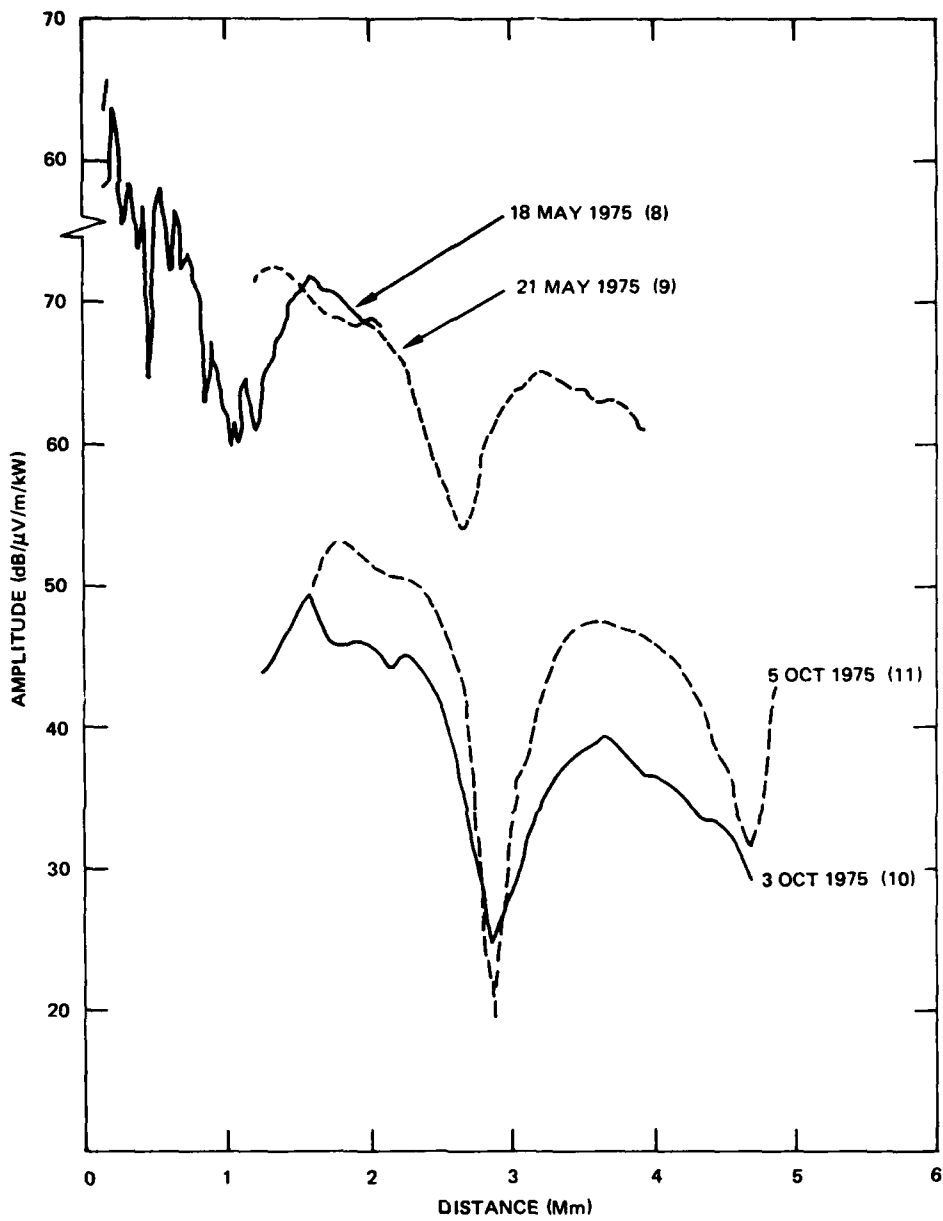
Figure 8. NAA (17.8 kHz) measured while flying across the Atlantic in 1975. Vertical field strength.
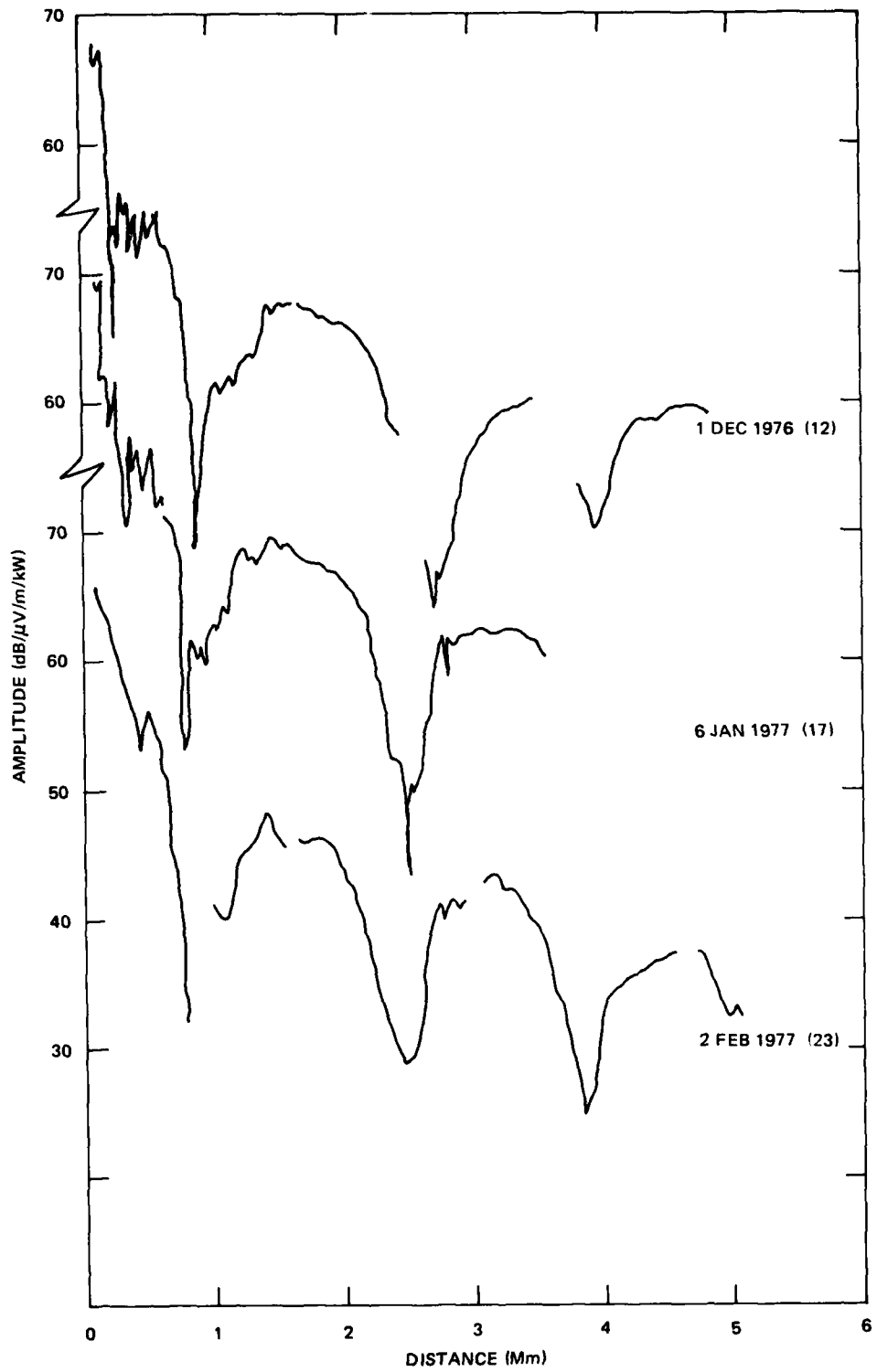
Figure 9. NAA (17.8 kHz) measured while flying across the Atlantic in 1976 and 1977. Vertical field strength.
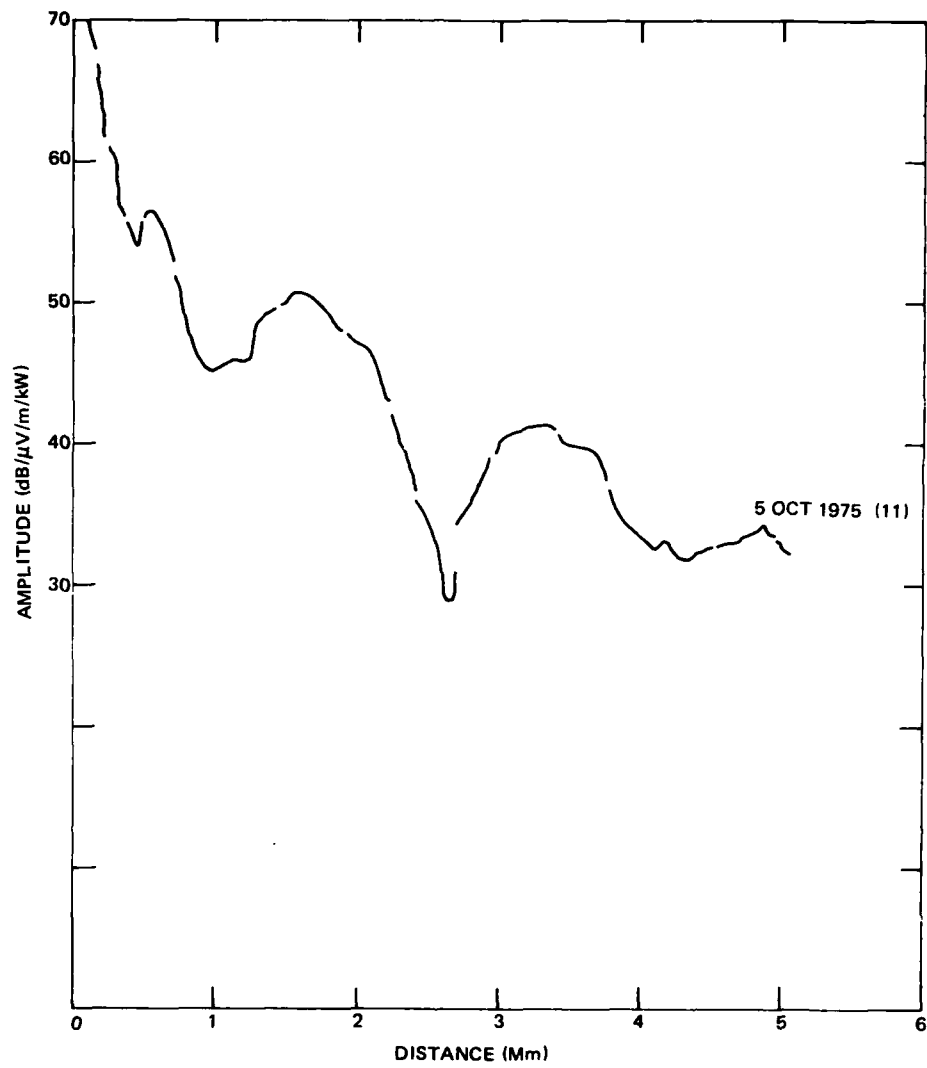
Figure 10. GBR (16.0 kHz) measured while flying across the Atlantic in 1975. Vertical field strength.
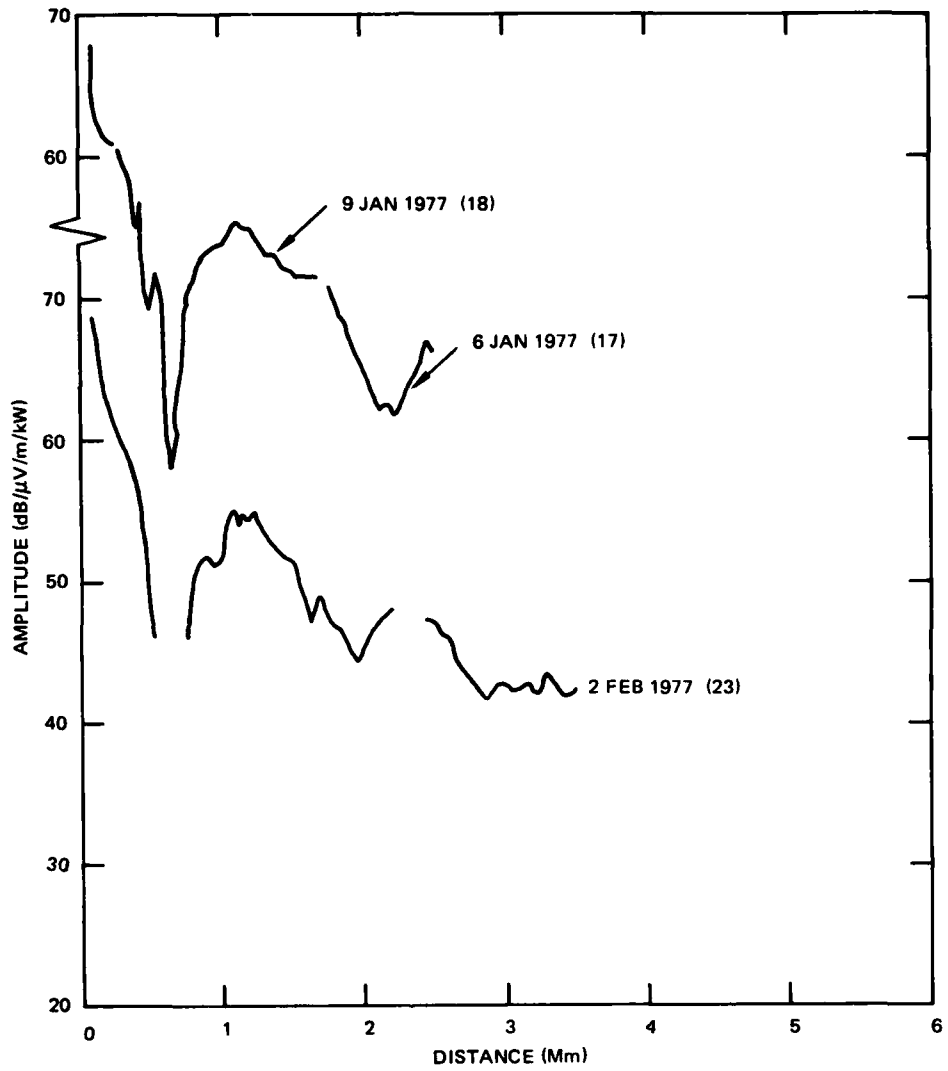
Figure 11. JHZ (16.4 kHz) measured while flying across the Atlantic in 1977. Vertical field strength.
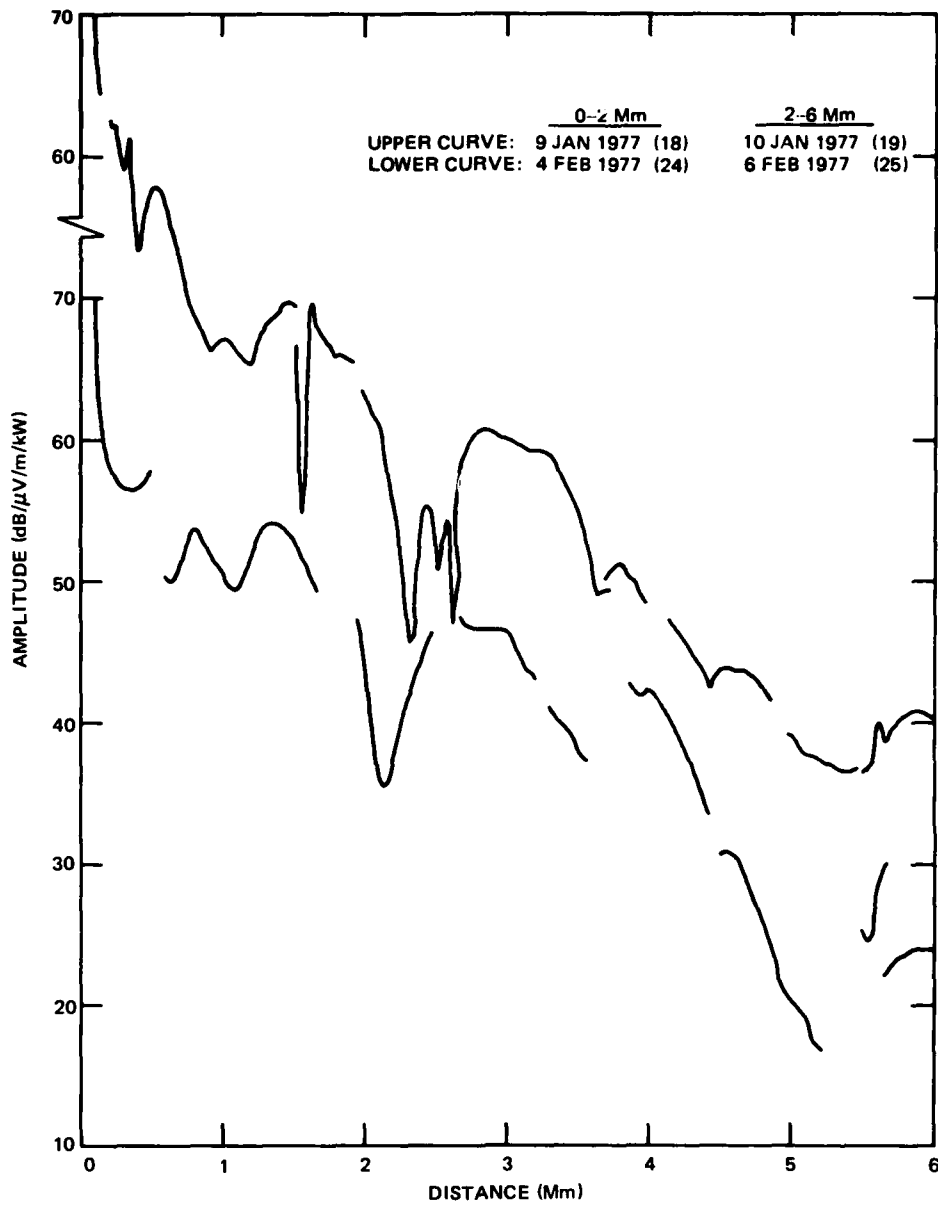
Figure 12. GBR (16.0 kHz) measured while flying toward the pole in 1977. Vertical field strength.
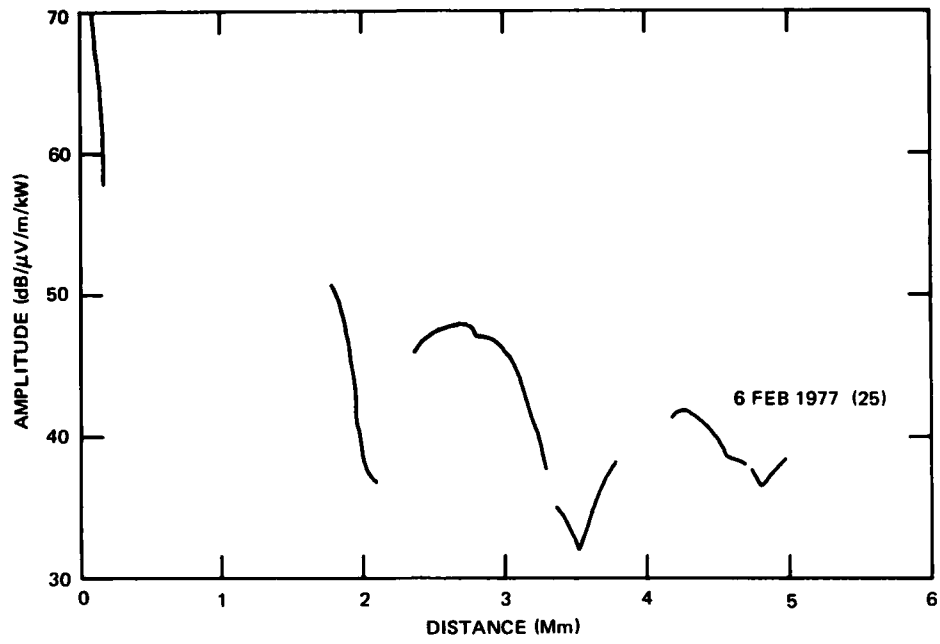
Figure 13. JHZ (16.4 kHz) measured while flying toward the pole in 1977. Vertical field strength.
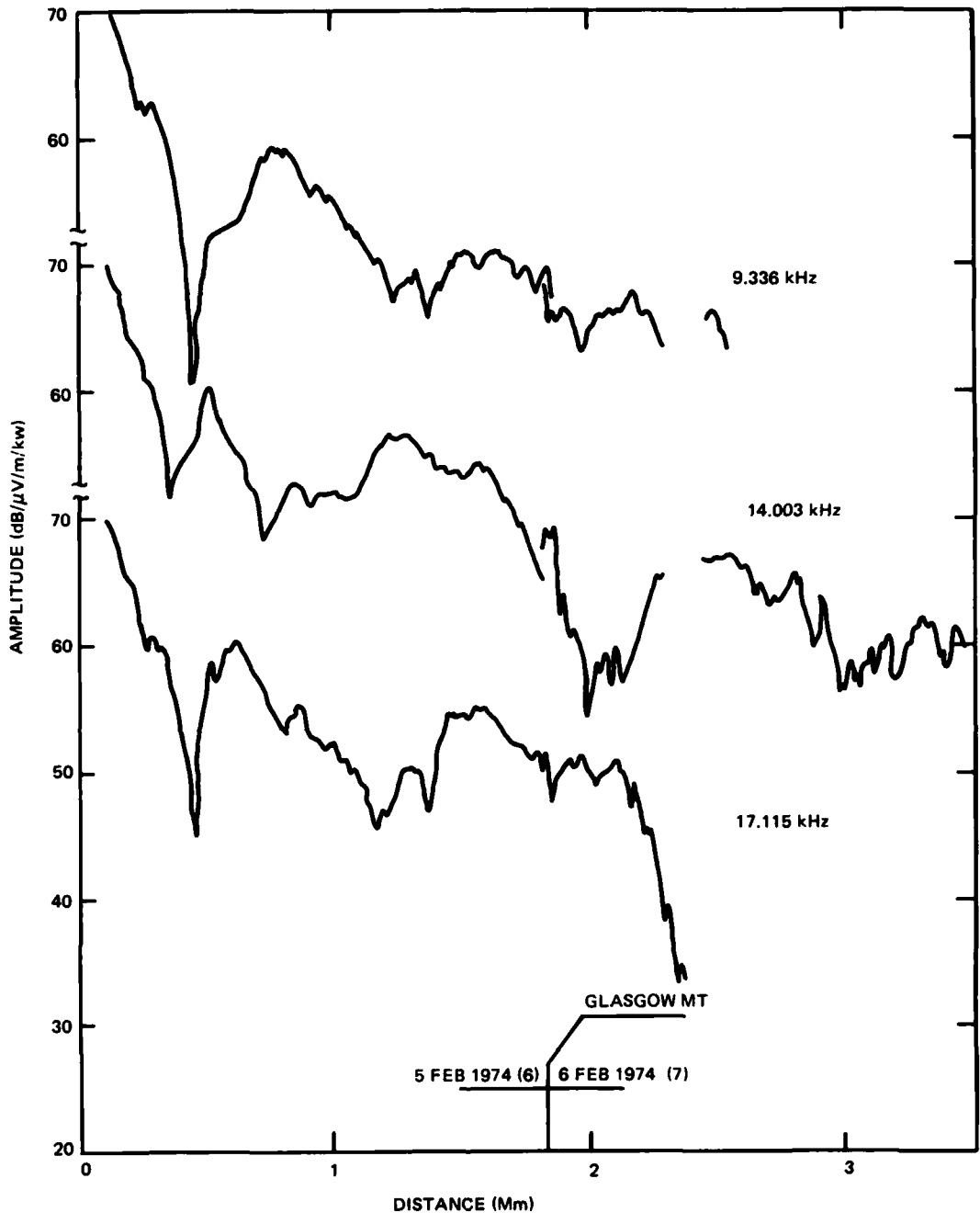
Figure 14a. Sounder data measured while flying between Sentinel and Thule, Greenland, in 1974. Vertical field strength.
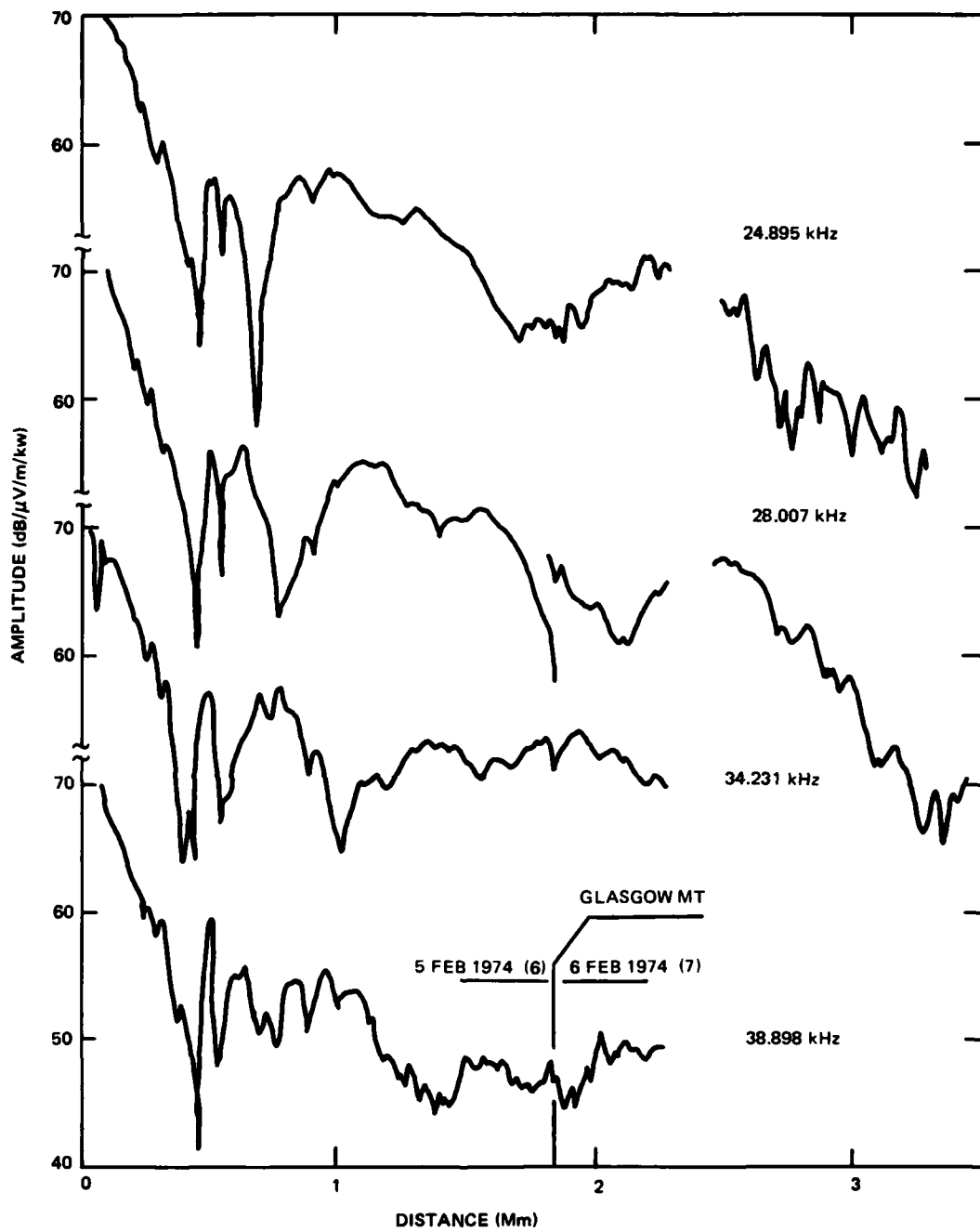
Figure 14b. Sounder data measured while flying between Sentinel and Thule, Greenland, in 1974. Vertical field strength.

43
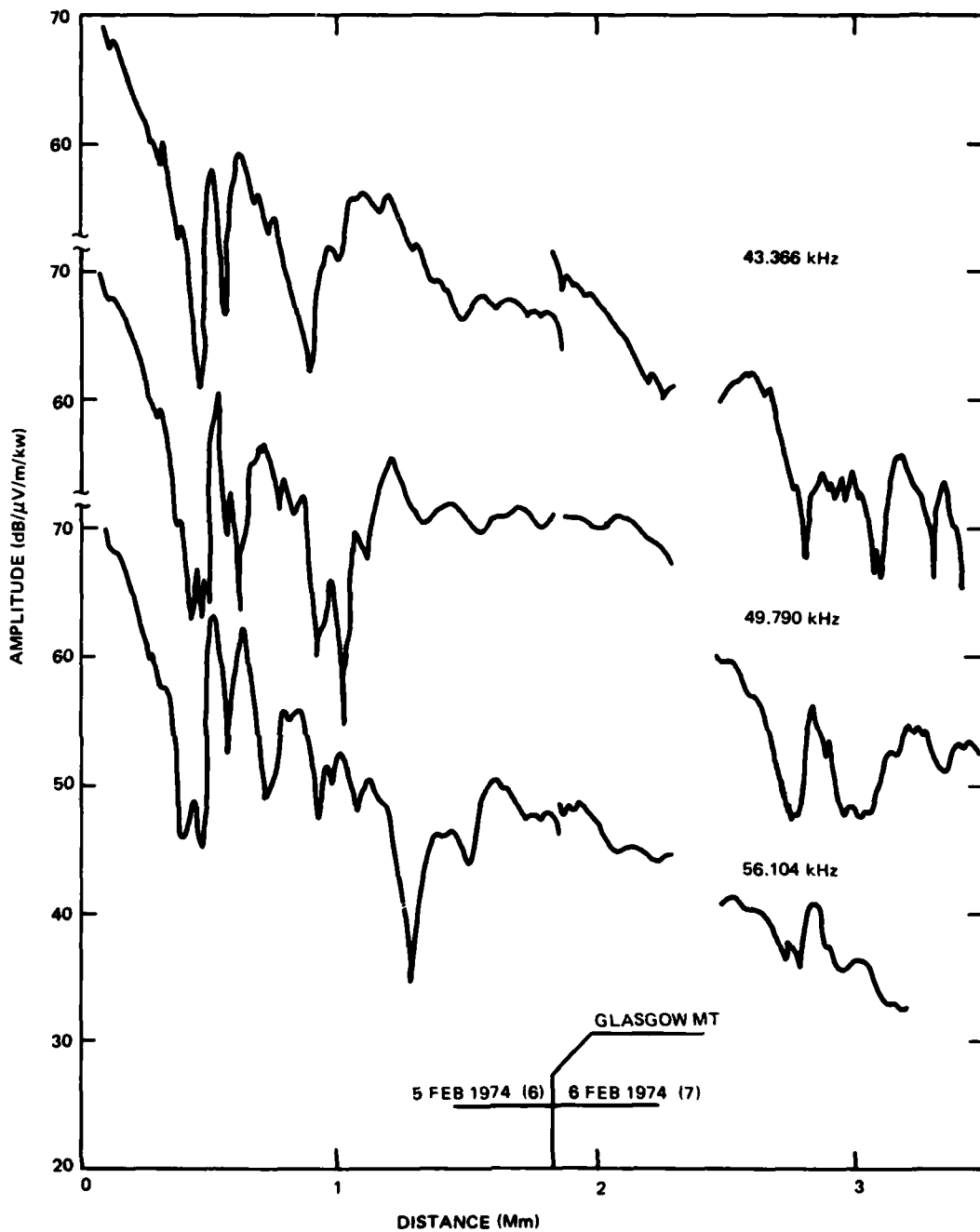
Figure 14c. Sounder data measured while flying between Sentinel and Thule, Greenland, in 1974. Vertical field strength.
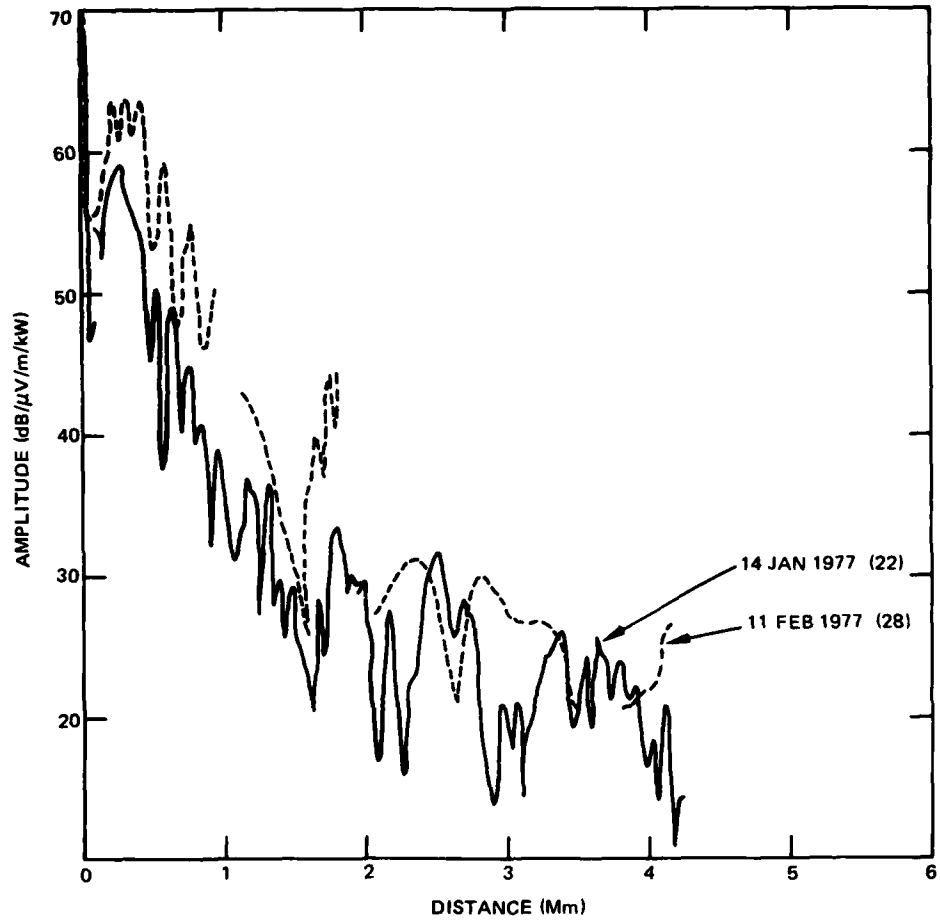
Figure 15. NLK (18.6 kHz) measured while flying between NLK and NAA in 1977. Horizontal field strength.
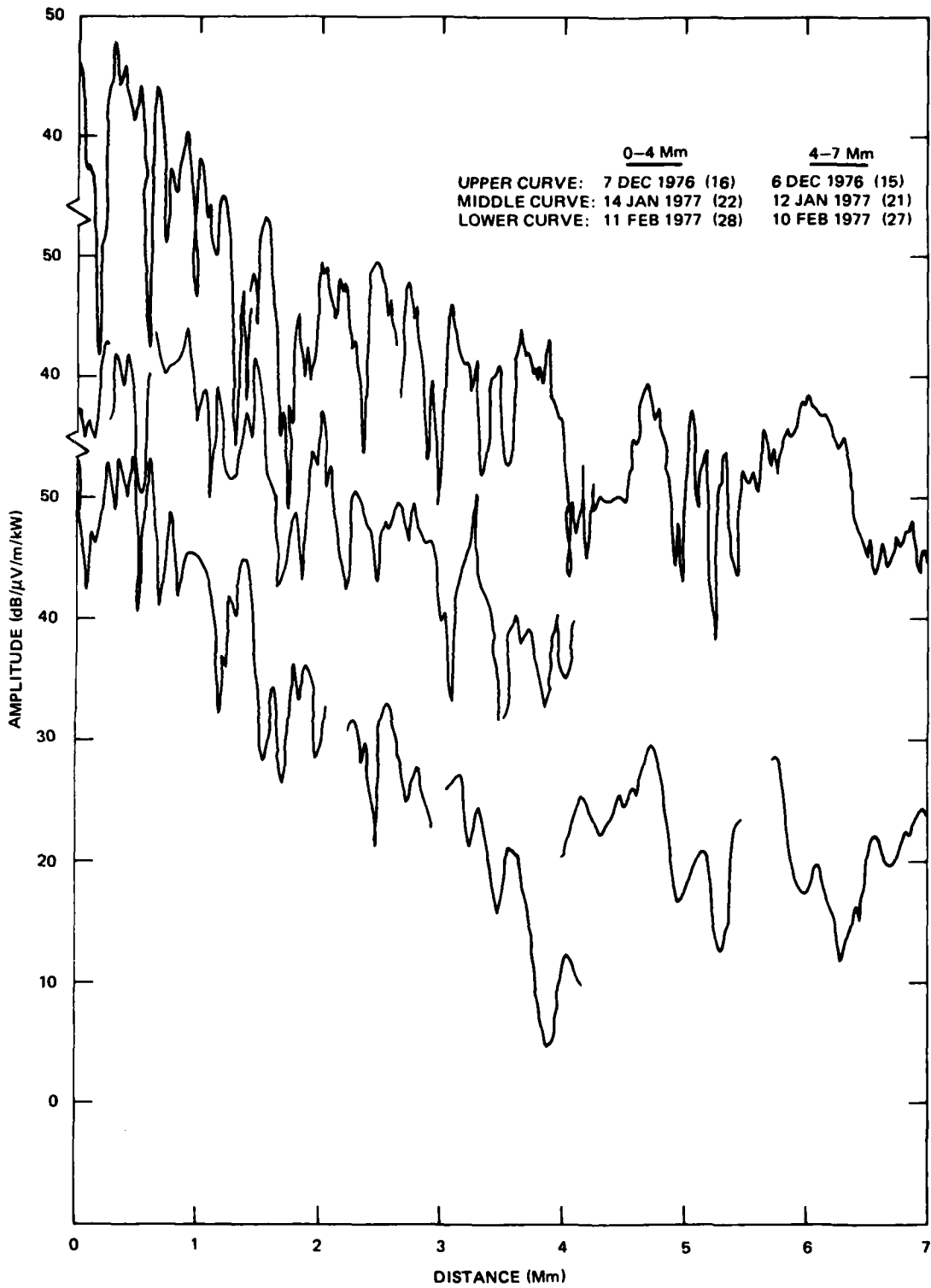
Figure 16. NAA (17.8 kHz) measured while flying from NPM to NLK to NAA in 1976 and 1977. Horizontal field strength.

46
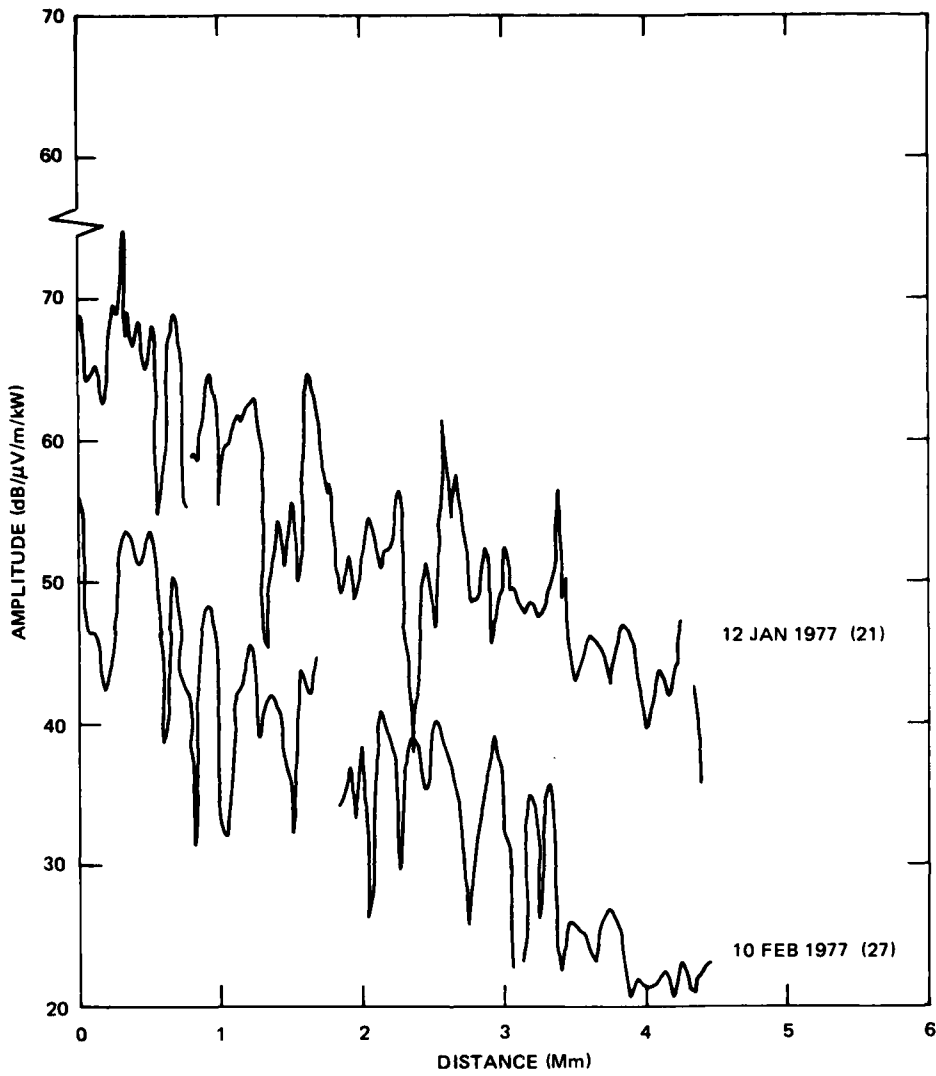
Figure 17. NLK (18.6 kHz) measured while flying between NLK and NPM in 1977.
Horizontal field strength.
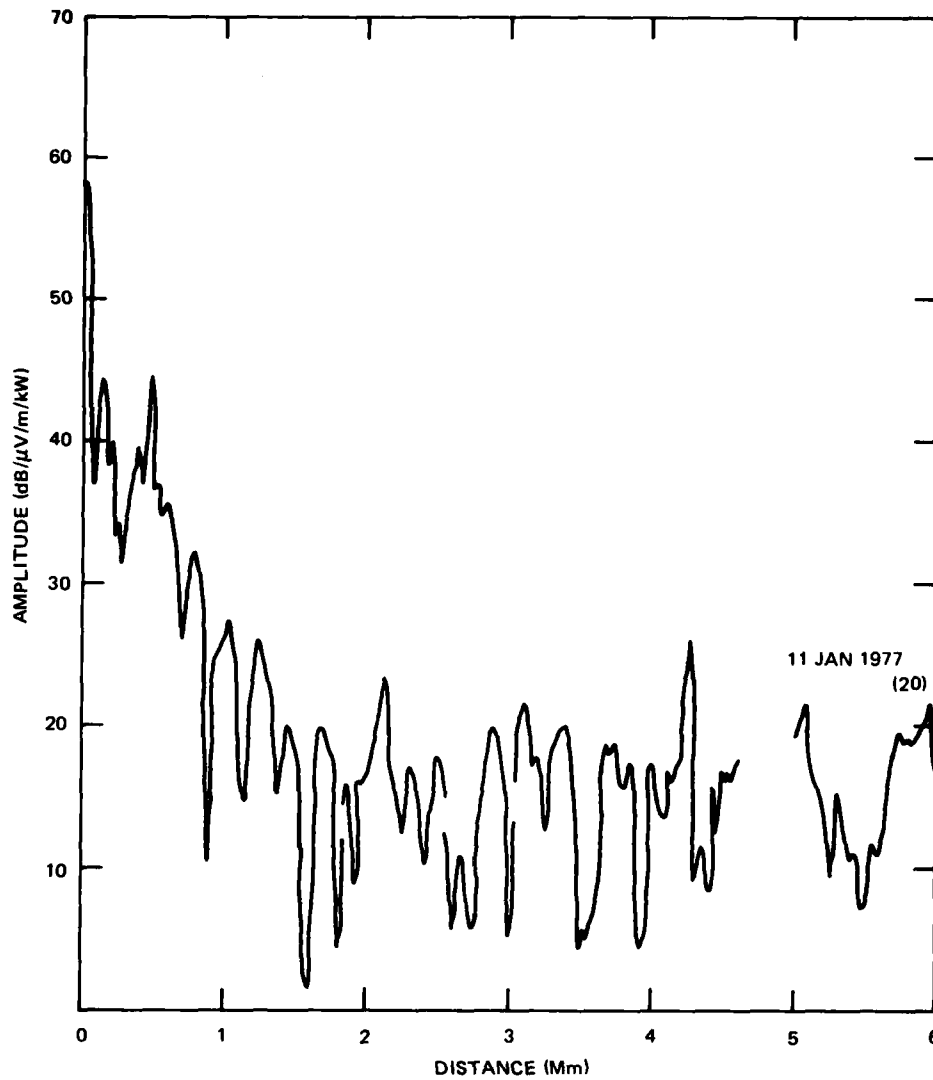
Figure 18. NPM (23.4 kHz) measured while flying between JHZ and NPM.
Horizontal field strength.

48
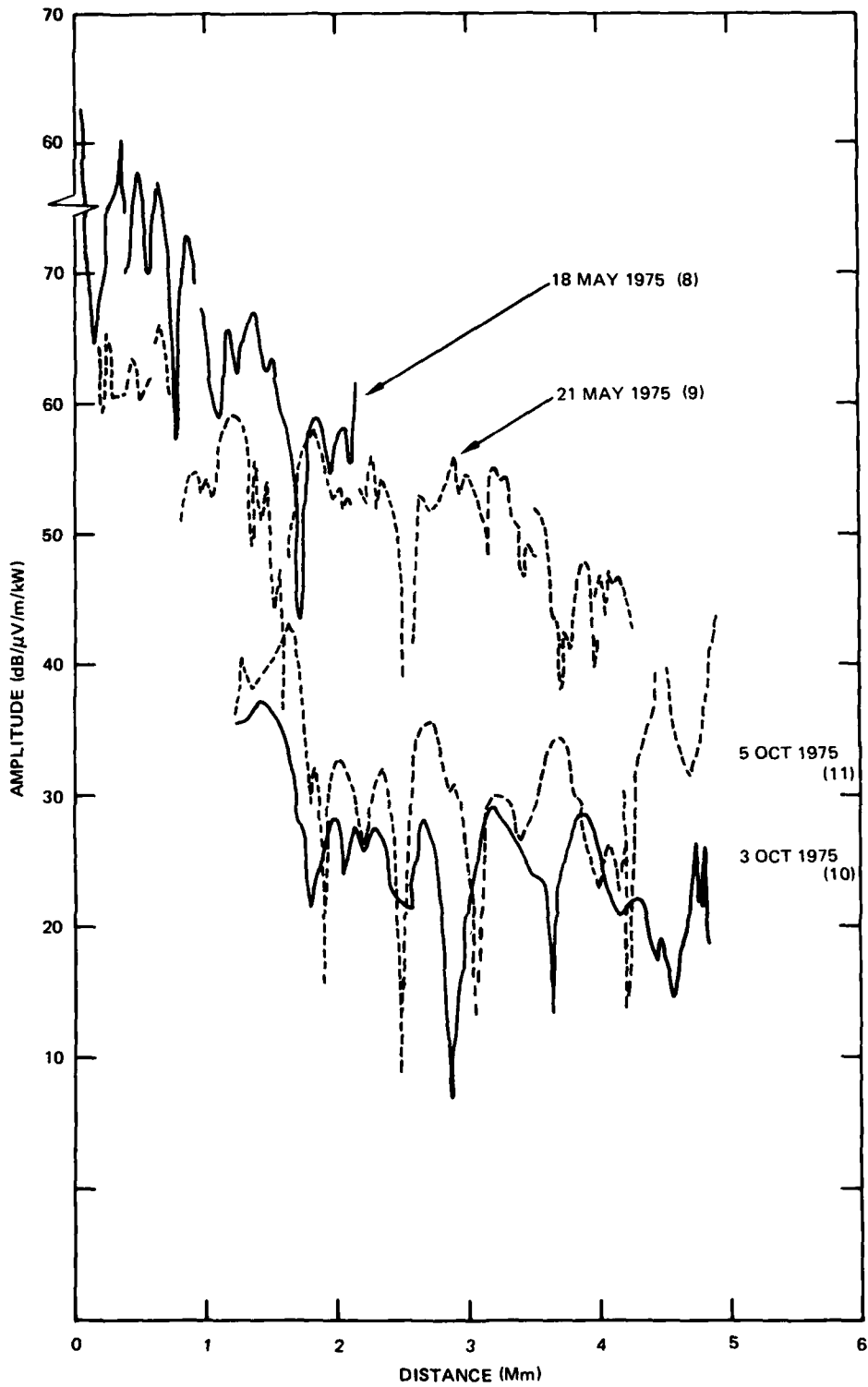
Figure 19. NAA (17.8 kHz) measured while flying across the Atlantic in 1975. Horizontal field strength.

49
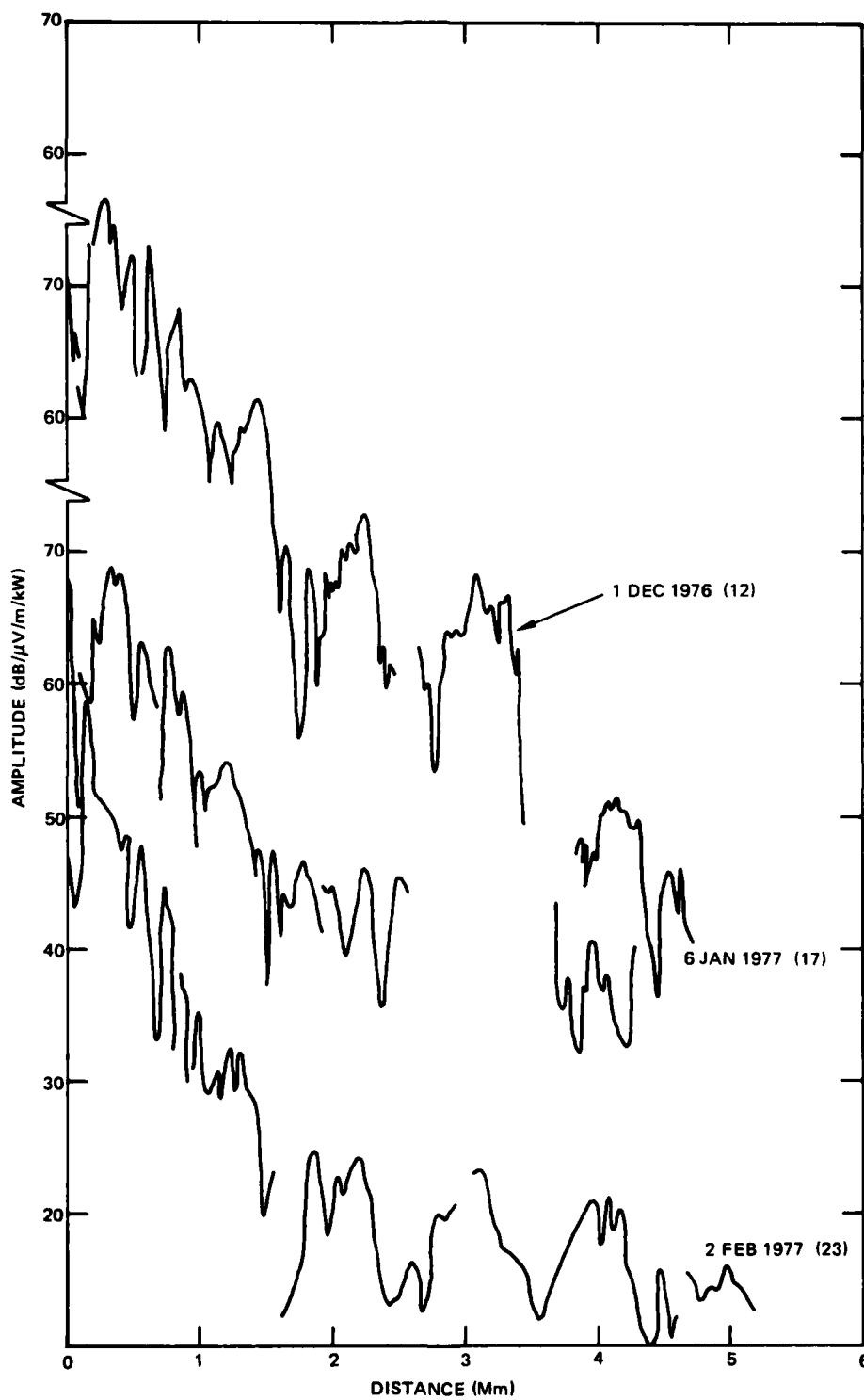
Figure 20. NAA (17.8 kHz) measured while flying across the Atlantic in 1976 and 1977. Horizontal field strength.
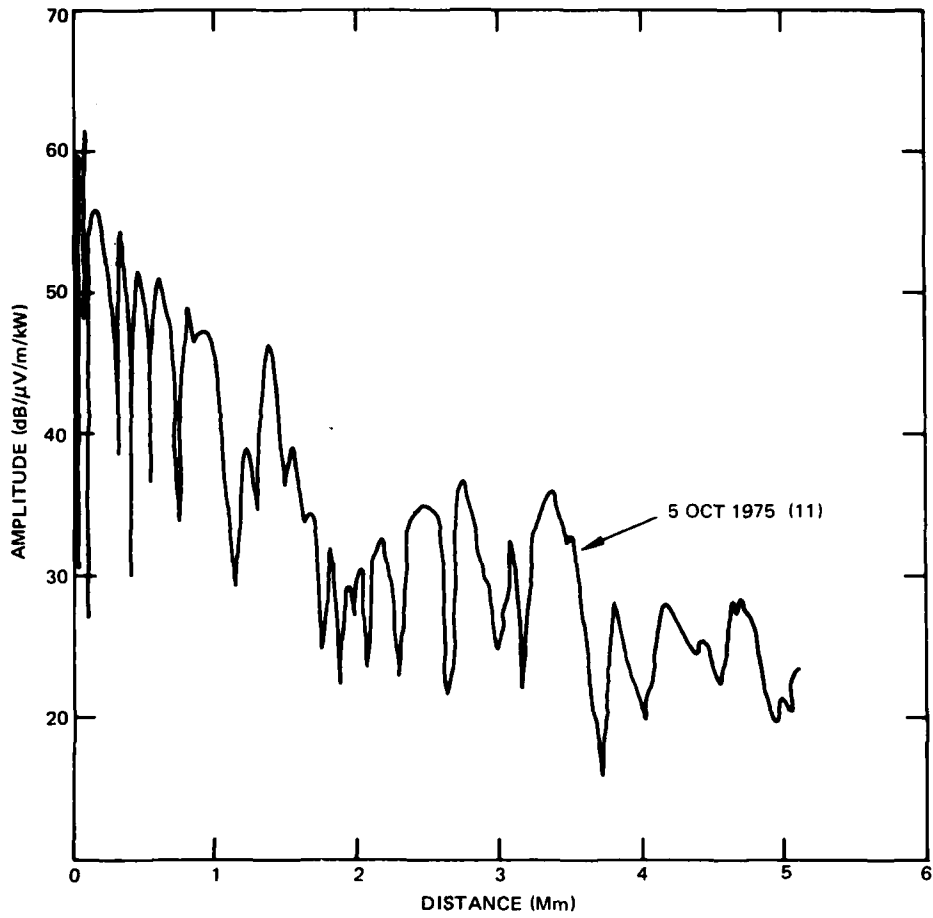
Figure 21. GBR (16.0 kHz) measured while flying across the Atlantic in 1975.
Horizontal field strength.

51
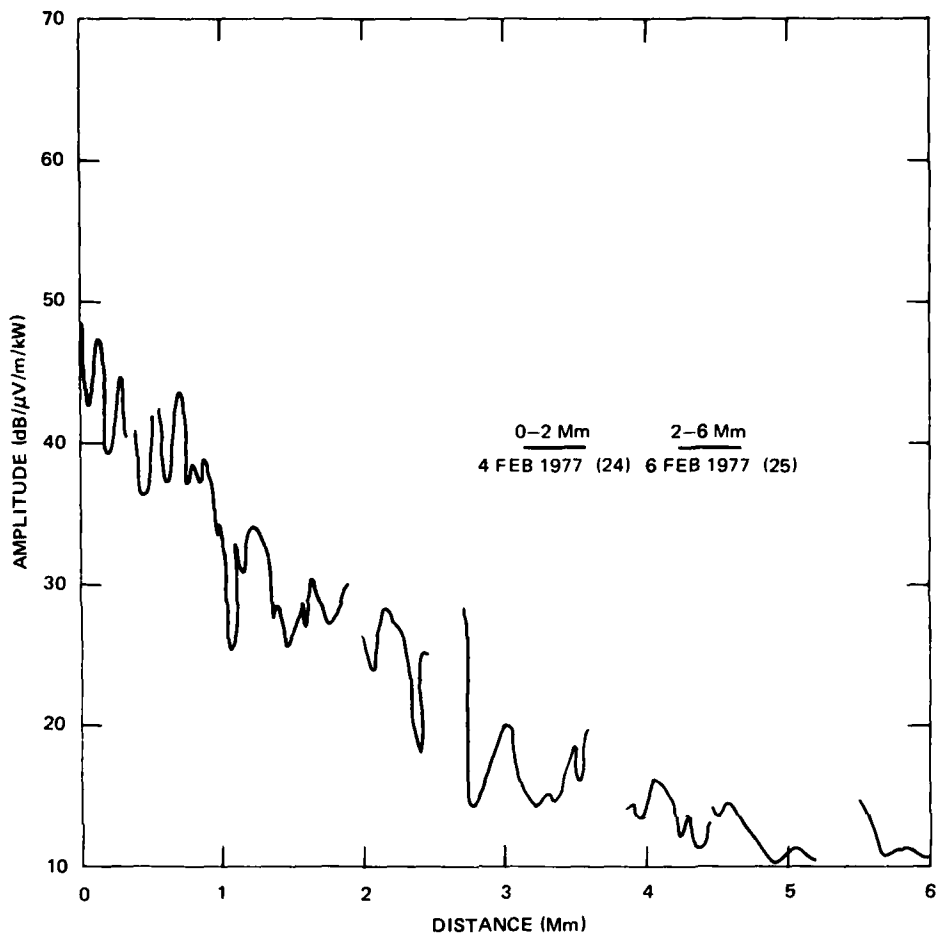
Figure 22. GBR (16.0 kHz) measured while flying toward the pole in 1977.
Horizontal field strength.
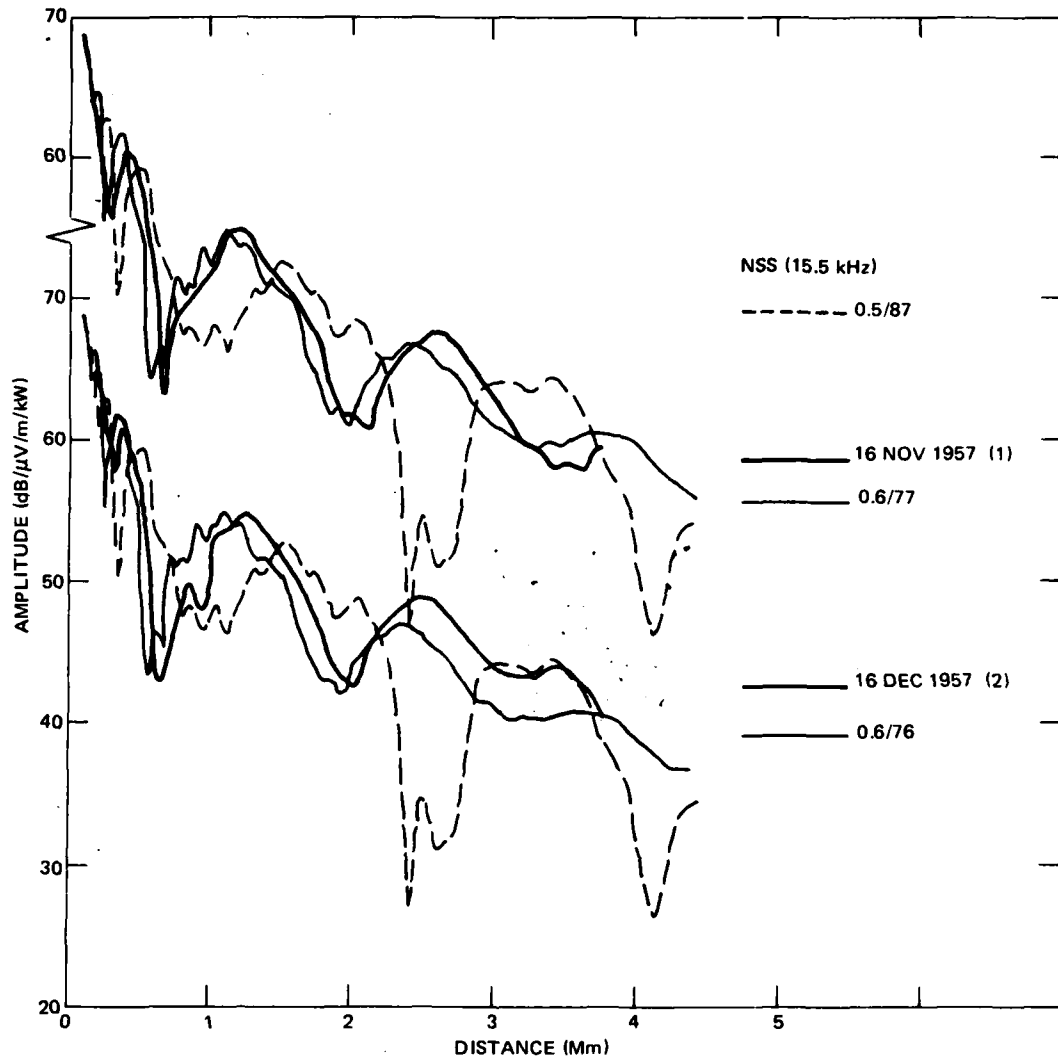
Figure 23. Best fit to measurements: NSS toward NLK, 1957.
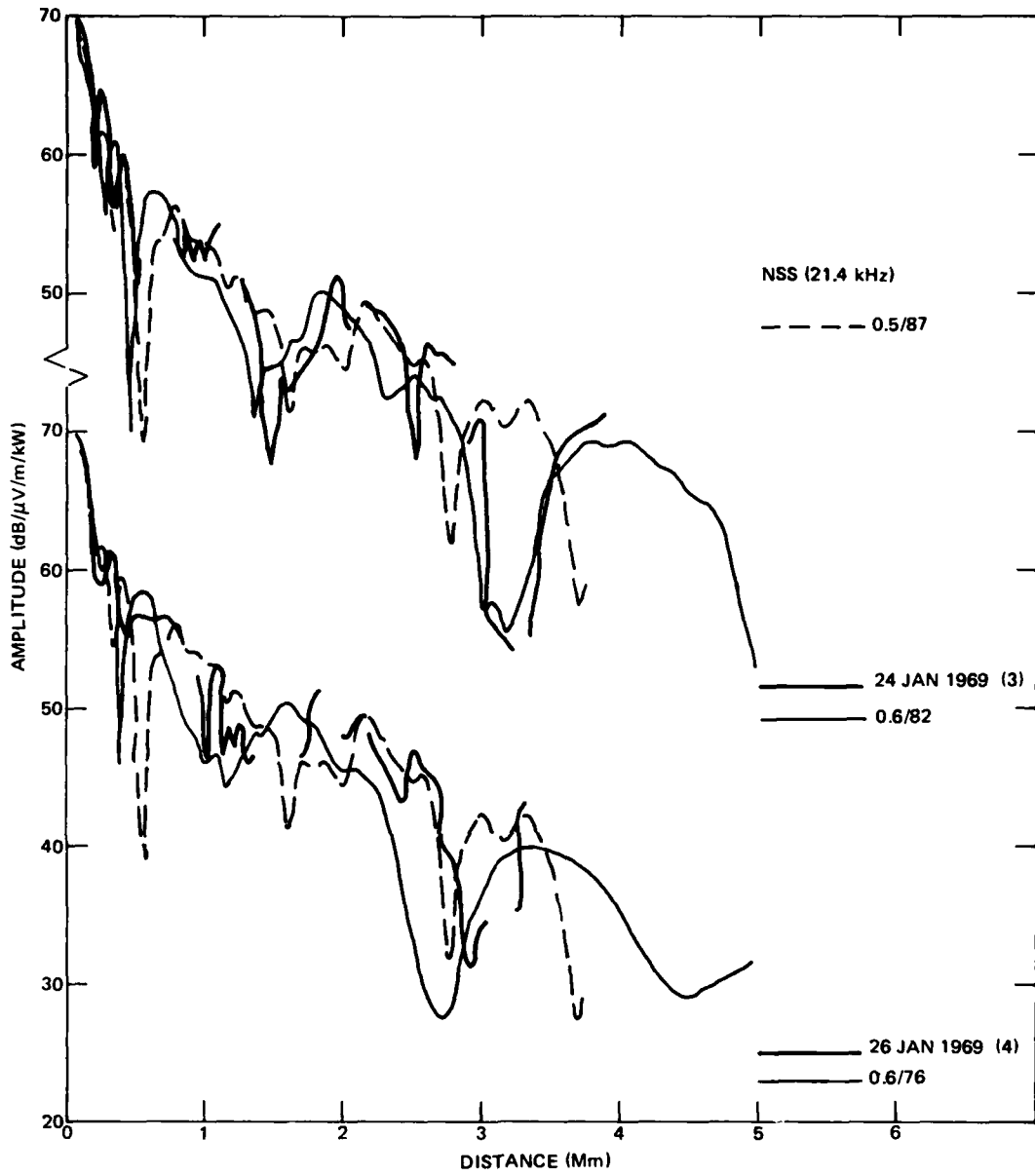
Figure 24. Best fit to measurements: NSS toward NLK, 1969.
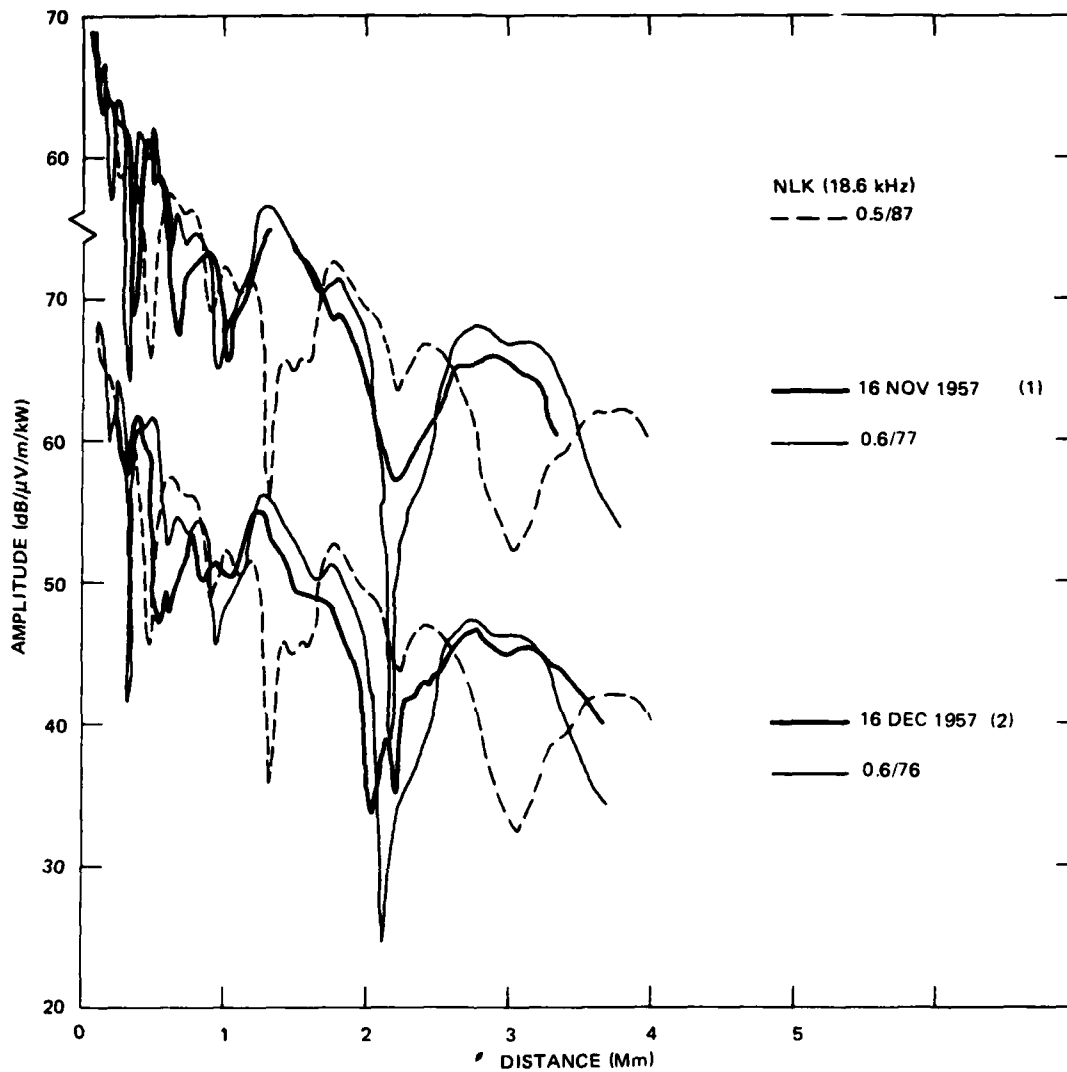
Figure 25. Best fit to measurements: NLK toward NSS, 1957.
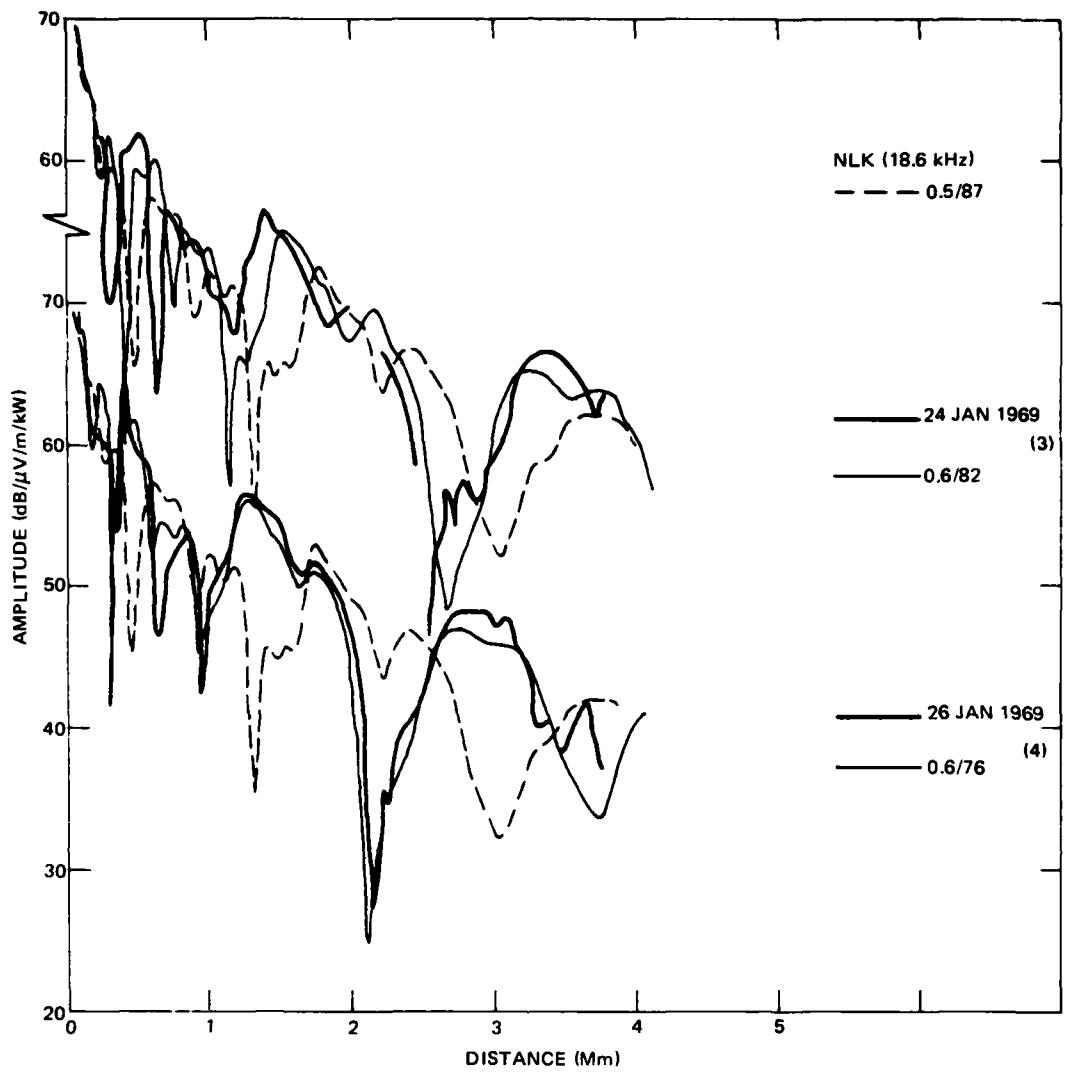
Figure 26. Best fit to measurements: NLK toward NSS, 1969.
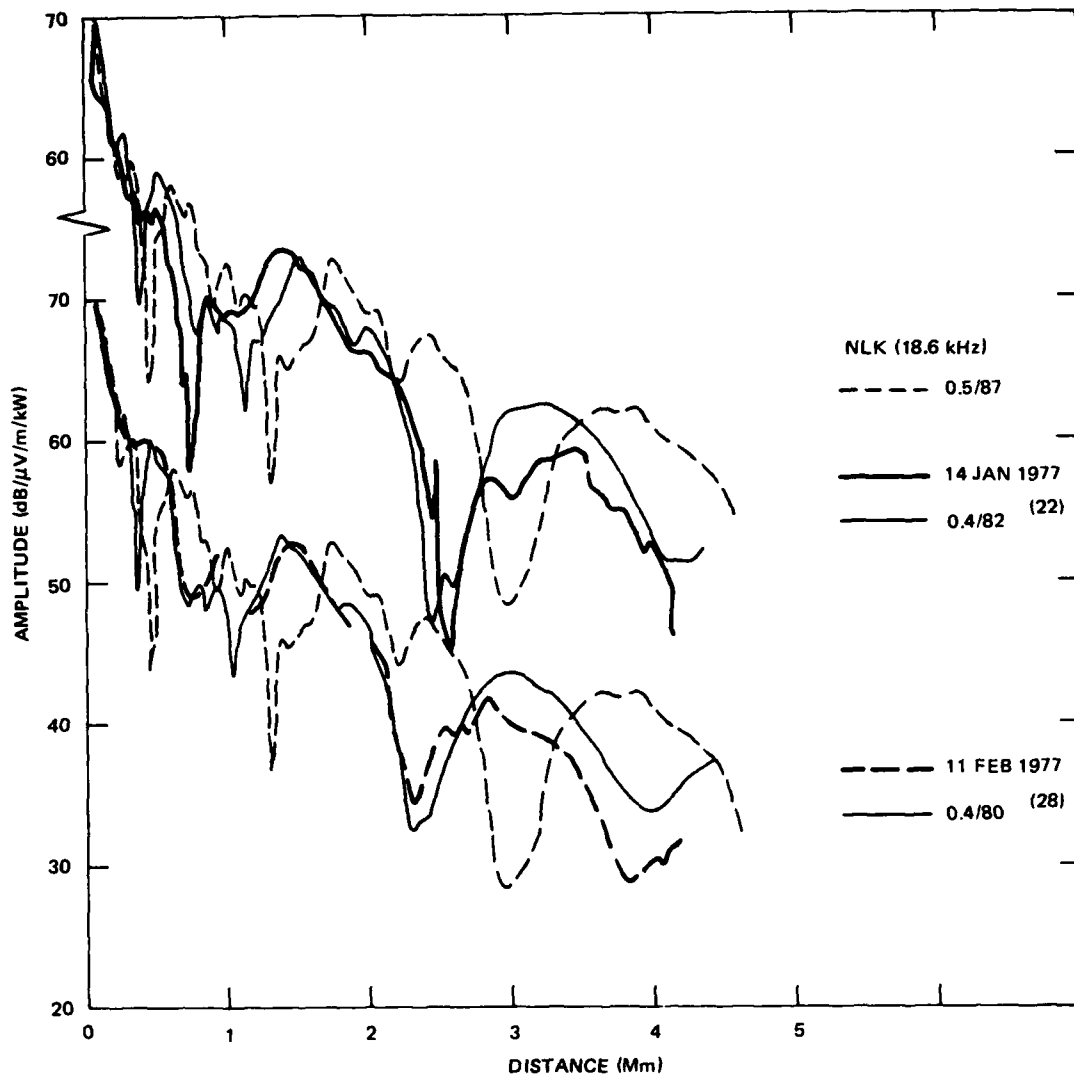
Figure 27. Best fit to measurements: NLK toward NAA, 1977.
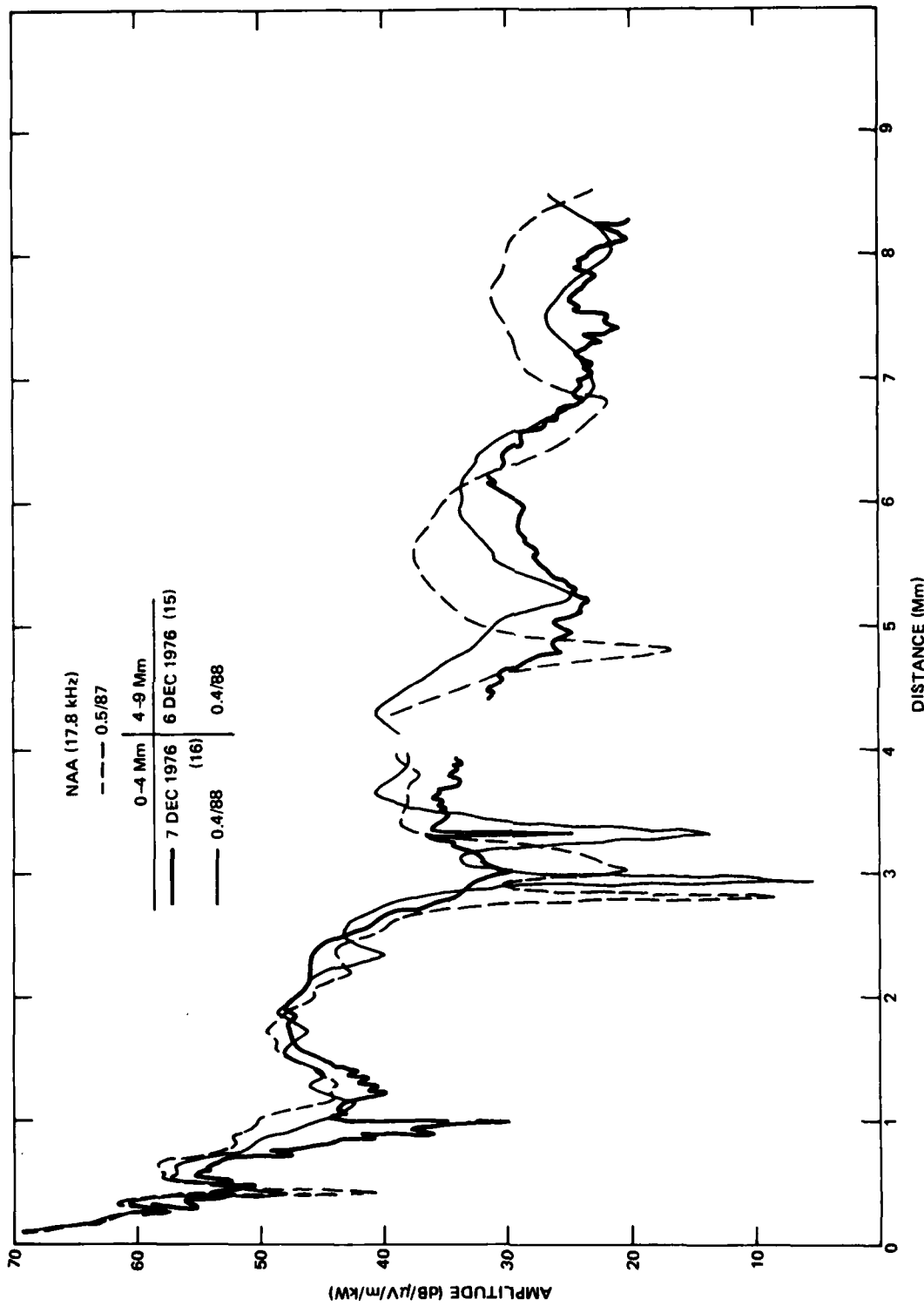
Figure 28a. Best fit to measurements: NAA toward NPM, 1976, 1977.
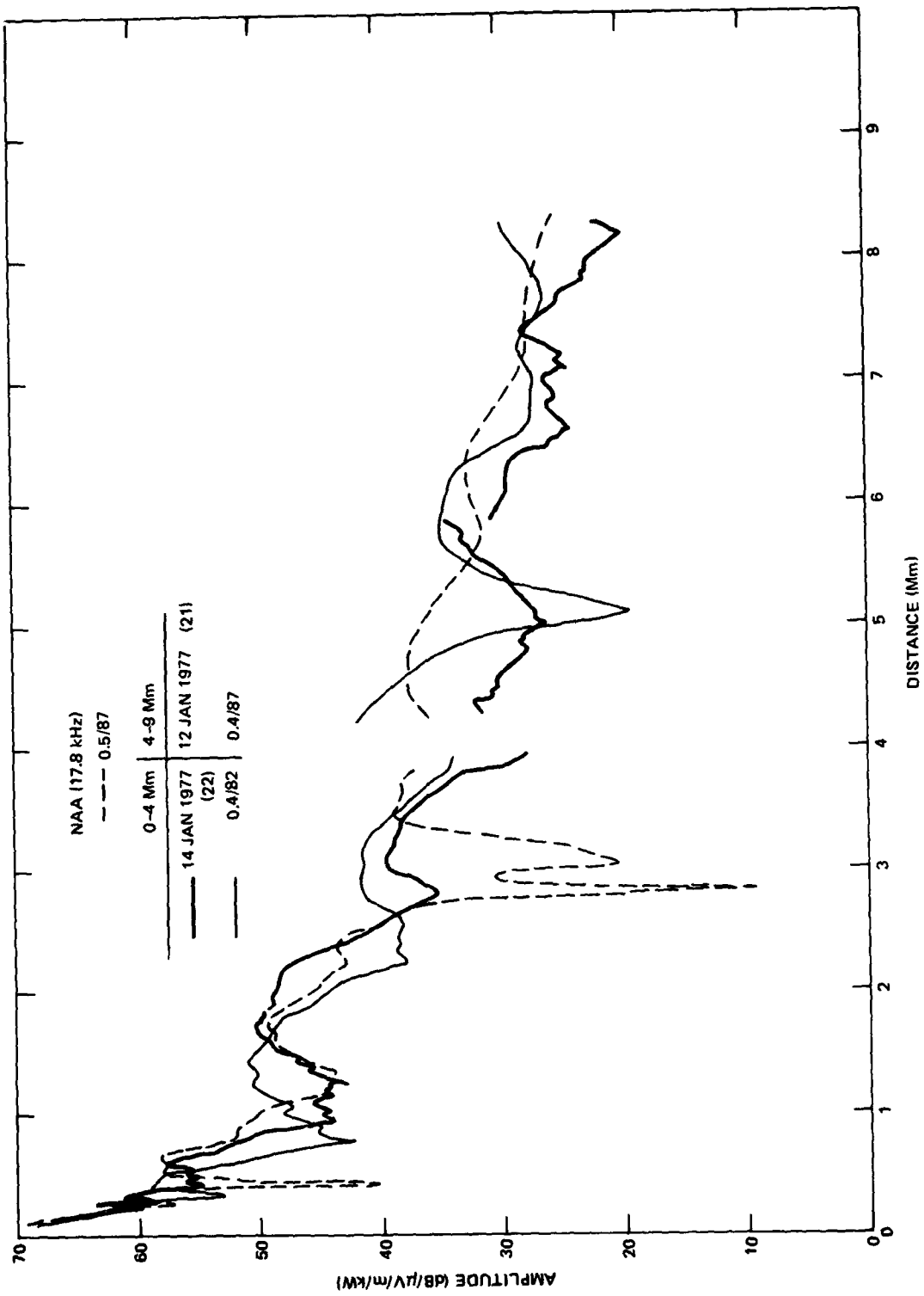
Figure 28b. Best fit to measurements: NAA toward NPM, 1976, 1977.

59
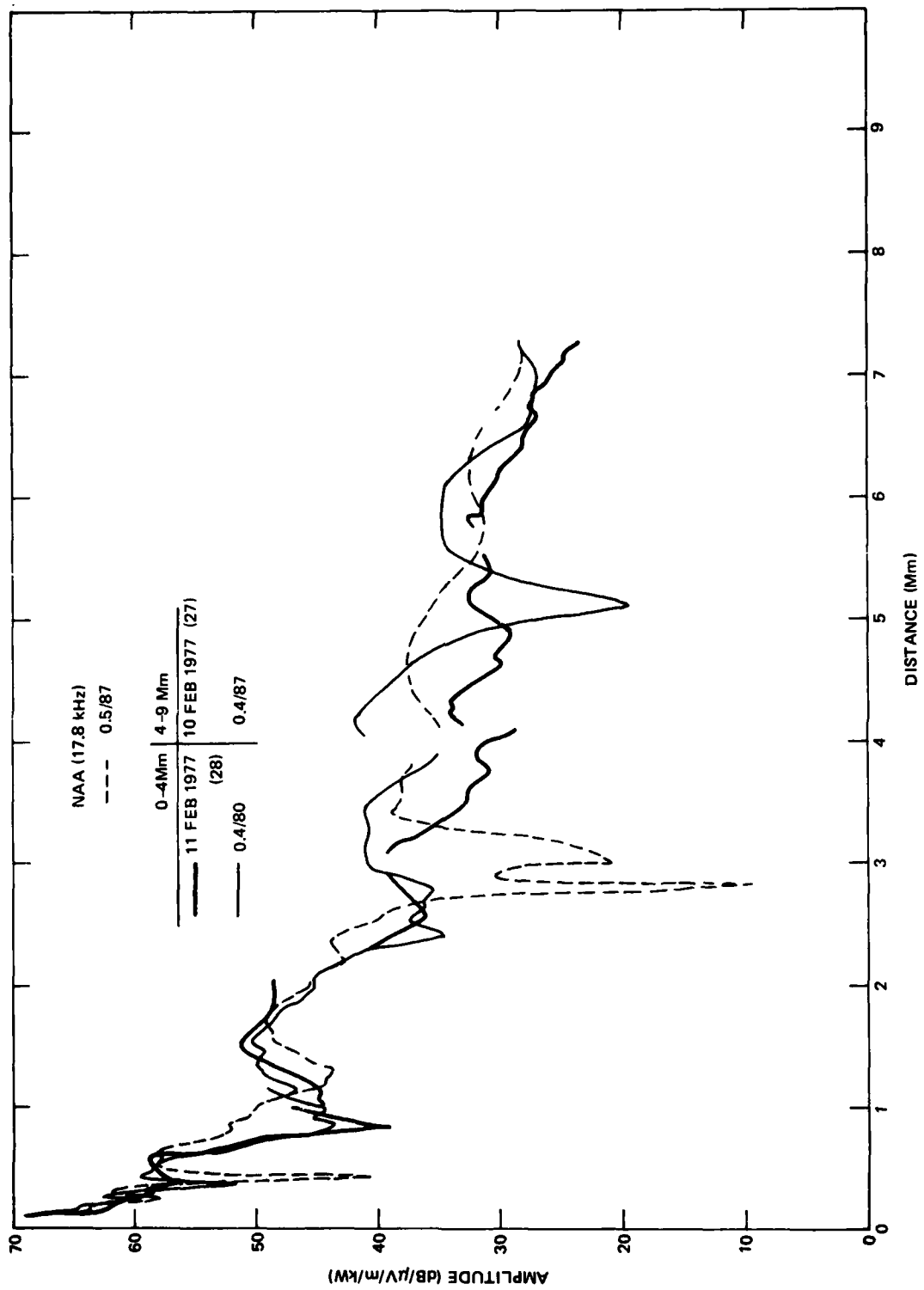
Figure 28c. Best fit to measurements: NAA toward NPM, 1976, 1977.

60
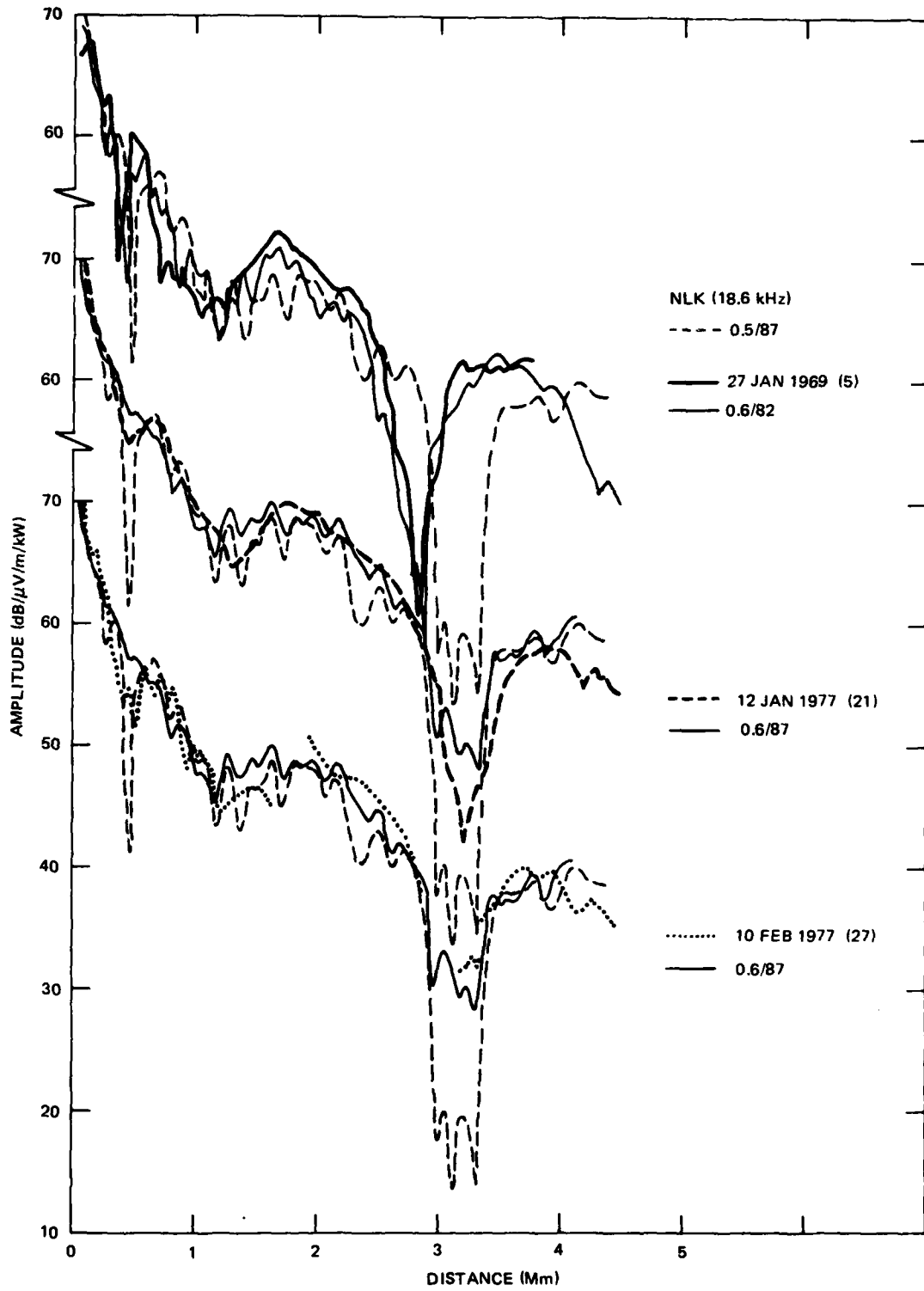
Figure 29. Best fit to measurements: NLK toward NPM, 1969, 1977.
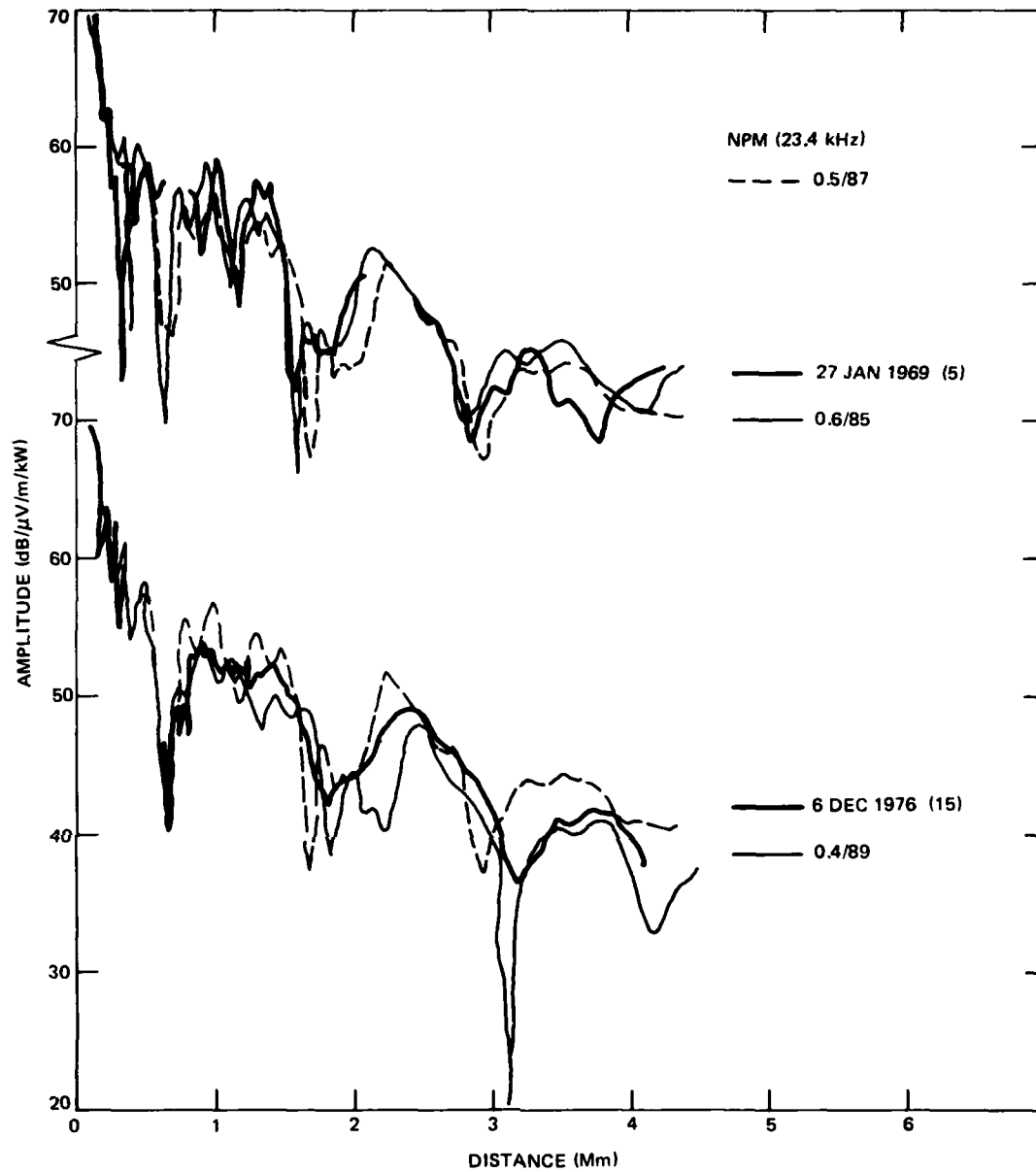
Figure 30. Best fit to measurements: NPM toward NLK, 1969, 1976.
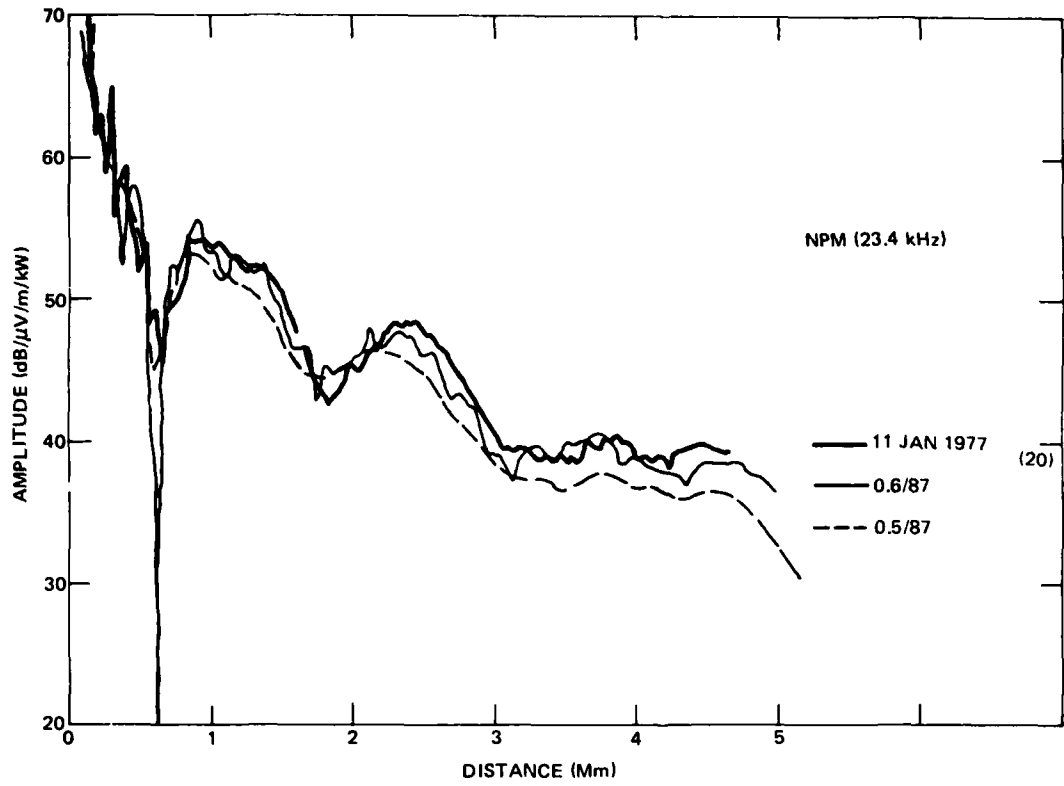
Figure 31. Best fit to measurements: NPM toward the pole, 1977.
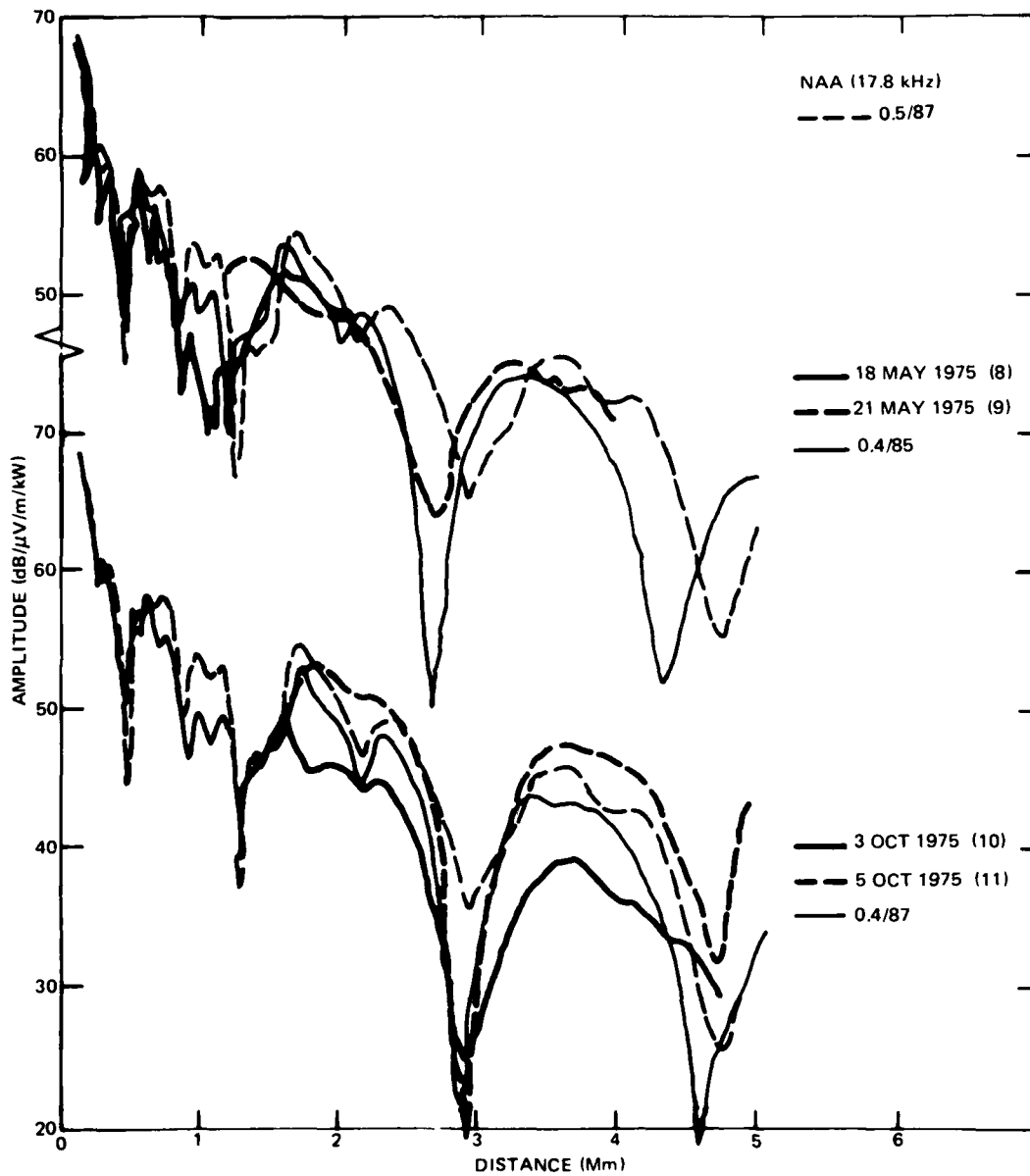
Figure 32. Best fit to measurements: NAA toward GBR, 1975.
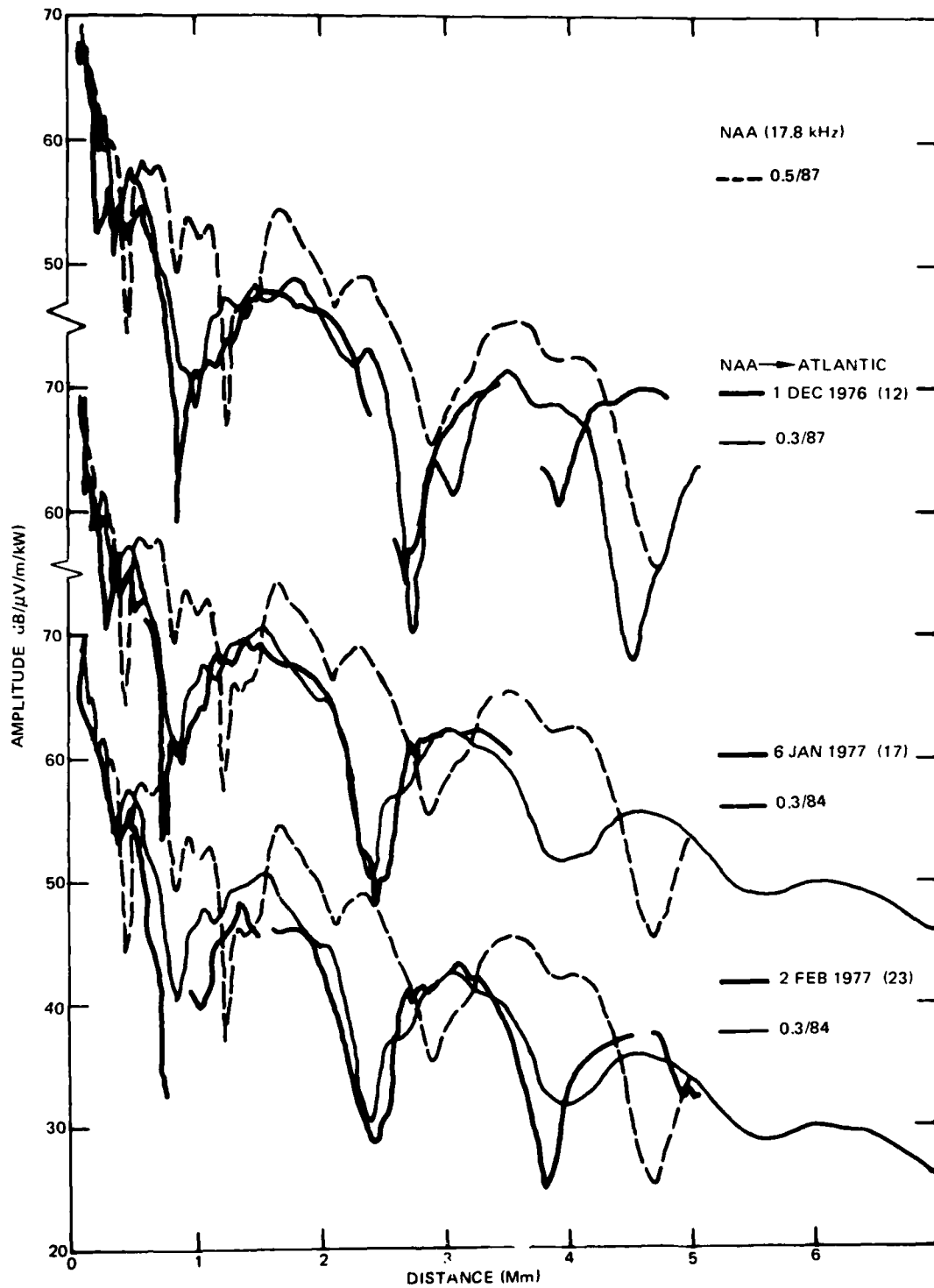
Figure 33. Best fit to measurements: NAA toward JHZ, 1976, 1977.
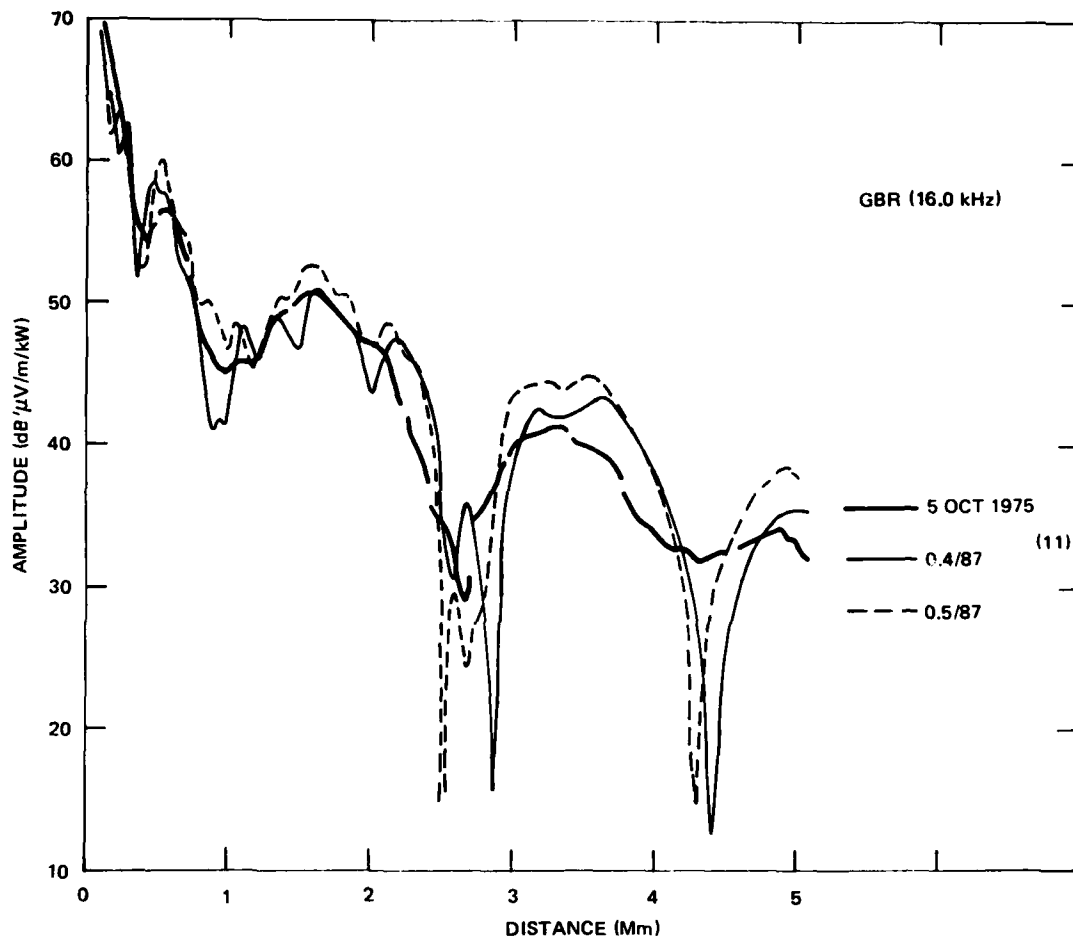
Figure 34. Best fit to measurements: GBR toward NAA, 1975.
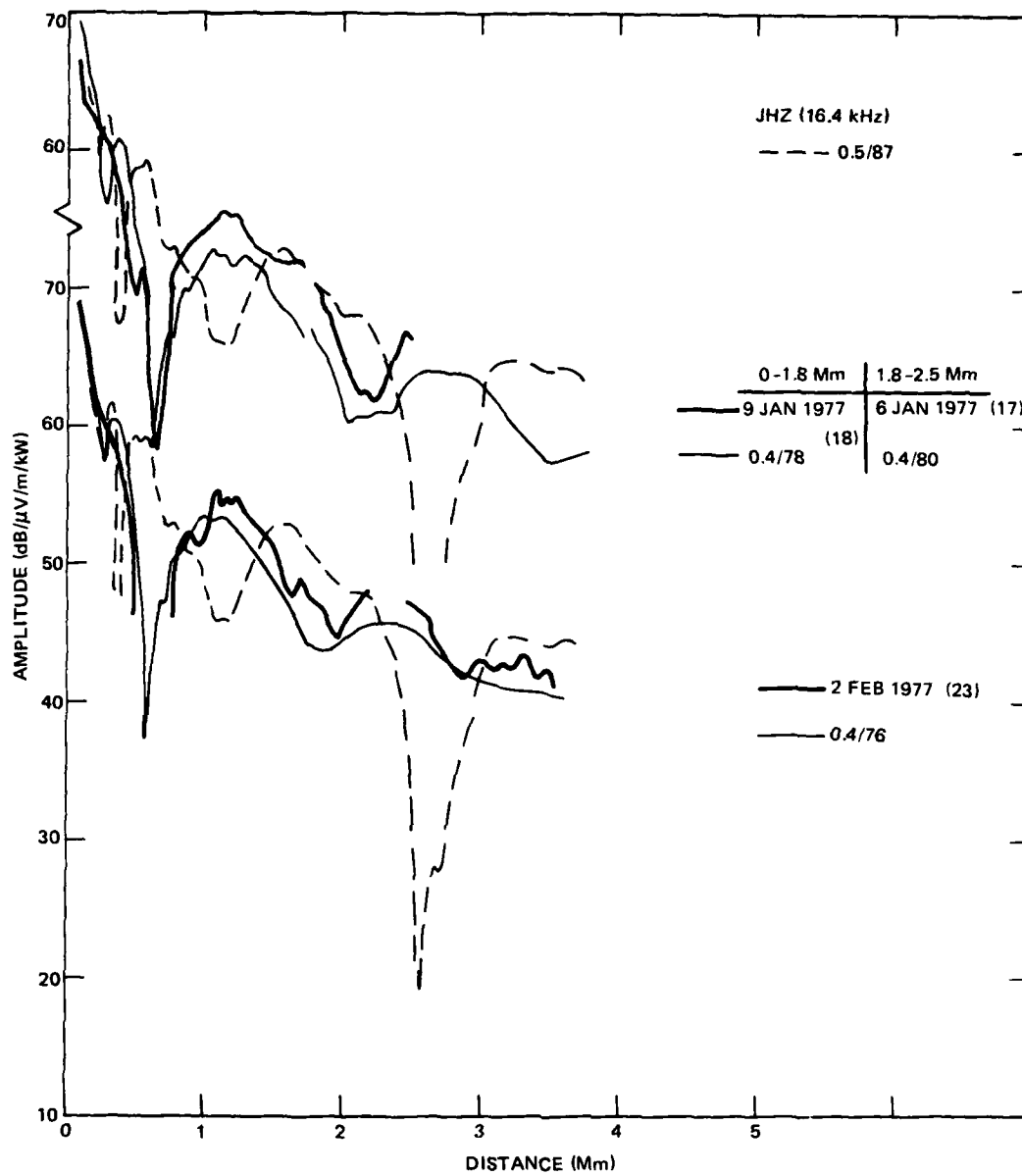
Figure 35. Best fit to measurements: JHZ toward NAA, 1977.
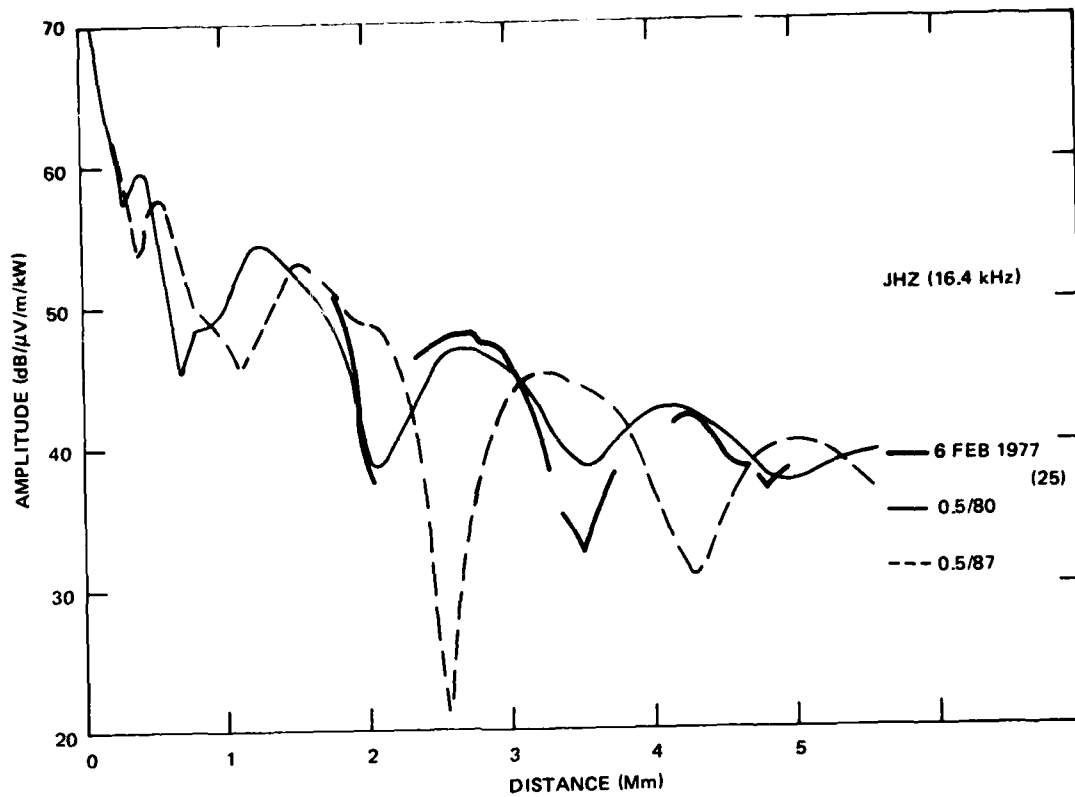
Figure 36. Best fit to measurements: JHZ toward the pole, 1977.
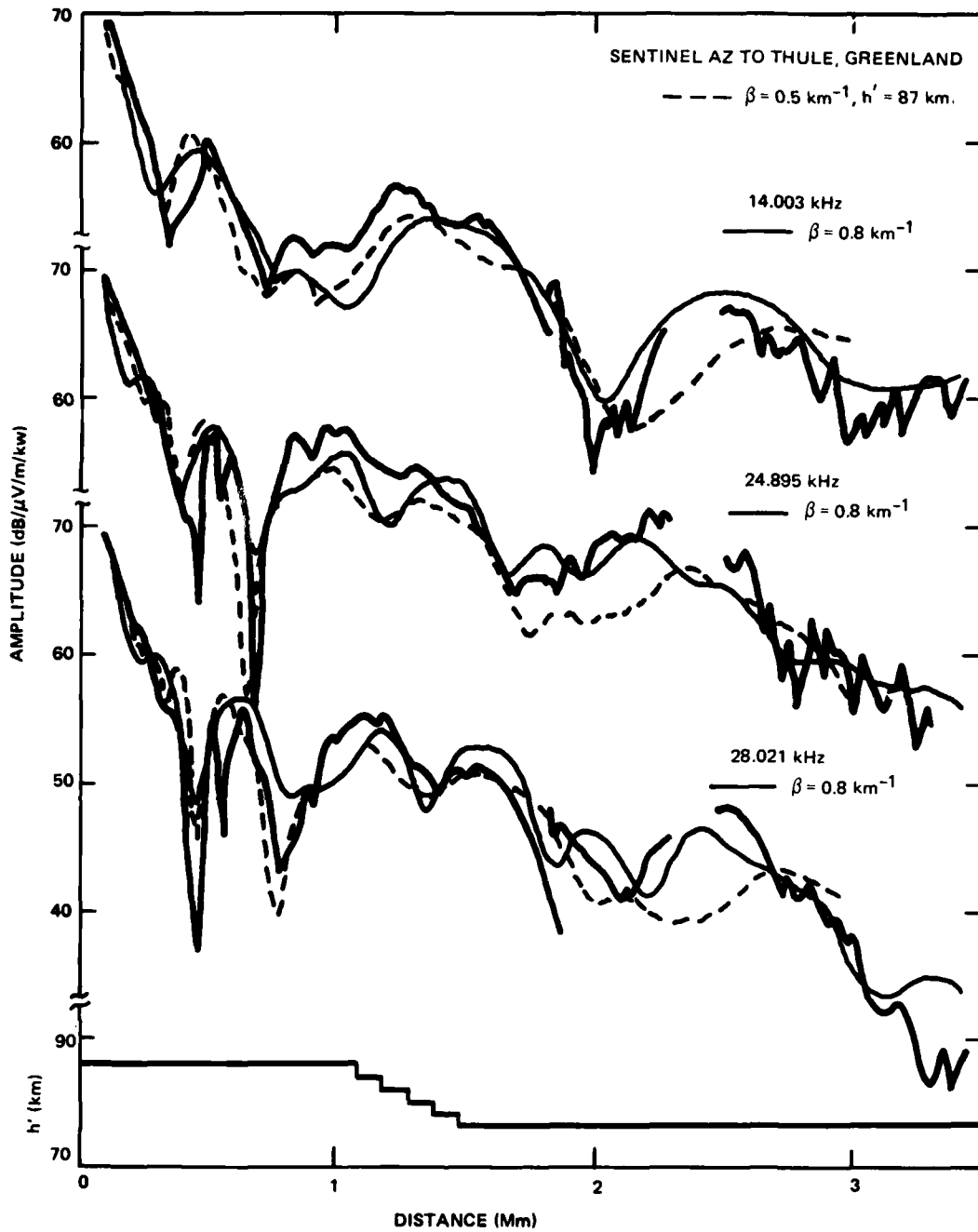
Figure 37a. Best fit to measurements, Sentinel AZ to Thule, Greenland, 1974.

69
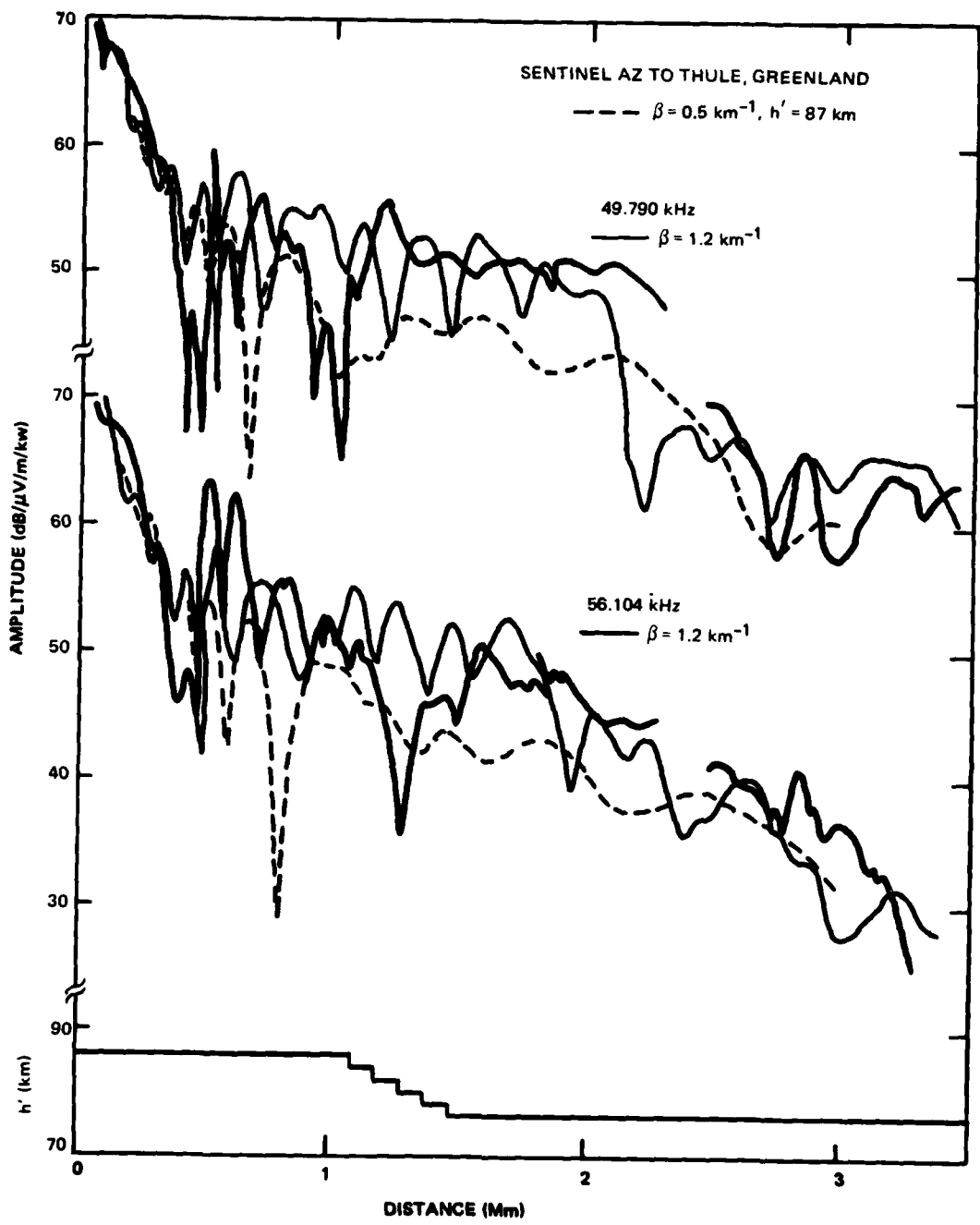
Figure 37b. Best fit to measurements, Sentinel AZ to Thule, Greenland, 1974.

70
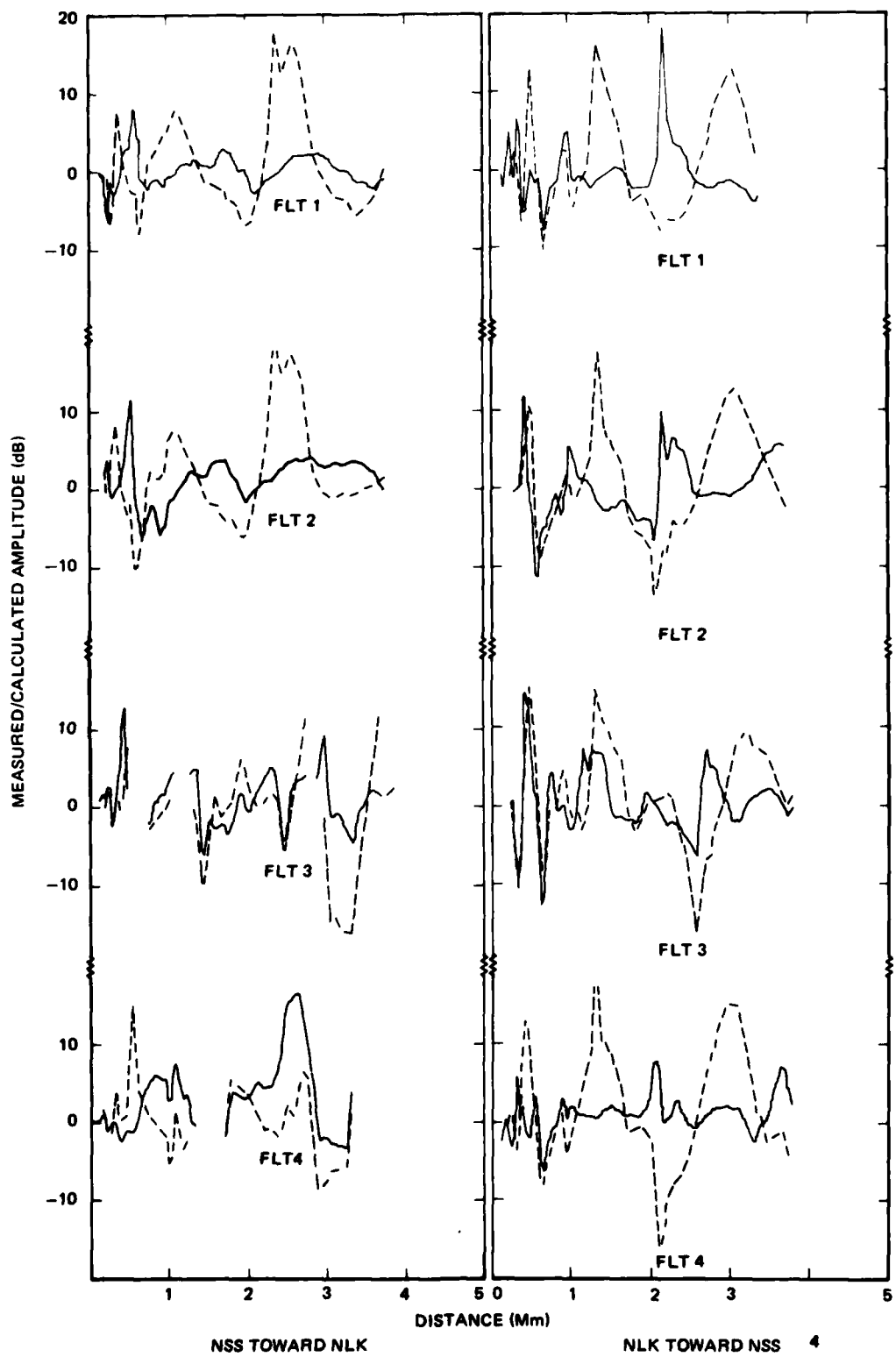
Figure 38. Ratio of measured to calculated amplitudes for the best fit profiles of table 4 (solid) and for the 0.5/87 profile (dashed) on the NLK -NSS path.

71
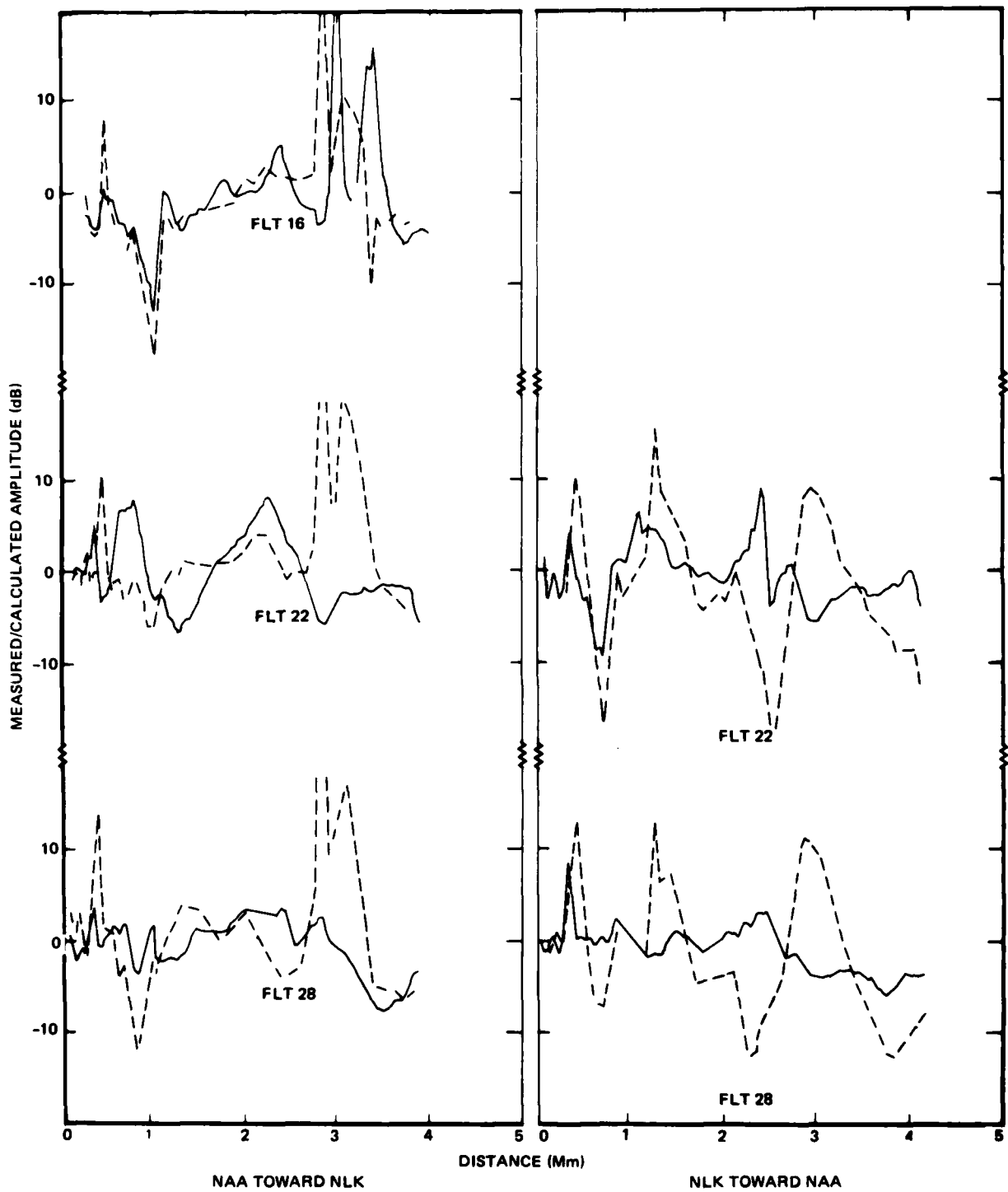
Figure 39. Ratio of measured to calculated amplitudes for the best fit profiles of table 4 (solid) and for the 0.5/87 profile (dashed) on the NLK-NAA path.

72
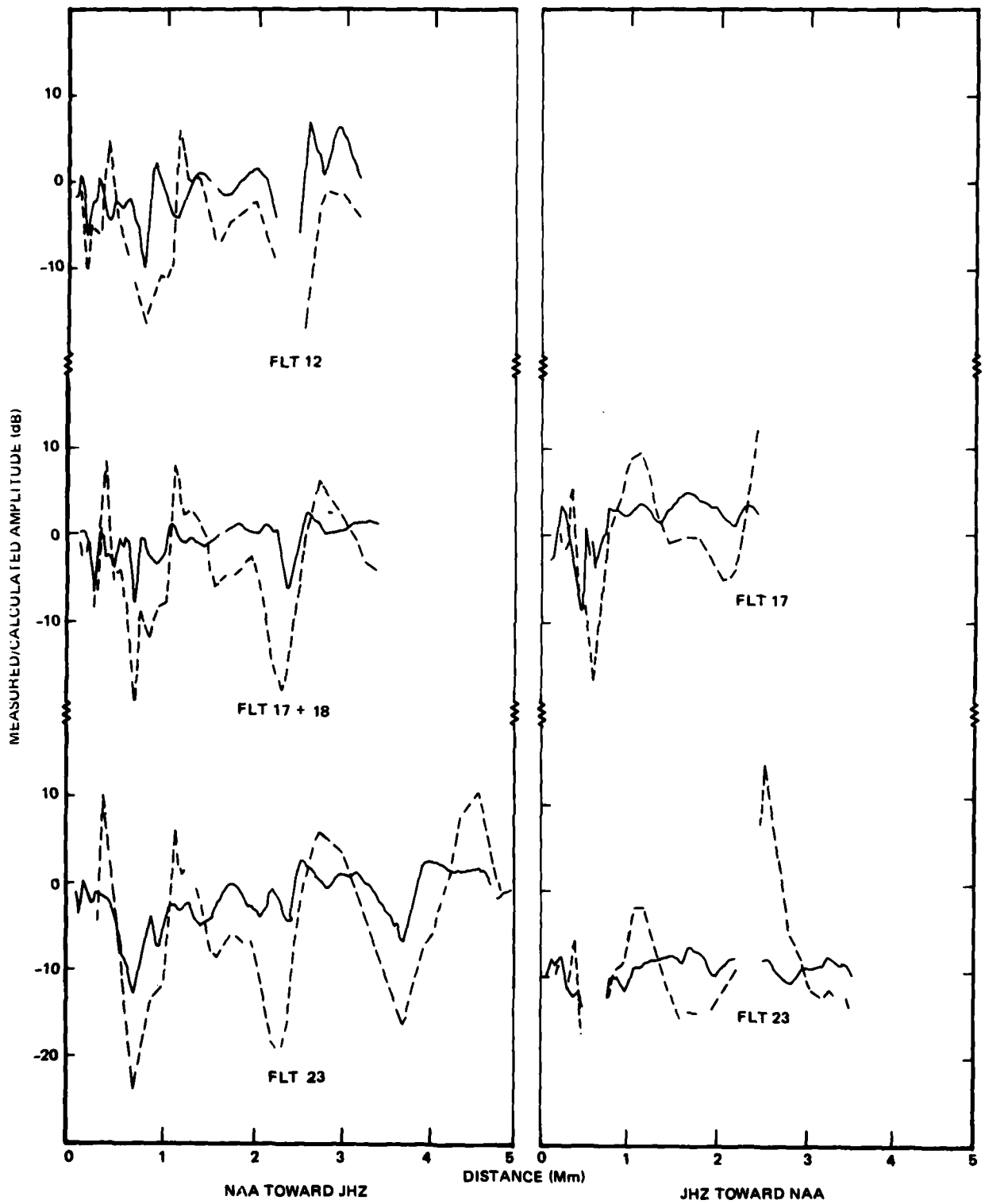
Figure 40. Ratio of measured to calculated amplitudes for the best fit profiles of table 4 (solid) and for the 0.5/87 profile (dashed) on the NAA-JHZ path.

73
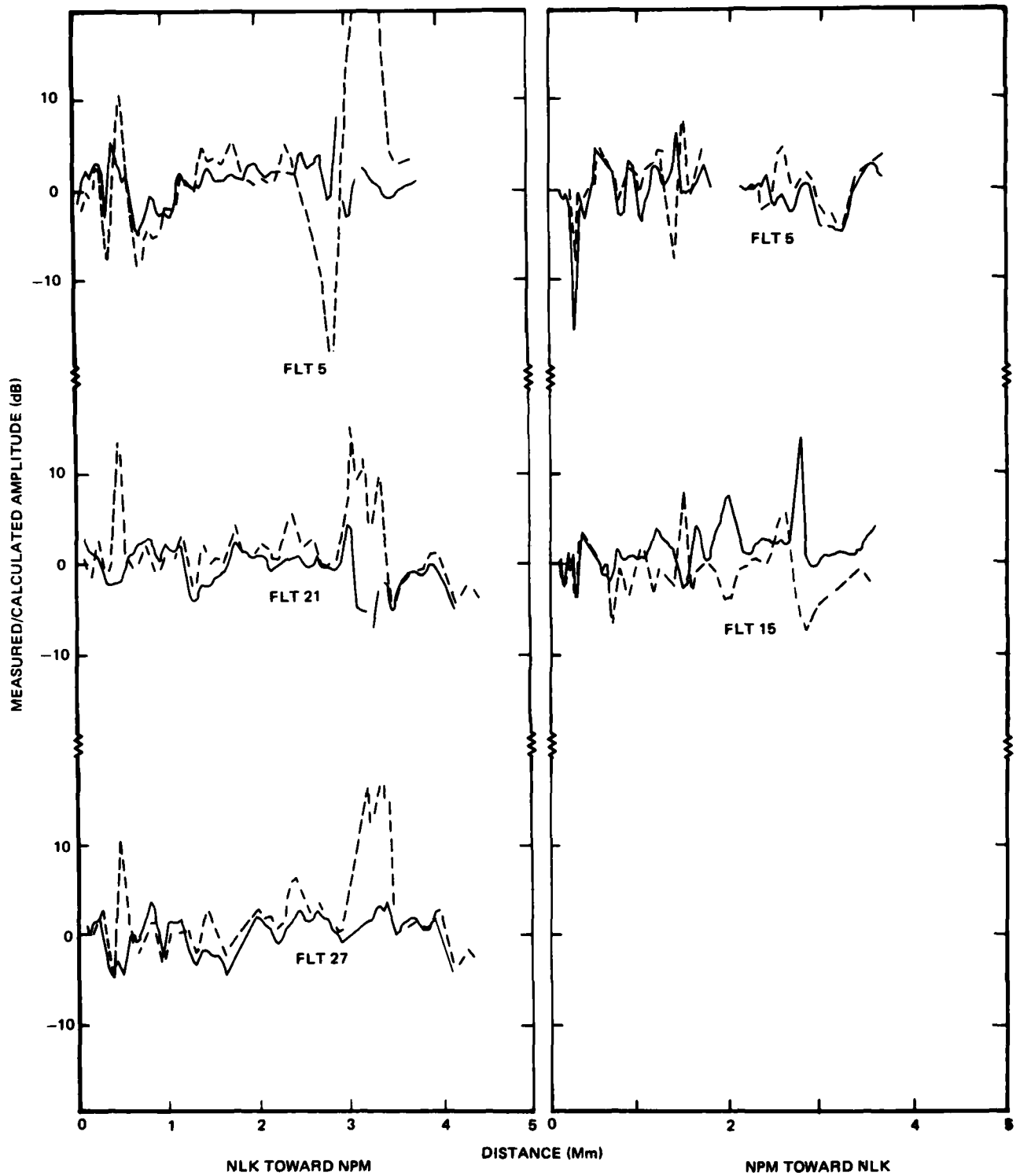
Figure 41. Ratio of measured to calculated amplitudes for the best fit profiles of table 4 (solid) and for the 0.5/87 profile (dashed) on the NLK-NPM path.

74

DEPARTMENT OF DEFENSE
ASSISTANT SECRETARY OF DEFENSE
CMD, CONT, COMM & INTELL
DEPARTMENT OF DEFENSE
WASHINGTON, DC 20301
    M EPSTEIN
    J BABCOCK

DIRECTOR
COMMAND CONTROL TECHNICAL CENTER
11440 ISAAC NEWTON SQUARE, N
RESTON, VA 22091
    C-650

DIRECTOR
COMMAND CONTROL TECHNICAL CENTER
ROOM ME682, THE PENTAGON
WASHINGTON, DC 20301
    C-312

DIRECTOR
DEFENSE ADVANCED RESEARCH PROJECT
    AGENCY
1400 WILSON BLVD
ARLINGTON, VA 22209
    NUCLEAR MONITORING RSCH
    STRATEGIC TECH OFFICE

DEFENSE COMMUNICATION ENGINEERING CENTER
1860 WIEHLE AVENUE
RESTON, VA 22090
    CODE R220 (M HOROWITZ)
    CODE R720 (JOHN WORTHINGTON)
    CODE R410 (JAMES W McLEAN)
    CODE R103

DIRECTOR
DEFENSE COMMUNICATIONS AGENCY
WASHINGTON, DC 20305
    CODE 810 (RW ROSTRON)
    CODE 480
    CODE 101B (MAJ ROOD)

DEFENSE COMMUNICATIONS AGENCY
WWMCCS SYSTEM ENGINEERING ORG
WASHINGTON, DC 20305
    RL CRAWFORD

DEFENSE TECHNICAL INFORMATION CENTER
CAMERON STATION
ALEXANDRIA, VA 22314
    TC   (12)

DIRECTOR
DEFENSE INTELLIGENCE AGENCY
WASHINGTON, DC 20301
    DIAST-5
    DIAAP (ALBERT L WISE)
    DB-4C (EDWARD OFARRELL)

DIRECTOR
DEFENSE NUCLEAR AGENCY
WASHINGTON, DC 20305
    DDST
    TISI ARCHIVES
    TITL TECH LIBRARY   (3)
    RAAE   (3)
    STVL

COMMANDER
FIELD COMMAND
DEFENSE NUCLEAR AGENCY
KIRTLAND AFB, NM 87115
    FCPR

DIRECTOR
INTERSERVICE NUCLEAR WEAPONS SCHOOL
KIRTLAND AFB, NM 87115
    DOCUMENT CONTROL

DIRECTOR
JOINT STRAT TGT PLANNING STAFF JCS
OFFUTT AFB
OMAHA, NB 68113
    JPST (CAPT DG GOETZ)

CHIEF
LIVERMORE DIVISION FLD COMMAND DNA
LAWRENCE LIVERMORE LABORATORY
PO BOX 808
LIVERMORE, CA 94550
    FCPRL

DIRECTOR
NATIONAL SECURITY AGENCY
FT GEORGE G MEADE, MD 20755
    W65
    OLIVER H BARTLETT W32
    TECHNICAL LIBRARY
    JOHN SKILLMAN R52

OJCS/J-3
THE PENTAGON
WASHINGTON, DC 20301
    OPERATIONS (WWMCCS EVAL
    OFF, MR TOMA)

OJCS/J-5
THE PENTAGON
WASHINGTON, DC 20301
    PLANS & POLICY (NUCLEAR DIVISION)

UNDER SECRY OF DEFENSE FOR RESEARCH
    AND ENGINEERING
DEPARTMENT OF DEFENSE
WASHINGTON, DC 2-301
    S&SS (OS)

DEPARTMENT OF THE ARMY
COMMANDER/DIRECTOR
ATMOSPHERIC SCIENCES LABORATORY
US ARMY ELECTRONICS COMMAND
WHITE SANDS MISSILE RANGE, NM 88002
    DELAS-AE-M (FE NILES)

COMMANDER
HARRY DIAMOND LABORATORIES
2800 POWDER MILL RD
ADELPHI, MD 20783
    DELHD-NP (FRANCIES N WIMENITZ)
    MILDRED H WEINER DRXDO-II

COMMANDER
US ARMY ELECTRONICS RESEARCH &
DEVELOPMENT COMMAND
FORT MONMOUTH, NJ 07703
    DRSEL-RD
    (JE QUIGLEY)

COMMANDER
US ARMY FOREIGN SCIENCE & TECH CENTER
220 7TH STREET, NE
CHALOTTESVILLE, VA 22901
 R JONES
 PA CROWLEY

COMMANDER
US ARMY NUCLEAR AGENCY
7500 BACKLICK ROAD
BUILDING 2073
SPRINGFIELD, VA 22150
 MONA-WE (J BERBERET)

CHIEF
US ARMY RESEARCH OFFICE
PO BOX 12211
TRIANGLE PARK, NC 27709
 DRXRD-ZC

DEPARTMENT OF THE NAVY
CHIEF OF NAVAL OPERATIONS
NAVY DEPARTMENT
WASHINGTON, DC 20350
 OP 941
 OP-604C3
 OP 943 (LCDR HUFF)
 OP 981

CHIEF OF NAVAL RESEARCH
NAVY DEPARTMENT
ARLINGTON, VA 22217
 CODE 402
 CODE 420
 CODE 421
 CODE 461
 CODE 464

COMMANDING OFFICER
NAVAL INTELLIGENCE SUPPORT CENTER
4301 SUITLAND RD BLDG 5
WASHINGTON, DC 20390

COMMANDER
NAVAL OCEAN SYSTEMS CENTER
SAN DIEGO, CA 92152
 CODE 81 (HD SMITH)
 CODE 532 (3)
 CODE 532 (WILLIAM F MOLER)

COMMANDING OFFICER
NAVAL RESEARCH LABORATORY
WASHINGTON, DC 20375
 CODE 5410 (JOHN DAVIS)
 CODE 7701 (JACK D BROWN)
 CODE 5461 TRANS IONO PROP
 CODE 5465 PROP APPLICATIONS
 CODE 5460 ELECTROMAG PROP BR
 CODE 2600 TECH LIBRARY (2)

OFFICER-IN-CHARGE
WHITE OAK LABORATORY
NAVAL SURFACE WEAPONS CENTER
SILVER SPRING, MD 20910
 CODE WA501 NAVY NUC PRGMS OFF
 CODE WX21 TECH LIBRARY

COMMANDER
NAVAL TELECOMMUNCATIONS COMMAND
NAVTELCOM HEADQUARTERS
4401 MASSACHUSETTS AVE, NW
WASHINGTON, DC 20390
 CODE 24C

COMMANDING OFFICER
NAVY UNDERWATER SOUND LABORATORY
FORT TRUMBULL
NEW LONDON, CT 06320
 PETER BANNISTER
 DA MILLER

DIRECTOR
STRATEGIC SYSTEMS PROJECT OFFICE
NAVY DEPARTMENT
WASHINGTON, DC 20376
 NSP-2141

DEPARTMENT OF THE AIR FORCE
COMMANDER
ADC/DC
ENT AFB, CO 80912
 DC (MR LONG)

COMMANDER
ADCOM/XPD
ENT AFB, CO 80912
 XPQDQ
 XP

AF GEOPHYSICS LABORATORY, AFSC
HASCOM AFB, MA 01731
 CRU (S HOROWITZ)
 PHP (JULES AARONS)
 OPR (JAMES C ULWICK)
 OPR (ALVA T STAIR)
 SUOL (RESEARCH LIBRARY) (2)

AF WEAPONS LABORATORY, AFSC
KIRTLAND AFB, NM 87117
 SUL (2)
 SAS (JOHN M KAMM)
 DYC (CAPT L WITTWER)

AFTAC
PATRICK AFB, FL 32925
 TN
 TD-3
 TD-5
 TF/MAJ WILEY

AIR FORCE AVIONICS LABORATORY, AFSC
WRIGHT-PATTERSON AFB, OH 45433
 AAD

COMMANDER
FOREIGN TECHNOLOGY DIVISION, AFSC
WRIGHT-PATTERSON AFB, OH 45433
 ETD BL BALLARD

HQ USAF/RD
WASHINGTON, DC 20330
 RDQ

HEADQUARTERS
NORTH AMERICAN AIR DEFENSE COMMAND
1500 EAST BOULDER
COLORADO SPRINGS, CO 80912
    CHIEF SCIENTIST

COMMANDER
ROME AIR DEVELOPMENT CENTER, AFSC
GRIFFISS AFB, NY 13440
    EMTLD DOC LIBRARY

COMMANDER
ROME AIR DEVELOPMENT CENTER, AFSC
HANSCOM AFB, MA 01731
    EEP JOHN RASMUSSEN

SAMSO/MN
NORTON AFB, CA 92409
    MINUTEMAN (NMML LTC KENNEDY)

COMMANDER IN CHIEF
STRATEGIC AIR COMMAND
OFFNUT AFB, NB 68113
    NRT
    XPFS (MAJ BRIAN G STEPHAN)
    DOK (CHIEF SCIENTIST)

US ENERGY RESEARCH AND DEV ADMIN
DEPARTMENT OF ENERGY
ALBUQUERQUE OPERATIONS OFFICE
PO BOX 5400
ALBUQUERQUE, NM 87115
    DOC CON FOR D W SHERWOOD

DEPARTMENT OF ENERGY
DIVISION OF HEADQUARTERS SERVICES
LIBRARY BRANCH G-043
WASHINGTON, DC 20545
    DOC CON FOR ALLEN LABOWITZ

DIVISION OF MILITARY APPLICATION
DEPARTMENT OF ENERGY
WASHINGTON, DC 20545
    DOC CON FOR DONALD I GALE

LAWRENCE LIVERMORE LABORATORY
PO BOX 808
LIVERMORE, CA 94550
    GLENN C WERTH L-216
    TECH INFO DEPT L-3

LOS ALAMOS SCIENTIFIC LABORATORY
PO BOX 1663
LOS ALAMOS, NM 87545
    DOC CON FOR T F TASCHEK
    DOC CON FOR D R WESTERVELT
    DOC CON FOR P W KEATON
    DOC CON FOR J H COON

SANDIA LABORATORIES
LIVERMORE LABORATORY
PO BOX 969
LIVERMORE, CA 94550
    DOC CON FOR B E MURPHEY
    DOC CON FOR T B COOK ORG 8000

SANDIA LABORATORIES
PO BOX 5800
ALBUQUERQUE, NM 87115
    DOC CON FOR SPACE PROJ DIV
    DOC CON FOR A D THORNBROUGH, ORG 1245
    DOC CON FOR W C MYRA
    DOC CON FOR 3141 SANDIA RPT COLL

OTHER GOVERNMENT
DEPARTMENT OF COMMERCE
NATIONAL BUREAU OF STANDARDS
WASHINGTON, DC 20234
    RAYMOND T MOORE

DEPARTMENT OF COMMERCE
OFFICE OF TELECOMMUNICATIONS
INSTITUTE FOR TELCOM SCIENCE
BOULDER, CO 80302
    WILLIAM F UTLAUT
    L A BERRY
    A GLENN JEAN
    D D CROMBIE
    J R WAIT

DEPARTMENT OF TRANSPORTATION
OFFICE OF THE SECRETARY
TAD-44.1, ROOM 10402-B
400 7TH STREET, SW
WASHINGTON, DC 20590
    R L LEWIS
    R H DOHERTY

DEPARTMENT OF DEFENSE CONTRACTORS
AEROSPACE CORPORATION
PO BOX 92957
LOS ANGELES, CA 90009
    IRVING M GARFUNKEL

ANALYTICAL SYSTEMS ENGINEERING CORP
5 OLD CONCORD RD
BURLINGTON, MA 01803
    RADIO SCIENCES

THE BOEING COMPANY
PO BOX 3707
SEATTLE, WA 98124
    GLENN A HALL
    J F KENNEY

UNIVERSITY OF CALIFORNIA
 AT SAN DIEGO
MARINE PHYSICAL LAB OF THE
 SCRIPPS INSTITUTE OF OCEANOGRAPHY
SAN DIEGO, CA 92132
    HENRY G BOOKER

COMPUTER SCIENCES CORPORATION
PO BOX 530
6565 ARLINGTON BLVD
FALLS CHUCH, VA 22046
    D BLUMBERG

UNIVERSITY OF DENVER
COLORADO SEMINARY
DENVER RESEARCH INSTITUTE
PO BOX 10127
DENVER, CO 80210
    DONALD DUBBERT
    HERBERT REND